THE ROLE OF THE OCEAN IN CONVECTIVE BURST INITIATION: IMPLICATIONS FOR TROPICAL CYCLONE INTENSIFICATION

DISSERTATION

Presented in Partial Fulfillment of the Requirements for

the Degree Doctor of Philosophy in the Graduate

School of The Ohio State University

By

Paula Ann Hennon, M.B.A

*****

The Ohio State University
2006

Dissertation Committee:

Dr. Jay Hobgood, Adviser

Dr. John Rayner

Dr. Lawrence Krissek

Dr. Jeffrey Halverson

Approved by

_____
Adviser
Atmospheric Sciences Graduate Program

ABSTRACT

The upper ocean significantly influences tropical cyclone structure and intensity. These effects, however, are not well understood mostly due to a lack of oceanic and atmospheric boundary layer observations within the inner-core region. This study relates ocean-atmosphere energy exchange processes to mid-to-upper tropospheric latent heating using mesoscale inner-core convective burst events.

A global survey of convective burst events in tropical cyclones from the year 1999 -- 2001 was constructed. This study shows that 80% of tropical cyclones have at least one convective burst event and that convective burst events usually occur during the intensification phase of the storm life cycle. Convective bursts are usually accompanied by a moderate (5-15 kt) wind speed increase, although some have little or no wind speed change during the burst itself. However, a period of intensification often follows a convective burst event within 18 to 24 hours.

To determine atmospheric and oceanic variables useful in identifying conditions typical of convective burst activity, an ensemble of discriminant analyses were performed. The first procedure tested solely atmospheric variables; the second tested the oceanic variables by themselves, and finally, a combined procedure attempted to distinguish convective burst events using both the atmospheric and oceanic variables. Four main atmospheric conditions characterize convective burst existence when compared to periods with no convective burst: 1) increased precipitable water at 200 km and 500 km, 2) increased 150 mb divergence at 600 km, 3) 2-1/2 times more convective instability in the large-scale environment, 4) 1-1/2 to 2 times more 850 mb moisture divergence at 200 km and 600 km. The main characteristic differences in ocean conditions during convective burst events are: 1) the mean climatological SST is 1.25°C greater 2) the "hurricane heat content" is double 3) less inner-core ocean cooling occurs. The combined analysis suggests that the moist static energy provided by the warm ocean is more influential on convective burst occurrence than simply having “enough” available atmospheric moisture.

A multivariate Lagrangian time series of the inner-core SST, the inner-core-wake SST, the ahead-of-storm SST, and measures of spatial variability of these variables for 30

tropical cyclones was constructed using an objectively interpolated SST tropical cyclone cold-wake climatology. Latent and sensible heat flux estimates and a measure of upper-ocean energy utilization were calculated for the inner-core (<.5° radius) and the near-core (.5° - 1° radius). This study found that tropical cyclones generally utilize only about 8% of the total enthalpy flux available from the ocean/atmosphere boundary layer. Storms with convective bursts utilize more energy from the ocean (11%) than storms with no convective burst (2%). Sea-air fluxes are greatly enhanced (doubled) during convective burst time periods.

These along-track ocean-atmosphere analyses were compared to vertical profiles of atmospheric latent heating calculated using a combined active and passive TRMM PR and TMI retrieval algorithm. Results show strong positive space and time correlations between ocean-air fluxes and mid-upper tropospheric latent heating.

Additionally, the 30 storms analyzed were categorized by the presence or absence of convective burst events during the storm lifecycle. Composite atmospheric latent heating profiles constructed for each group show a two-fold release in energy for the storms with convective burst events compared to storms with no convective burst event.

Finally, seven case studies are presented which attempt to resolve The upscale energy cascade of the tropical cyclone with a convective burst event from the ocean through the troposphere. For these case studies, the TRMM vertical profiles of latent heating are compared with AMSU temperature anomalies in an attempt to link the enhanced tropospheric latent heat release with a developing inner-eye warm core anomaly.

The findings of this study support the following scenario linking convective bursts to tropical cyclone intensification:

> *A very warm ocean with a deep mixed layer is the base of the energy supply for the intensifying tropical cyclone. The undilute convection of the mesoscale convective burst mines the enhanced boundary layer gaining almost twice the total enthalpy flux of a storm with no convective burst. This twofold energy utilization is apparent in the mid-upper troposphere as TRMM vertical profiles of latent energy release show 2 to 2-1/2 times the magnitude of profiles of non-convective burst time periods. Finally, in most cases and after a 12 to 24 hour lag, an enhanced warm core anomaly appears in AMSU analyses. This lag time is consistent with the convective timescale necessary for adiabatic warming through subsidence along the inner edge of the tropical cyclone eyewall.*

Dedicated to the Roses in the garden of my life: Mary Rose, Rosemarie, and Olivia Rose.
Thank you for your beauty.

ACKNOWLEDGMENTS

When I started my doctorate in Atmospheric Sciences I decided early on that if I wasn't "having fun" I wouldn't bother trying. So, I guess I was having fun. In fact, there was way too much fun to be had for just one person to enjoy so I spread the fun around -- a lot! I am happy to say that my life has taken some interesting turns throughout the process and I have tried to enjoy and learn from them all.

Interdisciplinary research required interdisciplinary support -- support that typically goes far beyond the realm of science. I want to acknowledge and offer my heartfelt gratitude for the fundamental contributions of my husband, Christopher, without whose love and support I would cease to be. I would also like to thank my family for their support and for always believing in me, even when I didn't give them much reason.

My adviser, Jay Hobgood has always trusted in my academic abilities even when I've approached learning in unorthodox ways. Thank you Jay for allowing me the intellectual freedom to pursue my education without much artificial restraint.

The work in this dissertation benefited from advice, comments, and friendship of many people over the years. Although I possessed no science credentials when I began this degree, many professors throughout my studies encouraged me to pursue a career as a scientist. Linda Leighton, my undergraduate honors adviser at Fordham University, a statistician herself, repeatedly tried with no avail to tempt me away from economics. Twelve years later a geology field trip around Lake Erie and a couple of courses with Larry Krissek finally convinced me to listen.

At Ohio State I had the excellent experience of working with Ellen Mosley-Thompson who has unceasingly taught me through example the value of playful thinking, a strong work-ethic, and of surrounding myself with positive, supportive people. Though my research interests in the tropical atmosphere eventually led me away from her area of expertise, her mentorship has been invaluable. Through Ellen, I befriended another exceptional scientist, Claire Parkinson at NASA Goddard Space Flight Center. Claire's exemplary NASA career and her excellent ability to explain hard science to non-scientists and children inspire me greatly.

Claire eventually arranged for me to meet Dr. Joanne Simpson. After two or three dishpan experiments staged to convince me of the role of background vorticity "seedlings" in tropical cyclogenesis, Joanne asked me if I had a dissertation topic. When I answered "not yet" she led me down the hall, and said, "You do now." She introduced me to Jeff Halverson. Funny. Jeff doesn't remember that day in 1999, but it changed my perspective forever. Since then I have come to understand much more fully not only the scientific topics of interest in this thesis but also my role as a scientist. Watching Jeff is witnessing "science in action." I am proud to have become a part of his team of investigators. Thank you Jeff for your support and friendship.

Without knowing it, my committee member Dr. John Rayner has had untold influence on this work. I am proud to be the last student to pass through his tutelage at Ohio State. Incidentally (or not!) Jay Hobgood, my adviser, Ellen Mosley-Thompson, Claire Parkinson, were all his students.

The multi-disciplinary work in this dissertation required gathering datasets from no fewer than eleven sources. All of the data used in this project was obtained at no cost. The multiple satellite platforms used in this dissertation added an extra layer of complexity to the project, but were necessary to trace tropical cyclone energetics. This complexity, however, opened the door to forge numerous valuable associations with scientists at many different institutions. Jeff Hawkins at the U.S. Naval Research Laboratory - Monterey provided the satellite imagery for the convective burst survey. Dan Cecil of the University of Alabama Huntsville and Marshall Space Flight Center provided the SSM/I data for thirty-one storms. Hal Pierce at NASA/GSFC found and dusted off scripts from the archive of the late Ed Rodgers to compute latent heating profiles from this SSM/I data. Bill Olsen and Mircea Grecu kindly provided TRMM latent heating estimates using their latest algorithm.

The ocean data came from multiple sources as well. Clark Rowley at the U.S. Naval Research Laboratory at Stennis Space Center provided surface temperature, surface height anomaly, Z26, and hurricane heat potential data despite his family being displaced while his home and work was underwater from Hurricane Katrina. Chelle Genetmann of Remote Sensing Systems, Inc. provided Lagrangian and Eulerian cold wake climatologies from the objectively interpolated TMI SSTs and programming support right up to the day before her wedding! Joe Cione and Eric Uhlhorn at the Hurricane Research Division of NOAA conceptualized the ocean variables and flux calculations and explained their ideas to me over beer at TCSP. I agree guys, the size of the gas tank is of little importance.

The first person to convince me about the importance of the role of the ocean in TC intensification was Michelle Mainelli of the Tropical Prediction Center. I don't know whether

to include you in the list of scientists who have provided support or as a personal inspiration and friend, Michelle, because you truly are both. Without you (and your Master's Thesis) the idea for this dissertation would never have been conceived. Your example of actually writing a thesis as a new mommy and finishing your degree was one of the biggest inspirations to me in the writing process.

I would like to acknowledge my friends who have provided personal support to me beyond belief. I am in awe and baffled by your generosity. Beth Mazzocco, the sister I never had, deserves the credit for encouraging me to persevere despite the weather. You truly saved the project in the eleventh hour! Amy Drew Thompson and Jorge and Margaret Reyes made two years in Miami worthwhile. Thank you Stephanie McMillen and Griselda Perez for lovingly caring for my daughter when she was very young. Bill Cotrill encouraged my competitive spirit and egged me on through the late stages of this work. Jeff and Kathleen Halverson generously shared their home and their lives with me for multiple weeks so I could afford to visit GSFC and keep up the momentum when the wheels started getting square. The Degrand Family provided the love and support of an extended family during my recent residence at their home in Columbus. Thank you Jim and Cynthia. Jens Blegvad has provided unending hours of support -- technical and philosophical-- to me over the past five years. Thank you for your friendship.

Finally, thank you Chris for not being a car mechanic. I love you and your scripts. Olivia, I hope you find Mommy to be an inspiration someday when you are older instead of thinking the Zygote Fairy must have made some sort of mistake.

This research has been supported by NASA Graduate Student Researchers Fellowship NGT5-131.

VITA

December 12, 1965	Born – Cleveland, Ohio, USA
1988	B.S., International Economics, Fordham University
1993	M.B.A., Operations Research,Kent State University
1999 – 2000	Graduate Research Assistant, Byrd Polar Research Center, Ice Core Paleoclimatology Group, The Ohio State University
2000 – 2001	Graduate Teaching Assistant, Department of Geography, The Ohio State University
2001 – 2005	Fellow, NASA Graduate Student Researcher Program, NASA Goddard Space Flight Center, Laboratory for Atmospheres, Mesoscale Processes Group

FIELDS OF STUDY

Major Field: Atmospheric Sciences

TABLE OF CONTENTS

LIST OF TABLES

LIST OF FIGURES

LIST OF ACRONYMS AND ABBREVIATIONS

AMSU	Advanced Microwave Sounding Unit
ATL	Atlantic Ocean Basin
AVHRR	Advanced Very High Resolution Radiometer
AXBT	Airborne Expendable Bathythermographer
AXCP	Airborne Expendable Current Profiler
CAMEX	Convection and Moisture Experiment
CAPE	Convective Available Potential Energy
CB	Convective Burst
CBLAST	Coupled Boundary Layers/Air-Sea Transfer Experiment
CCC	Central Cold Cover
CDC	Climate Diagnostics Center
CDO	Central Dense Overcast
CEC	Circular Exhaust Clouds
CPAC	Central Pacific Ocean Basin
DMSP	Defense Meteorological Satellite Program
EC	Extreme Convection
EDOP	NASA ER-2 Doppler Radar
EPAC	Eastern Pacific Ocean Basin
FNMOC	Fleet Numeric Meteorology and Oceanography Center
GOES	Geostationary Orbiting Environmental Satellite
GPROF	Goddard Profiling Algorithm
GRIB	Grid in Binary
GSFC	NASA Goddard Space Flight Center
HHC	Hurricane Heat Content
HRD	Hurricane Research Division of NOAA

H*Wind	Hurricane Wind Analysis
IO	Indian Ocean Basin
IR	Infrared
LF	Left Front
MCC	Mesoscale Convective Complex
MCS	Mesoscale Convective System
MSW	Maximum Sustained Wind
NCAR	National Center for Atmospheric Research
NCEP	National Centers for Environmental Prediction
NOGAPS	Naval Operational Global Atmospheric Prediction Scheme
NRL	U. S. Naval Research Laboratory
OPBL	Oceanic Planetary Boundary Layer
PR	Precipitation Radar
PV	Potential Vorticity
Q_H	Hurricane Heat Content (energy available to storm from ocean)
Q_{H_ext}	Energy extracted from ocean by storm
Q_{H_util}	Energy utilized by storm
RF	Right Front
SFMR	Stepped Frequency Microwave Radiometer
SHEM	Southern Hemisphere Ocean
SHIPS	Statistical Hurricane Intensity Prediction Scheme
SSHA	Sea Surface Height Anomaly
SSM/I	Special Sensor Microwave Imager
SST	Sea Surface Temperature
SST_A	Ambient Sea Surface Temperature
SST_{IC}	Inner-core Sea Surface Temperature
SST_{ICW}	Inner-core Wake Sea Surface Temperature
STY	Supertyphoon
TC	Tropical Cyclone
$TC_{transit\text{-}time}$	Tropical Cyclone Transit Time (seconds for storm to travel TC inner-core diameter)

TCSP	Tropical Cloud Systems and Processes Experiment
TMI	Thematic Mapper Imagery
TRMM	NASA's Tropical Rainfall Measuring Mission
UTC	Coordinated Universal Time
VHT	Vortical Hot Tower
WCR	Warm Core Ring
WPAC	Western Pacific Ocean Basin

CHAPTER 1
INTRODUCTION

1.1 Toward a global census of convective bursts in tropical cyclone intensity change

In spite of the tremendous progress made in improving forecasts of tropical cyclone track and landfall location in the past twenty years, the processes governing hurricane intensity change remain relatively poorly understood. Skill in predicting the sudden deepening or weakening of storms that threaten the lives of millions has not kept pace with the 25-30% reduction in track error incurred during the past twenty years. While synoptic scale factors such as sea surface temperature, the magnitude of vertical wind shear and certain upper tropospheric trough configurations are broadly known to favor intensification, there is a growing consensus that the smaller space and time scales play crucial roles. Only in recent years has satellite and other remote sensing technology advanced to the point where these mesoscale processes can be elucidated with sufficient detail.

Since about 1970 a line of thinking has evolved stating that unusually long-lived and intense clusters of thunderstorms, when present within the nascent cores of tropical cyclones, lead to storm intensification. In its simplest form, this idea is generally plausible: Tropical cumulonimbi warm the troposphere, through the release of latent heats of condensation and fusion. The pressure fall within the core of hurricanes derives from a core of air anomalously warmed in the middle troposphere. If concentrated in sufficient density close to the center of incipient rotation, might intense thunderstorms liberate enough energy to spin-up the storm core? This concept is predicated on the theory that a tropical atmosphere with high vorticity or rotational inertial stability will efficiently retain heat energy, minimizing energy loss to the environment in the form of gravity waves (Schubert 1980, Ooyama 1969).

1.2 Convective bursts in the literature

These mesoscale regions of persistent convection are generally referred to (both operationally and in the journal literature) as *convective bursts* (CBs), although the term *supercell* has also been used to characterize inner core hurricane convection of an extreme nature. A succinct definition of convective burst follows from Rodgers et al. (2000): "a mesoscale (100 km by hours) cloud system consisting of a cluster of high cumulonimbus towers within the inner core region [of a tropical cyclone] that approaches or reaches the tropopause with nearly undiluted cores." In the satellite presentation, convective bursts stand out as rapidly expanding, circular regions of cold convective cloud, within which are embedded several smaller overshooting convective turrets. Examples of convective bursts in several storms are seen in Figure 1.

Gentry et al. (1970) were perhaps the first to recognize the significance of these spatially and temporally coherent cloud features, which they termed Circular Exhaust Clouds (CECs). In Skylab photos, these massive features were identified by their highly symmetric appearance and great height, often casting shadows on the undercast of hurricane spiral cloud tops (Black 1978). Such eruptive events, occurring close to the storm inner core often presaged intensification by 12-36 hours (Black 1978; Rogers and Fritsch 2001) (Gentry, Rodgers et al. 1980) (Black, Burpee et al. 1986) (Steranka, Rodgers et al. 1986) (Zehr 1988; Lyons and Keen 1994) Gentry et al. concluded that "the CEC…is a prominent link in the three-dimensional [hurricane] circulation and may be typical of a type of cloud developed in hurricane genesis situations." Gray (1998) provided evidence that unusually strong and concentrated "Extreme Convection (EC)" events, contained within a larger envelope of mesoscale convection, are a key step in the transformation of tropical waves and depressions into rotating cyclonic storms. He also underscored the role of convective bursts, on a time scale of 6-12 hours, in the formation of middle-level, mesoscale vortices that serve as embryonic sources of hurricane spin. The presence or absence of bursts, Gray argues, is a crucial determinant in whether a tropical cyclone will mature.

While most studies of convective bursts have focused on Atlantic basin hurricanes, Ebert and Holland (1992) describe an exceptionally vigorous series of convective bursts that occurred during the rapid intensification of tropical cyclone Hilda in the Coral Sea off Australia. One CEC in Hilda attained minimum cloud top temperatures of -100 °C, equivalent to convective towers penetrating the stratosphere to a height of 19 km and updrafts at tropopause height on the order of 15-40 m s^{-1}. Zehr (1988) identified tropical cyclones in the northwest Pacific containing convective bursts prior to deepening.

The great majority of these papers identify a positive correlation between the occurrences of a convective burst and ongoing or subsequent storm intensification. Work by Lander (1999) provides an example of a massive convective burst in Hurricane Gloria that was attended by a surprisingly small increase in wind speed. Lander states an interesting facet of Dvorak's (1975) satellite-based intensity estimation technique: "Ironically, one of the largest and coldest eruptions of convection near the core of a tropical cyclone (TC), the central cold cover (CCC), indicates slowed or arrested development." Such CCCs characteristically begin as an explosive growth of deep convection near the storm core, then spread into a very large, smooth and very cold cirrus canopy. The Gloria CCC expanded to 500,000 km^2; half its area was colder than -90 °C. This is similar to the Ebert and Holland ECC, but in contrast to Hilda, satellite techniques revealed only modest intensification of Gloria in the next 36 hours (+35 kt). This increment is seemingly out of proportion to the magnitude of the convective eruption. While there may have been environmental factors limiting the intensification potential of Gloria (not identified by Lander), the study raises an important point: An explosive convective event near the inner core does not necessarily equate to an equally dramatic change in hurricane intensity. In fact, recent work by Cecil and Zipser (1999) failed to show a relationship between the frequency of a developing tropical cyclone's inner core lightning - a marker of deep convective intensity - and storm deepening, for a large sample of storms in the Pacific and Atlantic.

1.3 Hypothesis 1: Tropical cyclone intensity change and convective bursts are positively related

Thus, it would seem that the hypothesis linking TC intensity change with remarkable bursts of convection requires a more rigorous test, or at least a robust sampling of storms, since most of the aforementioned studies address only isolated cases. The studies by Lander and Cecil and Zipser appear to downplay the role of convective bursts. Only two intensive surveys appear in the literature, and each of these is limited to a single ocean basin, i.e. Steranka et al., 1986 (Atlantic) and Zehr, 1992 (Pacific). The first goal of this paper is, *to present a more comprehensive census of the natural phenomenon termed convective bursts, develop statistical relationships for a large sample of storms that is global and multi-year in coverage, and evaluate the central hypothesis in the more rigorous context of physical mechanisms associated with bursts and storm intensification.*

1.4 Dynamical significance of convective bursts -- upscale energy cascade.

The literature to date provides clues about the convective scale dynamics and thermodynamics associated with bursts of convection in TCs, the initiation of bursts, and the upscale feedback of bursts on the larger storm. However the only published studies attempting to tie the processes together have been case studies of a single storm.

1.4.1 Literature survey regarding convective scale atmospheric dynamics and thermodynamics.

Kelley et al. (2004) document 163 eyewall overpasses using the Precipitation Radar of the Tropical Rainfall Measurement Mission (TRMM) satellite. For the subset of cases containing tall convective towers, convective tower height (and thus vigor) scales directly with the probability of tropical cyclone intensification. In the population of eyewalls with convective towers taller than 14.5 km, 71% were intensifying; if towers were 10.0 km tall, the probability was 46%; towers below 10.0 km incurred only a 13% likelihood of intensification. Kelley et al. (2005) expand the sample of tall convective towers by examining their incidence in developing Atlantic tropical cyclones within range of the coastal NEXRAD radar network. Here, repeated observation of tall precipitation in the eyewall provides more information about wind intensification. If the frequency of tall precipitation is at least 33% for the radar imagery of a storm, there is an 82% chance of intensification. If this threshold is not met, the probability of intensification drops to just 17%. In both studies, the authors assumed that the radar identified tall convective eyewall towers constitute the larger mesoscale entities termed convective bursts, but the scale linkage has yet to be established.

Several researchers have examined the thermodynamic perturbation or response of the troposphere in and around convective bursts. Simpson et al. (1997) used aircraft data to probe twin convective bursts in developing Tropical Cyclone Oliver. They identified two small regions of enhanced tropospheric warming: one in the middle layers, embedded within the cloudy mass of the burst, (likely due to the release of latent energy), and a second in the lower troposphere, on the edge of the burst in clear air (likely associated with subsidence-induced warming.) The nascent eye later developed on the edge of the convective mass. Stossmeister and Barnes (1992) note a similar case in Tropical Storm Isabel, whereby an intense burst of convection produced strong subsidence along its periphery, inducing the formation of a new circulation center through adiabatic warming. Heymsfield et al. (2001) revealed the multicellular structure of a convective burst in Hurricane Bonnie. Using aircraft observations, they measured a 10-km deep mesoscale subsiding current on the

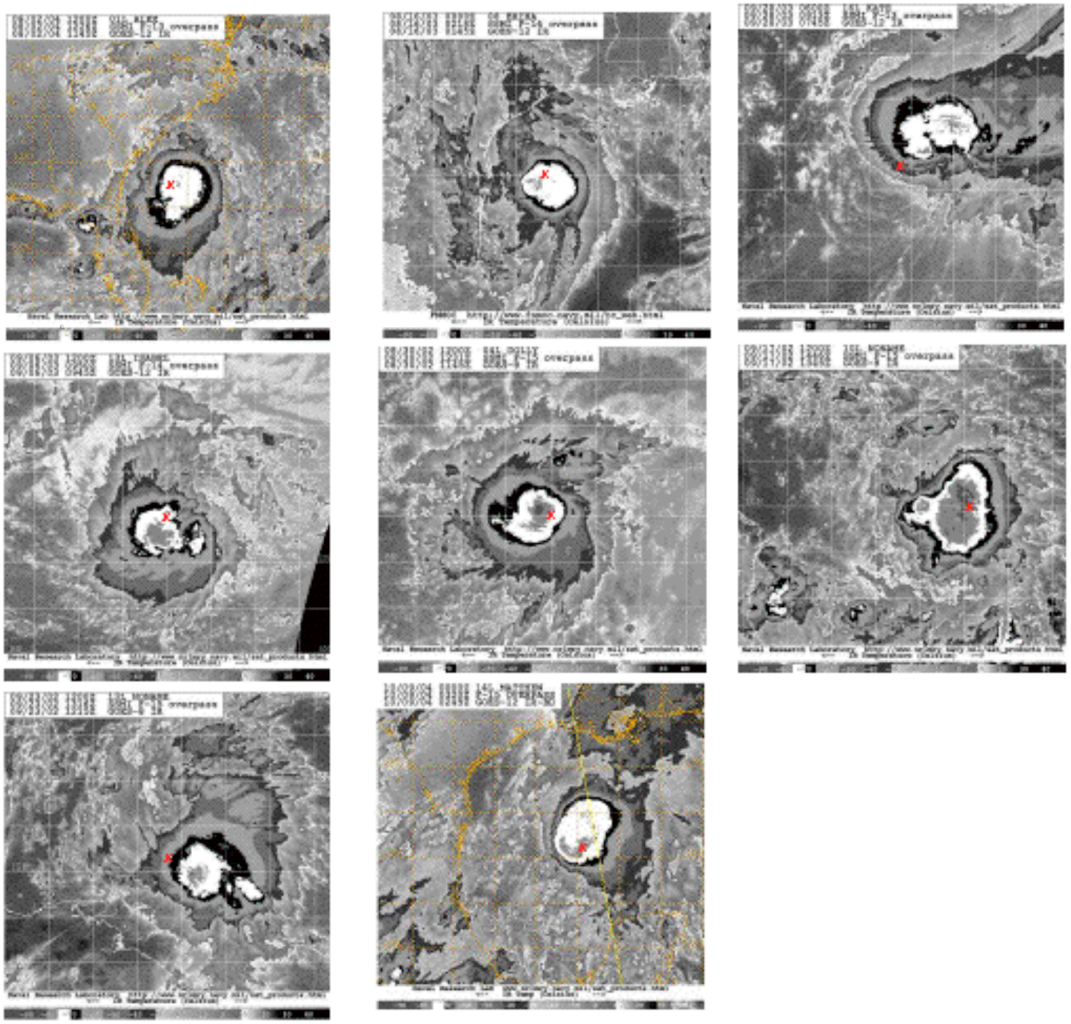

Figure 1: Examples of convective bursts from various storms (1999-2001).

periphery of the burst within the eye, with downward vertical velocities on the order of several ms^{-1}. In contrast to these studies, which highlight the important effects of a thermally-induced hydrostatic pressure reduction, Lackmann and Yablonski (2004) argue that intense rain-out in the vigorous convective regions of developing cyclones effectively reduces the mass of the vertical air column, thereby lowering the surface pressure.

Paradoxically, the presence of moderate vertical wind shear may be tied to the development of convective bursts in storms that are undergoing genesis or intensifying. Heymsfield et al. (2005) use aircraft data to investigate the thermodynamics and physical properties of a convective burst with supercell-like properties in highly sheared Tropical Storm Chantal. The convective burst was hypothesized to develop as a result of a pronounced shear-induced wave number one asymmetry. Molinari et al. (2005) investigated the role of moderate shear in inducing convective outbreaks and accelerating the genesis of Hurricane Danny. The downshear convective bursts became progressively more intense and located closer to the center during the development process. The downshear reformation of Tropical Storm Gabrielle (2005) was also associated with a highly asymmetric convective outbreak in a strongly sheared environment.

Since convective bursts are associated with strong upward vertical motions and typically occur within a region of consolidating low-mid level spin, they likely play a key role in the vorticity dynamics of genesis. As will be illustrated later several instances of bursts develop a closed eyewall in their cloudy remnants during dissipation. Stewart and Lyons (1996) show an example of mesocyclones within intense convection that developed as Supertyphoon Ed underwent rapid intensification. The mesoscyclones evolved into the eye of the storm and engendered large surface pressure falls. Hendricks et al. (2004) postulate that vortical hot towers (VHTs) stretch local vortex tubes within regions of intense convection and are therefore critical to the tropical cyclone spinup process.

The energetics of convective bursts are documented in two papers, one for rapidly intensifying Hurricane Opal in the Atlantic (1998) and the other for rapidly deepening Supertyphoon Paka in the Pacific (2000). In both cases, there was a succession of convective blowups preceding episodes of rapid deepening. Using data from satellite-based microwave profilers, Rodgers et al. (1998, 2000) computed the vertical distribution of latent heating at various times throughout the evolution of both storms. Periods of enhanced, deep tropospheric heating coincided with episodes of extreme convection. There was a time lag between the period of energy release and subsequent intensification that decreased as each storm became stronger. The decrease in lag is hypothesized to result from the growth of inertial stability, which effectively "stiffens" the atmosphere as the storm vortex strengthens,

and thus becomes more effective at retaining convective heating against energy loss in gravity waves.

Using a suite of mesoscale satellite observations, Ritchie et al. (2003) were able to construct the entire sequence of events defining the birth and intensification of Hurricane Floyd. Two convective bursts identified in the enhanced infrared and passive microwave imagery played key roles in initiating genesis and development of Floyd's eyewall. In the manner noted by Gray (1998) Floyd's bursts were triggered by a low-level wind surge (as noted in QuickSCAT imagery) impinging on a region of high surface equivalent potential temperature. During and immediately after the burst episodes, AMSU-derived tropospheric temperature profiles revealed that Floyd's middle tropospheric warm core greatly amplified as the surface pressure fell. The Ritchie et al. study thus provides the first compelling evidence connecting the occurrence of bursts directly to the energy content of the developing storm's inner core.

The operational arm of the NOAA Hurricane Research Division (HRD) and the Science Mission Directorate of NASA have a keen interest in promoting advanced field studies of tropical cyclone genesis and intensification. As part of the joint NASA-NOAA Tropical Cloud Systems and Processes (TCSP) field experiment in July 2005, convective bursts were intensively sampled using multiple research aircraft in two Atlantic storms. In one of these systems, a predefined convective burst flight module was flown to specifically target the meso-convective structure of episodic, intense convection in a developing tropical system. In particular, the goals were to better understand the role of the burst in modifying convective downdrafts, to map the energy content of the boundary layer and ocean mixed layer fueling the burst, and to identify any mid-level mesovortex interactions and downward vortex growth occurring within the burst. Given the current research focus on hurricane intensity change, it is likely that there will be continued interest in process studies associated with convective bursts well into the foreseeable future.

While providing valuable insights into the convective-scale processes operating within convective bursts, the aforementioned papers once again address only isolated, individual storms. To date, there is no systematic survey of the mesoscale and synoptic scale causative factors for a large sample of convective bursts.

1.5 From the bottom up – The role of the ocean as a modulator of tropical cyclone intensity change in the literature

The vertical distribution and magnitude of energy release has been quantified only for two named systems. *All of the studies neglect the role of the ocean, the primary energy*

reservoir of tropical cyclones. The ocean lies at the base of the upward cascade of energy, from mixed layer heat content, through sea surface skin temperature, thence up into the troposphere through the action of boundary layer fluxes. Undilute convection mines the boundary layer, where a transfer of deep tropospheric energy warms the upper levels through latent heats of condensation and subsidence-induced warming of the eye. The hydrostatic response of the column is to lower the surface pressure. Ultimately, moist static energy is acquired by the atmosphere from the ocean, which then powers the hurricane heat engine through a series of transformations involving latent energy, increase in geopotential, and sensible heating in adiabatic processes. This hypothesis chain is illustrated in Figure 2 at the end of this chapter.

1.6 Hypothesis 2: A convective burst effectively channels the flow of moist static energy from the ocean through the troposphere through the action of boundary layer fluxes.

This paper posits that convective bursts act as an ignition source to spark the heat engine. As a second major objective, this paper addresses the flow of energy from ocean through the troposphere for a set of tropical cyclones containing convective bursts, compared to a set of null cases.

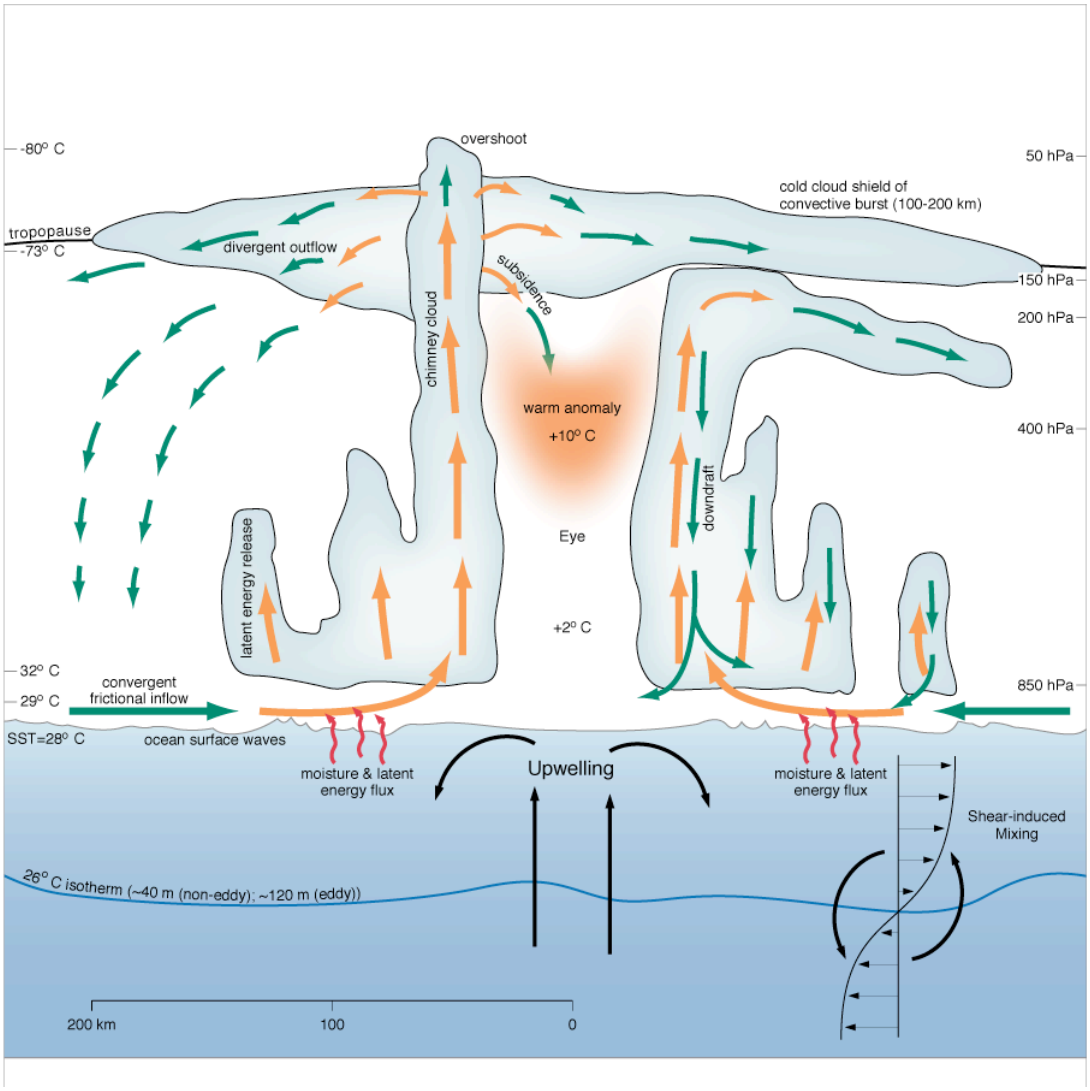

Figure 2: Overview of hypothesis chain: enhanced surface convergence and/or sea-air fluxes produce a favorable environment for convective burst occurrence. Sustained upper tropospheric energy release occurs, and subsiding air leads to an upper-level warm anomaly.

CHAPTER 2
A NATURAL HISTORY OF CONVECTIVE BURSTS

As noted in previous studies, convective bursts are most readily identified from their presentation in the visible, infrared and microwave satellite channels. The high temporal resolution and global coverage of GMS, Meteosat, GOES, and DMSP sensors makes it possible to compile incidence metrics and morphological characteristics for a large population of bursts. In this study, the criteria for identifying bursts incorporates geometrical cloud properties, cloud top temperature and unique infrared cloud-scale and passive microwave signatures.

2.1 Morphology of convective bursts

In comparison to convective cloud lines, isolated cumulonimbus clouds and transient, small convective clusters, a few salient morphological characteristics of convective bursts identify them as uniquely mesoscale (i.e. a temporal scale of hours and a spatial scale on the order of 10^2 km) circulations or entities. These properties, illustrated in Figure 3, include: (1) the size of the horizontally contiguous cold cloud shield, which can exceed 2×10^5 km^2, and more importantly the large gradient in cloud top temperatures that defines the burst's physical boundaries; (2) the tendency to develop as isolated cloud features with a propensity for suppressing deep convective growth in a large radius surrounding the active cloud shield; (3) the lifetime of the events, which can stretch to 12-18 hours and beyond; and (4) frequent observations of cyclonic curvature in the cloud fields, suggesting that bursts are dynamically active entities containing one or more vortical circulations.

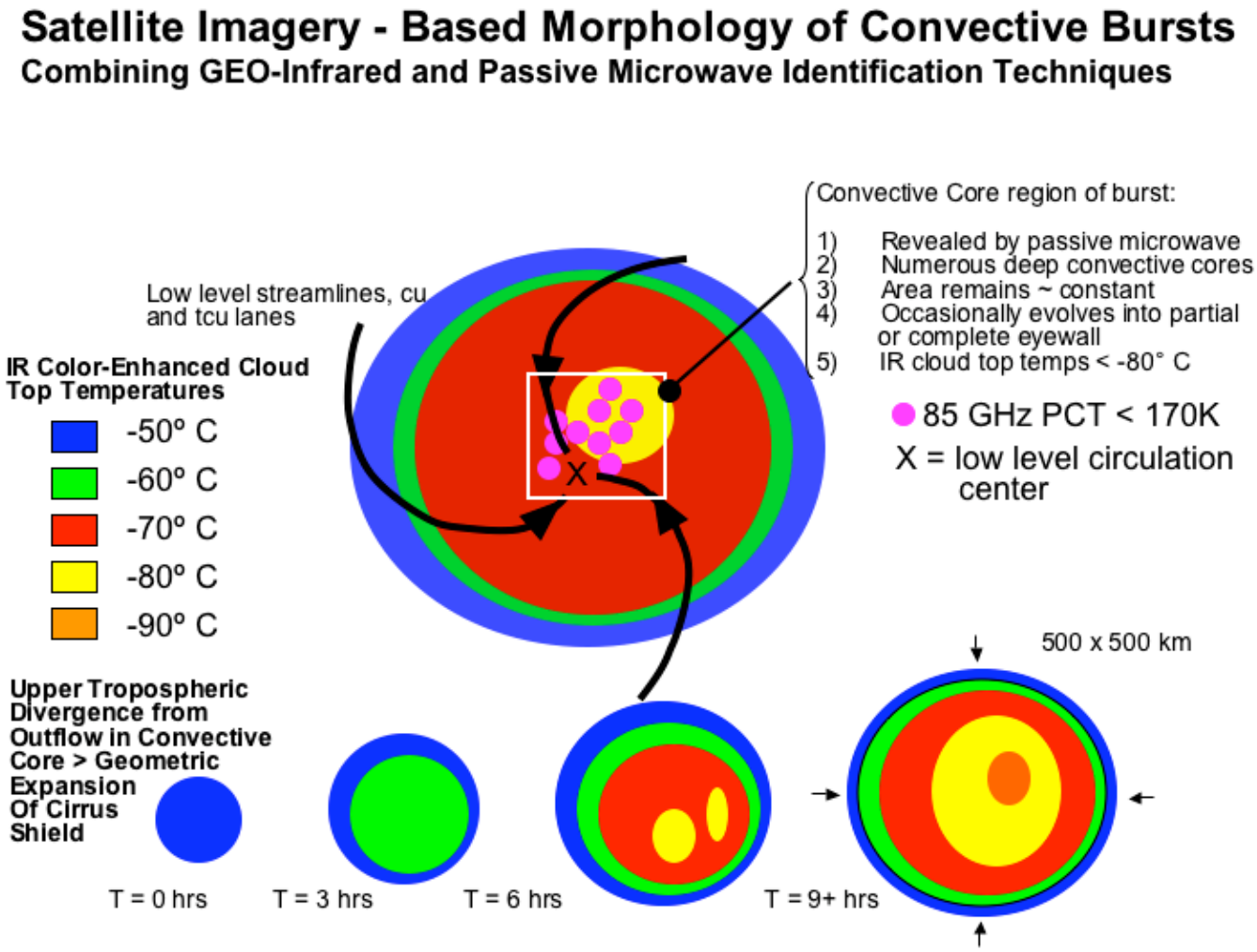

Figure 3: Morphology of a Convective Burst.

2.2 Methods of satellite identification

The following physical, mesoscale time and space criteria are used to identify candidate bursts for incorporation into a three-year, global sample of n = 350 burst events in the context of developing tropical cyclones:

Infrared Channels

1. Total cloud top area during maximum intensity of the burst exceeds 2° x 2°;
2. Circular or elliptical shape of the stratiform cloud shield is maintained throughout the burst lifecycle;
3. Minimum cloud top temperature contour of the circular burst area is less than or equal to -70° C;
4. Lifespan exceeds 3 hours

Passive Microwave Channels

1. An active region of intense, deep moist convection is contained within the stratiform infrared cloud shield, with 85 GHz (ice scattering) brightness temperatures equal to or less than 190 K;
2. Locus of active convection occurs within 100 km of a defined center of circulation

The sample years chosen span 1999-2001 and incorporate the following six ocean basins: Atlantic (ATL), East Pacific (EPAC), Central Pacific (CPAC), Western Pacific (WPAC), Indian Ocean (IO) and Southern Hemisphere Pacific (SHEM). These three years encompass a total of 240 named, tropical storms and tropical cyclones. This comprehensive satellite-based observation was greatly facilitated by systematically mining the Naval Research Laboratory's Tropical Cyclone image database, accessible through the World Wide Web. Spreadsheets were compiled on burst incidence, properties and association with Dvorak-estimated intensity change. The SPSS statistical software package was used to develop numerical relationships and compile statistics among the various census observables.

It is important to mention a few limitations associated with this methodology. Because satellite images were not strictly evaluated on a half-hourly basis for the three years of the study, it is possible that the true frequency of convective bursts is underestimated by 5-10%. The Dvorak satellite-based intensity estimation technique has associated errors, which are on the order of 5-7 kt., such that the correlation between burst incidence and storm intensity change is imperfect. And finally, tropical cyclogenesis is a multi-scale, multi-factorial process. While this study will demonstrate that a positive correlation exists between the incidence of convective bursts, and concurrent or subsequent storm

intensification, correlation herein only implies that an *association* exists between the burst *phenomenon* and the *process* of intensification, and not necessarily an unambiguous cause-effect relationship.

2.3 Scale hierarchy of structure

As Figure 4 illustrates, convective bursts are a multi-scale phenomenon. The cirro-stratiform cloud shield is a mesoscale entity that contains the envelope of cloud- and precipitation-forming upward vertical motions. Since bursts typically clear out a large annulus of troposphere outside their boundaries, it is likely that mesoscale subsidence extends the dynamical envelope of bursts even further.

Embedded within bursts is an active core of deep moist convection. In the case of the example shown for Super Typhoon Damrey (Figure 4), an archetype for many well-developed bursts, GMS infrared imagery reveals a broad, circular region encompassing -80° C cloud top temperatures, with some smaller embedded regions approaching -90° C. The TRMM microwave imager reveals a compact knot of active convection near the center of the burst, and a vortex is present - wrapping the convection into a nearly closed eyewall. The area of active convection is typically much smaller than the radial extent of the burst's cirrostratus shield, occupying perhaps only 10-20% of the total shield area during maximum expansion.

Adjacent images in Figure 4 focus on the convective scale structure of the Damrey convective burst, as shown by the TRMM Precipitation Radar (PR). Within the region of 85 GHz microwave temperatures < 200 K, the PR divulges the vertical structure of precipitation. Extremely tall convective towers are embedded in the principal spiral band wrapping around the southeastern quadrant of the eye, with surface rain rates in excess of 100 mm hr^{-1}. As is typically the case, deep moist convection repeatedly fires in multi-cellular fashion in one location of the burst, which may remain stationary relative to the quadrants of the translating low-level center of circulation. Convection in the Damrey inner-core convective band overshoots to a height of 18-19 km, which is 2-3 km above tropopause level. The extreme vigor of this cloud feature (what is sometime termed a "chimney cloud") attests to the rapid intensification of Damrey during the active phase of its convective burst. These convective-scale cloud features, although short-lived, occur throughout the multi-hour (or day!) lifecycle of a burst. The convective towers and their positive correlation with probability of intensification are individually documented in (Kelley, Stout et al. 2005). The Venn intersection of the population of hot towers and larger, mesoscale bursts has yet to be determined. There are, quite possibly, numerous cycles of convective-scale growth and decay within a burst. Each successive generation adds cloud (liquid water and ice) mass to the

upper troposphere as active updraft cores decay and merge into a rapidly expanding outflow of stratiform rain remnants. The rapid expansion of the decaying cloud tower aggregate simply follows from the principle of mass continuity. The fact that expansion can be ongoing and steady-state for more than 12 hours implies that successive initiation of convective towers *must* also be sustained for an equally long period.

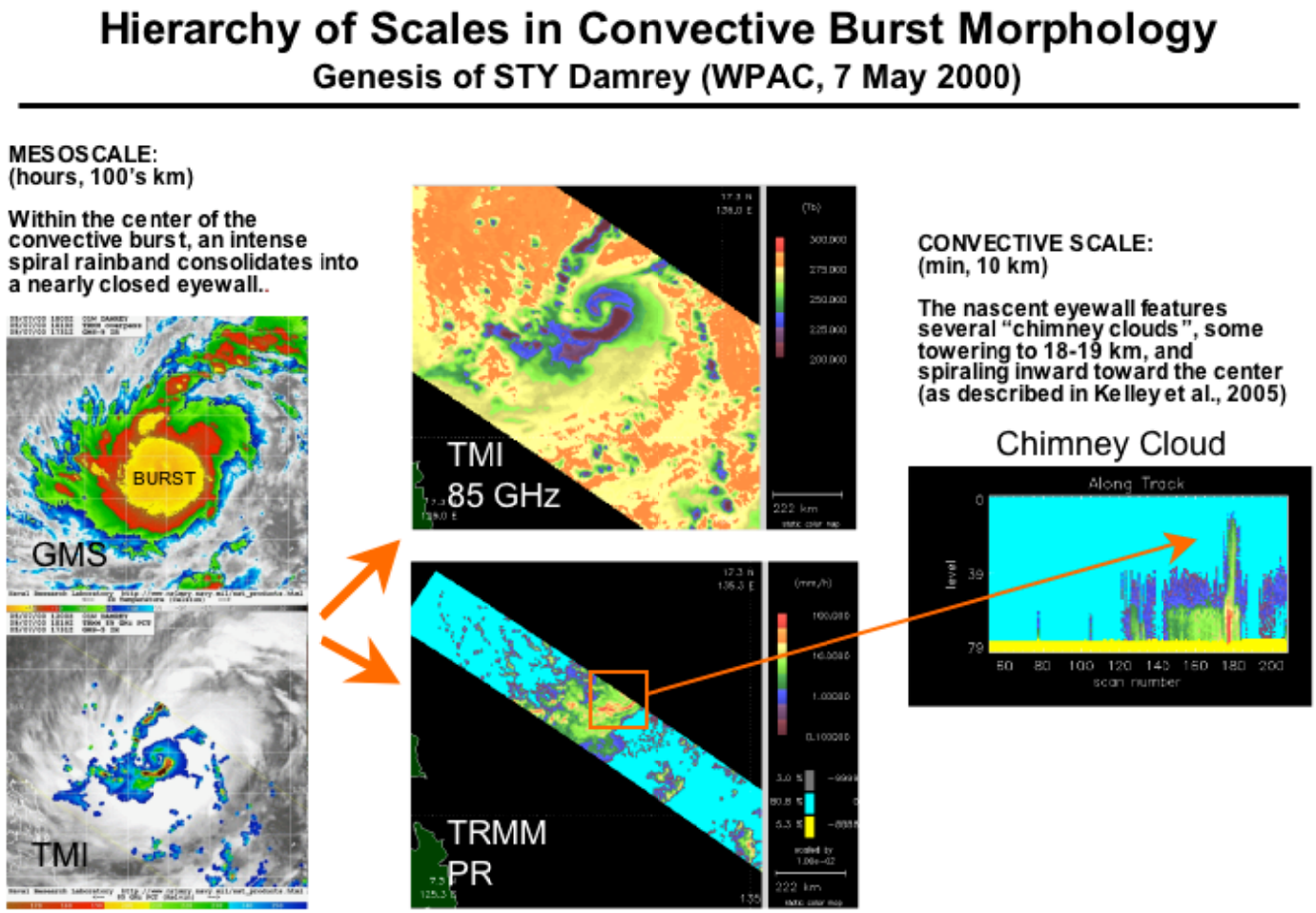

Figure 4: Archetypal convective burst in STY Damrey illustrating the hierarchy of Scale Interaction

2.4 Similarity to mesoscale convective clusters (MCCs)

As Figure 5 illustrates, convective bursts display a striking resemblance to Mesoscale Convective Complexes (MCCs). MCCs typically develop over land, in mid-latitude baroclinic zones and downwind of mountain ranges. However, they are also very common over tropical Africa and occasionally develop over the tropical oceans (Laing and Fritsch 2000). MCCs produce a large fraction of summertime, nocturnal rainfall over the U.S. Great Plains, and account for a large share of the severe weather there. They appear as very coherent structures in the infrared imagery, and frequently contain cyclonic rotation. Of the two types of MCC development scenarios, the tropical oceanic bursts are perhaps akin to the Type II category of Fritsch and Forbes (2001) which typify a moist, barotropic environment. Type II bursts initiate from the interaction of a surface cool pool generated by moist downdrafts and relatively weak shear. The interaction sustains the mesoscale uplift that evolves into the characteristic large stratiform cloud shield of the MCC.

Based on the three-year natural history of convective bursts, many meet the Maddox (1980) threshold for size, shape and persistence: a) cold cloud area < -33° C greater than 10^5 km^2; b) cold cloud area < -52° C in excess of 5 x 10^4 km^2; c) ellipticity > 0.7; and d) persistence > 6 hrs. According to Laing and Fritsch (2000), the majority of MCCs have total cloud dimensions of 2 x 10^5 km^2, which is close to the value of the median diameter of convective bursts sampled in this study. Many MCCs are also primarily nocturnal, a characteristic also identified in the three-year sample of convective bursts.

MCCs contain balanced, mid-level vortices, hypothesized to develop as a result of differential diabatic heating within the cloud mass. The diabatic phase change profile warms the middle troposphere and cools the tropopause and lower troposphere, creating a positive potential vorticity (PV) anomaly in midlevels and negative PV anomaly in upper levels (Fritsch and Forbes, 2001). The near-neutral, moist static stability environment in the extensive stratiform rain region of MCCs also lowers the Rossby radius, which favors the development of a balanced, long-lived mesoscale system (Schubert, Hack et al. 1980), (Chen and Frank 1993). Additionally, Fritsch and Forbes suggest that the combination of middle-tropospheric convergence and the stretching term of the vorticity equation enhances spin-up of planetary vorticity in the middle levels of MCCs. Thus, stability and kinematic fields act in the same sense to generate positive PV anomalies, which become manifest as warm core meso-circulations in MCCs (Figure 6). It is tempting to speculate that similar processes may be at work in the convective bursts that so frequently attend tropical cyclogenesis. The aforementioned MCC studies underscore the possible role of convective bursts as sources of precursor rotation in tropical environments.

While more definitive work is needed, it is possible that convective bursts in evolving tropical cyclones are the tropical oceanic counterparts of "classic" MCCs. It is also likely that some of the MCCs over water as classified by Laing and Fritsch are the *de facto* convective bursts of this study, in light of the fact that these maritime mesoscale convective systems frequently turn into tropical storms and hurricanes (Velasco and Fritsch 1987), (Miller and Fritsch 1991).

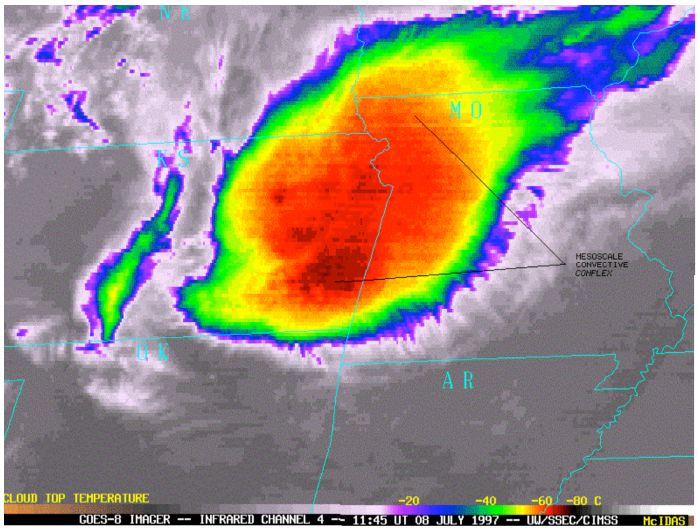

Figure 5: Midwestern midlatitude MCC bears a striking resemblance to a CB

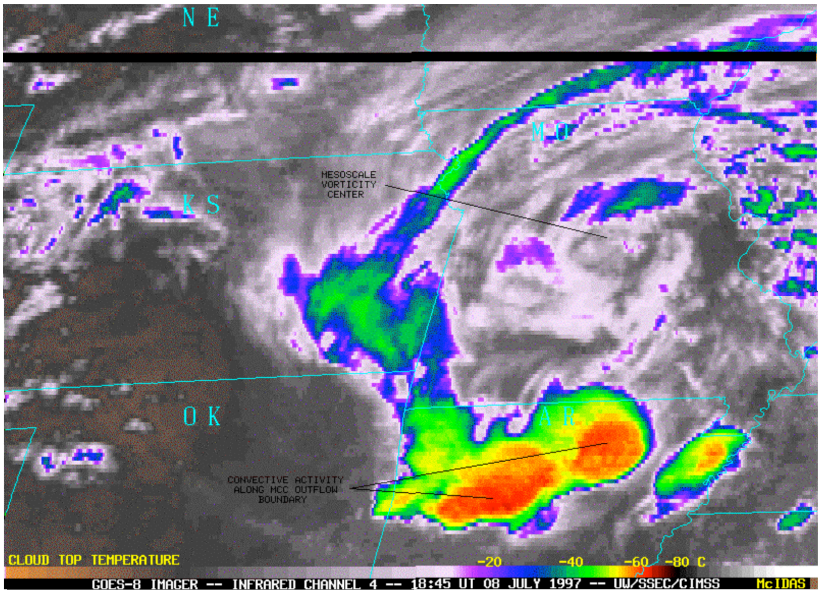

Figure 6: Example of warm-core meso-circulation in a MCC.

2.5 Dynamic evolution of convective bursts

Figure 7 and Figure 8 typify the evolution of convective bursts in developing tropical cyclones, in this case Supertyphoon Damrey. The sequence of three GMS infrared image captures the dramatic radial expansion of the principal -80° C cold cloud shield (yellow area), often termed the Central Dense Overcast (CDO), which also displays near-perfect symmetry. Such remarkable symmetry indicates a low-shear environment, which is favorable for cyclogenesis. The divergence of cold cloud area (-80° C envelope) over the 18 hour period shown in the images works out to -1.2×10^{-5} s^{-1}, corresponding to an increase in area of 110%. The cloud mass demonstrates cyclonic rotation throughout its evolution, indicative of the broader circulation of the developing tropical storm phase. On the small scales, the image sequence shows that broad environmental spin is probably consolidated by vigorous convergence and upward motion contained within the burst's convective core. This active convection is revealed in the accompanying passive microwave (SSM/I and TMI) images.

Within the space of 6-7 hours (1137 to 1819 UTC), microwave data shows that the core of hot towers spins up into an annular eyewall. The vertical stretching of storm-scale vorticity may play a role in amplifying and extending the eyewall circulation into low-levels. It is also important to note that while the area of cold convective cloud debris undergoes a nearly geometric doubling with time, the area of the convective core remains constant. This implies that within the hot tower "conduit" of a burst, the upward mass flux *must* be significant. Some combination of intense, sustained release of latent energy and compensating mass subsidence should contribute to development of the warm core needed to hydrostatically lower the surface pressure and intensify the storm. Direct evidence for this thermodynamic influence of convective bursts on storm deepening is illustrated in the case of Hurricane Floyd by Ritchie et al. (2003).

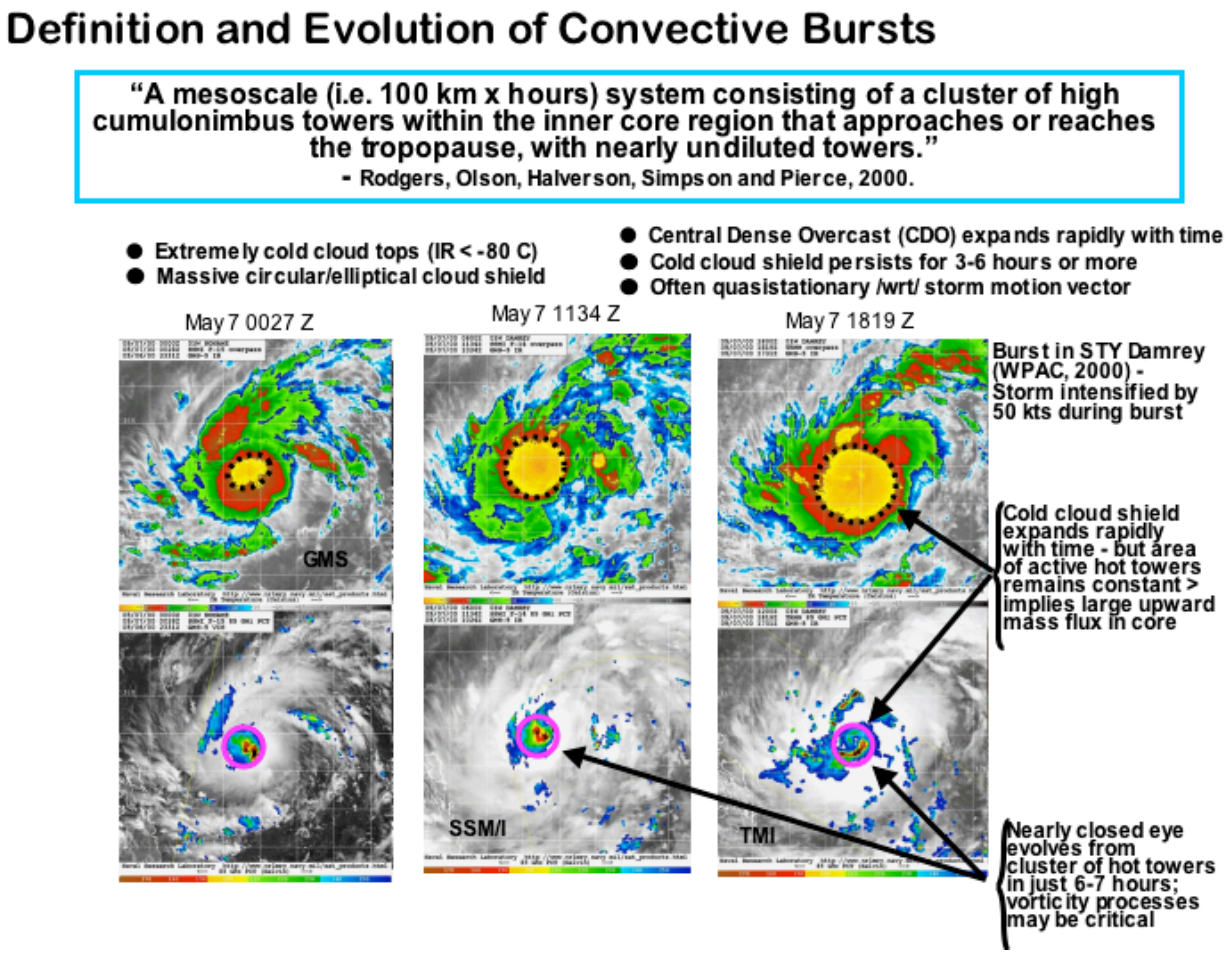

Figure 7: Evolution of convective burst in STY Damrey.

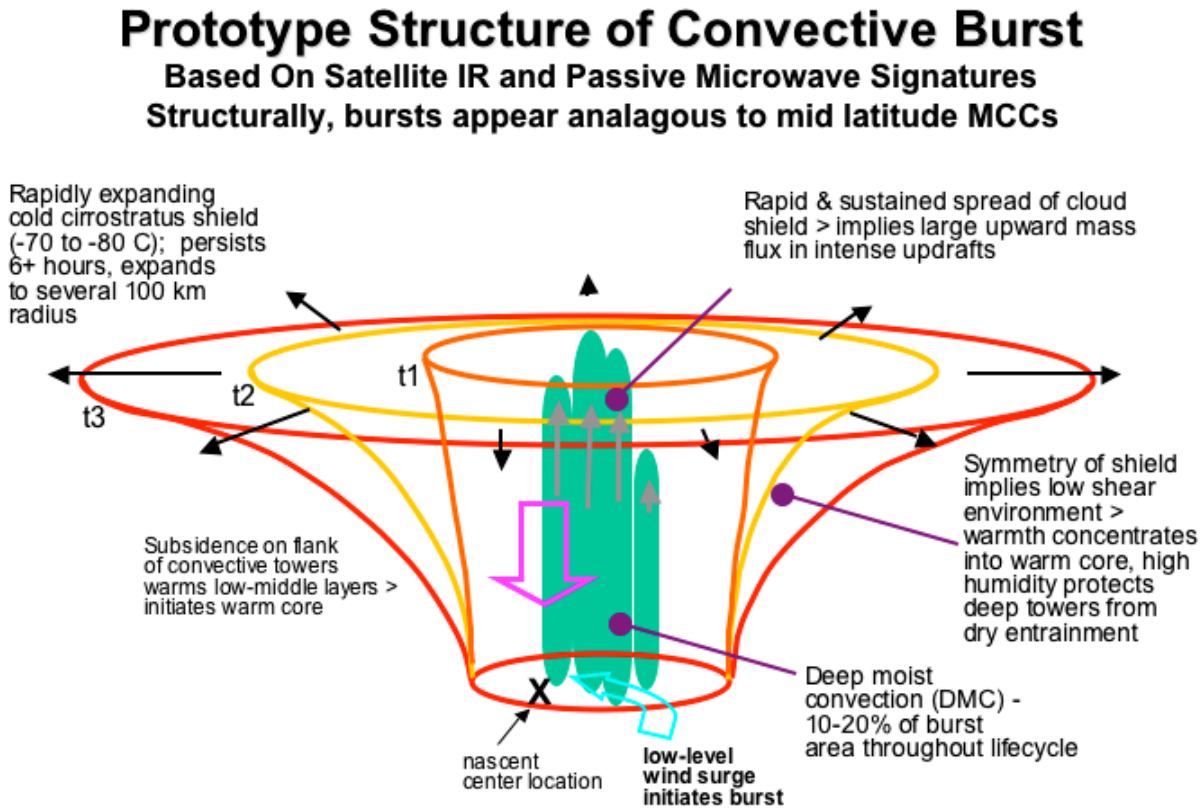

Figure 8: Prototype structure of a convective burst.

2.6 A global census of convective bursts

2.6.1 Incidence of convective bursts by ocean basin and entire globe

As seen in Table 1, convective bursts are globally ubiquitous features of tropical cyclones, and most storms contain more than one burst during their lifecycle. Figure 10 shows the global distribution of convective bursts for 1999, 2000, and 2001. On an annual basis, an average of 80% of tropical cyclones contain one or more bursts. The incidence ranges from a low of 73% of storms in the Atlantic to 100% in the Indian Ocean. Of the tropical cyclones that contain convective bursts, 79% demonstrate a positive association with increased intensity as measured by the Dvorak technique (best track statistics).

	IO	SH	WPAC	ATL	EPAC	GLOBE
# storms	10	62	75	37	42	223
# CBs	15	107	106	60	56	344
ratio	1.5	1.7	1.4	1.6	1.3	1.5
% storms with CB	100%	81%	76%	73%	90%	80%
% storms intensify	100%	79%	76%	73%	85%	79%

Table 1: Convective bursts by ocean basin

2.6.2 Average intensity change associated with bursts - by basin and entire globe

The majority of convective bursts (68% globally) are associated with positive intensity change. (See Table 2 and Figure 9.) The magnitude of the intensification averages +14 kt. Relatively few bursts (20%) exhibited zero apparent change in intensity, while only 12% had a negative association with intensification. The wind speed changes on average are relatively modest, and are comparable with the average value (+10 kts) identified by Steranka et al. (1986) in a small survey of 12 Atlantic basin tropical cyclones. Note, however, that these metrics only consider storm strengthening that occurs during the duration of the burst, which is inherently shorter than the typical timescale of

	IO	SH	WPAC	ATL	EPAC	GLOBE
mean intensity Δ	+29%	+15%	+14%	+11%	+11%	+14%
% (+) intensity Δ	80%	64%	71%	63%	78%	68%
% no change	13%	25%	21%	29%	11%	20%
% (-) intensity Δ	7%	11%	8%	17%	11%	12%

Table 2: Intensity change during convective burst events.

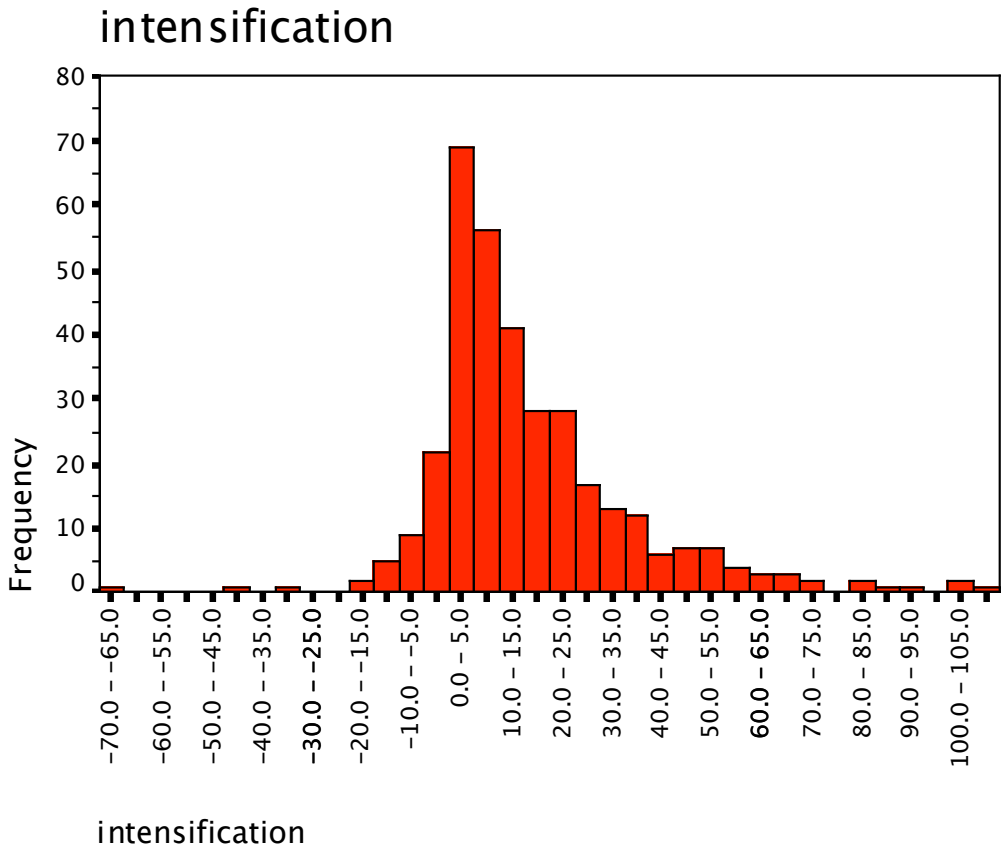

Figure 9: For n = 344 burst events (1999-2001), frequency distribution of intensity change (wind speed change in kt.) associated with convective bursts.

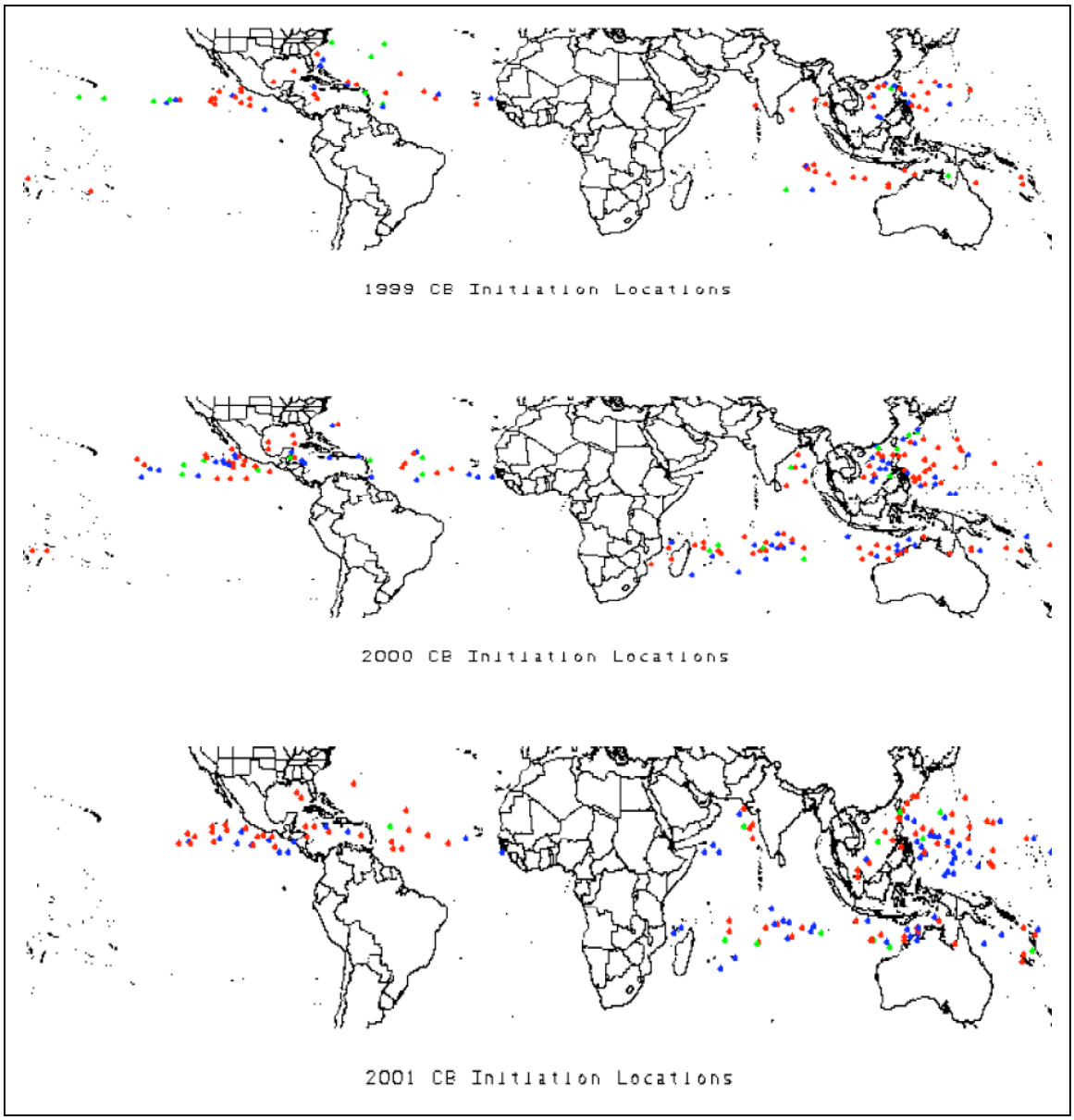

Figure 10: CB initiation locations for 1999 (top), 2000 (middle), 2001 (bottom). Increasing wind speeds during CB are red. Bursts with decreasing intensity are indicated in blue. Neutral cases are green.

intensification. These metrics also do not account for the likely importance of time lag between burst initiation and peak maximum sustained wind (MSW). The lag time between a convective burst event and storm intensification, which Steranka et al. (1986) found to be about 24 hours, is further considered in Chapter 8. Additionally, increases in MSW for individual cases can be quite large, up to +100 kts. Finally, note here that *association* between the occurrence of bursts and subsequent storm strengthening does not necessarily imply that bursts *cause* the intensification, as intensity change is an inherently multi-factorial process that is influenced by multiple scales of interaction.

2.6.3 Metrics that imply the forcing mechanisms for convective bursts

2.6.3.1 Monthly trends in convective burst initiation

Aside from the Pacific southern hemisphere storms, which show peak incidence of bursts during the summer (February), the incidence of bursts climbs steadily throughout the summer months in all other ocean basins, with a peak frequency in late August-early September. (See Figure 11.) It is well known that tropical cyclone incidence closely parallels secular trends in ocean surface temperature and ocean heat content, which culminate in mid-September for the northern hemisphere ocean basins. However, since convective bursts are driven by buoyancy contained in intense updrafts, it is also possible that the likelihood of burst initiation increases as the energy content of the lower thermal boundary rises. That is, increases in equivalent potential temperature or moist static energy are expected to accompany the rise in sea surface temperature (SST). This would increase the reservoir of convective available potential energy (CAPE) tapped by hot tower updrafts - enhancing both the magnitude and depth of their tropospheric penetration. The increased upward mass flux in hot towers likely explains many of the observed properties of the convective burst, including the large mass divergence in the cloud shield outflow and exceptionally cold (deep) cloud tops discussed in Section 2.1.

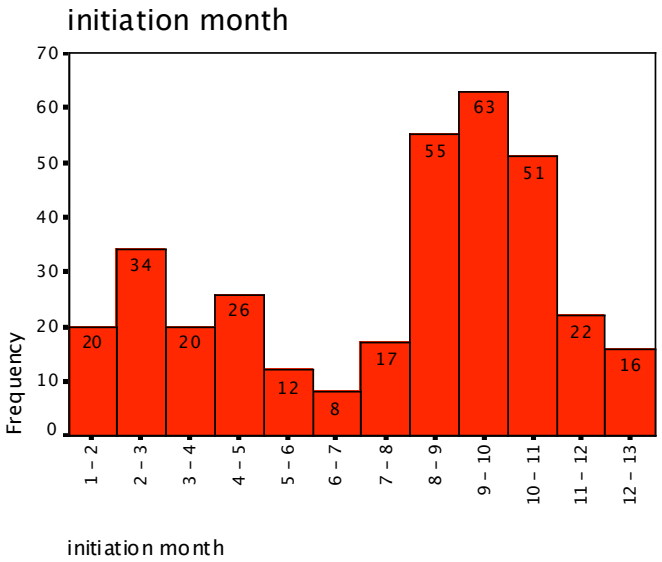

Figure 11: For n = 344 burst events (1999-2001), frequency distribution of convective burst incidence associated with month of year (1 = January).

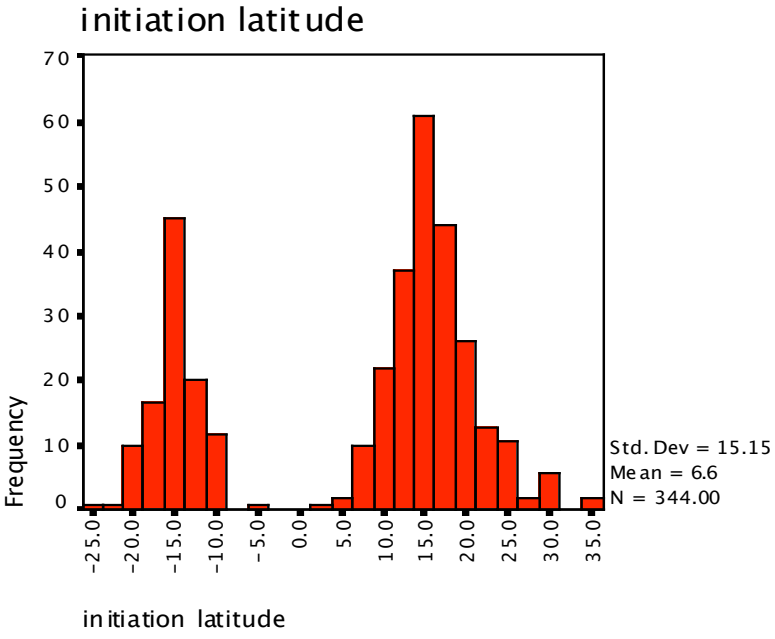

Figure 12: For n = 344 burst events (1999-2001), frequency distribution of convective burst latitude of initiation (negative values connote southern hemisphere).

2.6.3.2 Latitude of convective burst initiation

As seen in Figure 12, the most frequent latitude of burst initiation is 15° N and S. More events are endemic to the northern hemisphere. The latitudinal distribution simply reflects the climatologically preferred regions of tropical cyclone genesis in all ocean basins, underscoring the overlap of sufficiently warm ocean surface temperatures with the non-zero component of planetary vorticity necessary to initiate storm spin-up. As will be noted in Section 2.6.3.5, convective bursts may provide an important mesoscale linkage between environmental or background vorticity contained on the synoptic scale, and the process of consolidating this rotation down to the scale of the storm vortex.

2.6.3.3 Local time of day

In terms of the 24 hour (diurnal) cycle of solar heating and longwave cooling over oceans, convective burst initiation time displays a curious bimodal frequency, with both an early morning (6 AM - 7 AM local) and late afternoon (4 PM - 5 PM) maximum. This is the case for all six ocean basins examined. The early morning maximum is consistent with the results of studies that show a nocturnal maximum in the areal extent and intensity of mesoscale convective system (MCS) rain over the tropical oceans (Nesbitt and Zipser 2003). The late afternoon maximum is more characteristic of continental land regions. To explain the nocturnal maximum, it is possible that the extensive and cold cirrostratus shield present during the burst mature stage promotes enhanced longwave cooling of the upper troposphere. This would destabilize the mesoscale region of atmosphere contained within the envelope of the burst, promoting continued growth of vigorous convection and/or sustaining mesoscale updrafts and downdrafts within the stratiform region of the burst. The generation of a cool temperature anomaly near the tropopause can also enhance generation of PV in mid-levels and thus provide an embryonic source of tropical cyclone spin (Fritsch and Forbes 2001).

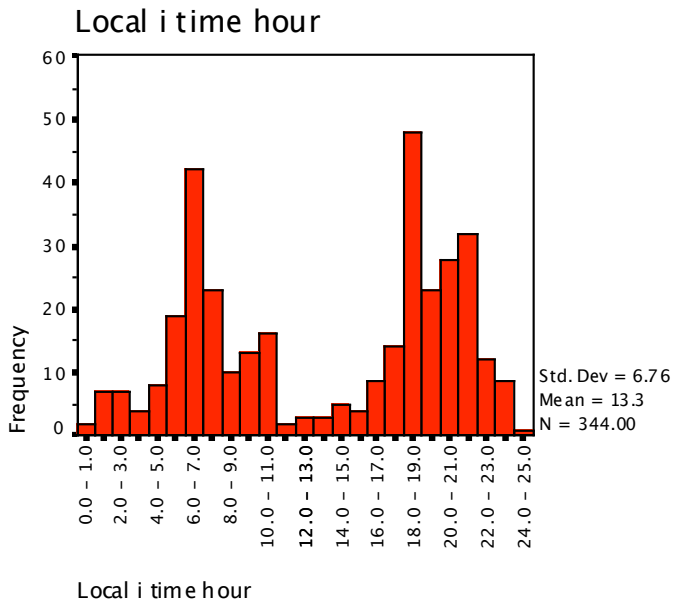

Figure 13: For n = 344 burst events (1999-2001), frequency distribution of convective burst initiation as a function of local time of day.

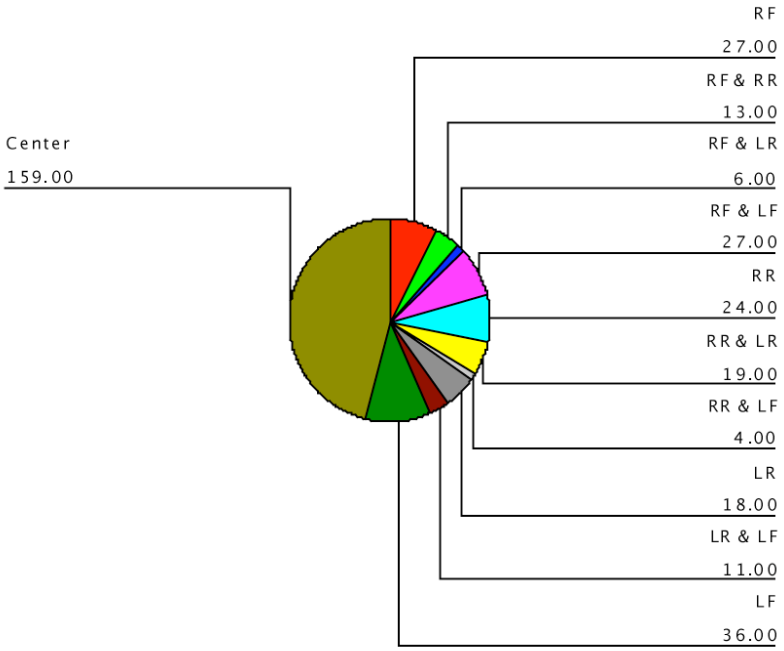

Figure 14: For n = 344 burst events (1999-2001), distribution of convective burst initiation within quadrants around vortex center. RF = Right Front, LF = Left Front, LR = Left Rear, RR = Right Rear. All quadrants are relative to the local motion vector of the storm center, as determined through best track data.

The late afternoon/early evening maxima in burst incidence may be coupled with the maximum in solar heating during this time of day. While such heating typically does not enhance lower tropospheric temperatures over tropical oceans by more than 2-3° C, a secondary afternoon maximum in oceanic tropical rainfall is noted in other studies (Gray and Jacobson 1977). Solar destabilization is the most likely mechanism accounting for heightened convective burst activity in the afternoon hours. Any process or set of processes that leads to long duration of the secondary circulation (in-up-down) within a convective burst, or serial occurrence of bursts (such as the posited radiative and solar destabilization processes) may be crucial for cyclogenesis.

2.6.3.4 Location of convective burst initiation relative to tropical cyclone center of circulation

Most convective bursts (46%) initiate very close to the tropical cyclone center of circulation (typically within 1°). Otherwise, Figure 14 indicates the distribution around the center, in the four orthogonal sectors oriented relative to the direction of storm translation. The Left Front (LF; 10%) and Right Front (RF; 8%) quadrants account for the second largest spatial distribution of bursts. This is because the storm's motion generates a relative wind that enhances low-level convergence of high θ_e air into the forward quadrants. In northern hemisphere storms, bursts initiate in the RF quadrant and are advected into the LF quadrant by the swirling wind, maturing as they do so. In the southern hemisphere, initiation occurs in the LF quadrant, with growth and advection into the RF quadrant. The metrics computed for each of the basins (not shown) support this model. Many of the bursts that apparently initiate close to the center may still have begun in one of these forward quadrants; however, precise diagnosis was hampered by the limited resolution of satellite images, and subjective determination of the burst centroid. Storms in which the burst is located close to the circulation center are probably more likely to intensify. This is because the upscale coupling of energy within the larger circulation should be most efficient when subsidence-induced warming is located adjacent to (or even within) the region of incipient eye formation and also contained within the vortical Rossby radius of deformation.

2.6.3.5 Burst incidence relative to the composite storm lifecycle

Figure 15 illustrates a simplified, composite lifecycle of a tropical cyclone, with a sequence of four stages defined as Pre-Intensification > Intensification > Maximum Intensity > Dissipation. The majority of convective bursts in the global population occur during the intensification phase of the storm. This not only suggests that bursts are integral to storm

deepening, but may underscore the role of thermodynamic instability in modulating their occurrence. Work by Cione et al. (2000) shows that CAPE is unevenly distributed within tropical cyclones. Dropsonde observations reveal that there is more CAPE in the outer circulation than within the eyewall and core region. This is because the deep tropospheric warm anomaly thermally stabilizes the inner core region, where convective ascent is close to moist neutral. Before the warm core is definitively established, i.e. during the pre-genesis and intensification phases of TC evolution, CAPE should be most abundant. During maturity, CAPE is small within the core. The type of deep, extensive and sustained convective overturning characteristic of bursts is therefore most likely to occur during the pre-maturity phases of TC growth. Once CAPE is depleted, one would expect the incidence of inner-core bursts to diminish.

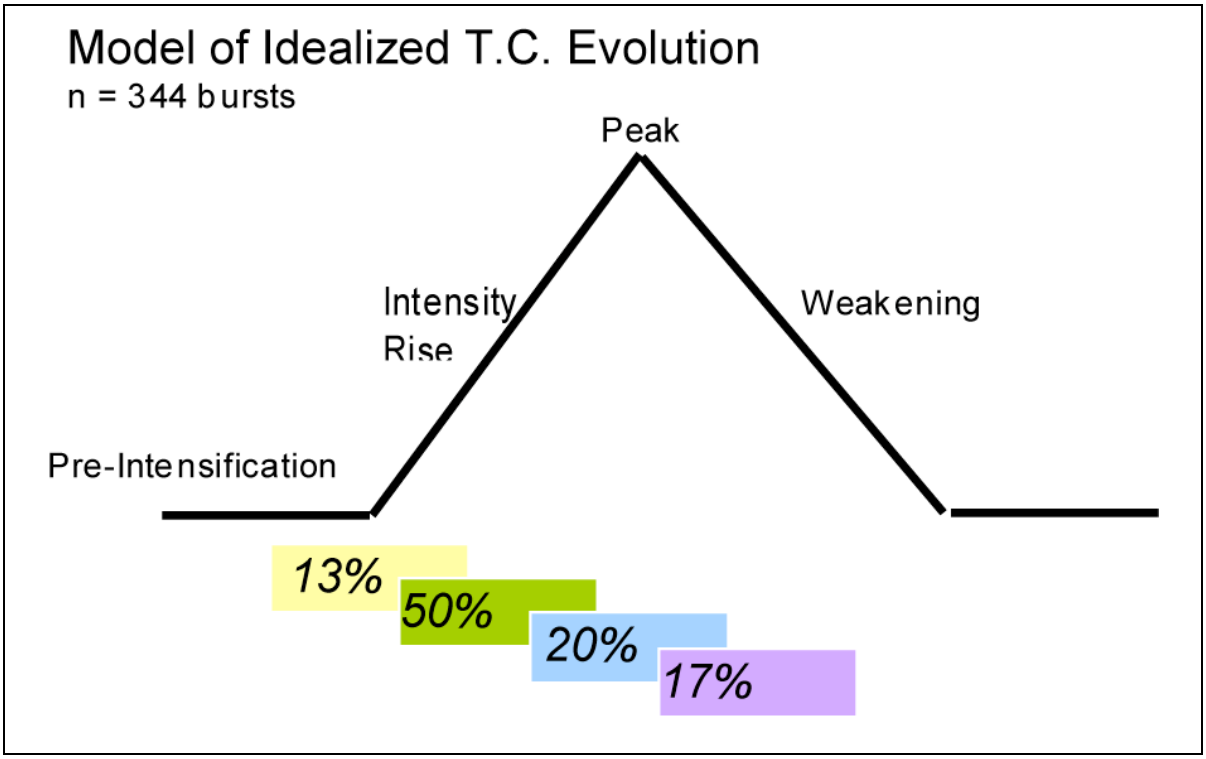

Figure 15: Percentage of convective bursts throughout the TC lifecycle.

2.6.4 Possible connections to storm dynamics

2.6.4.1 Eyewall formation during convective burst events

About 30-40% of convective burst events were associated with partial or complete formation of an inner core eyewall; in the majority of cases the eyewall closed off by the time the burst dissipated. The percentage of bursts during the time of eyewall formation can be broken down according to basin as follows:

Basin	% of CBs
ATL	31.5
CPAC	29.5
EPAC	18.5
IO	40.0
SHEM	28.0
WPAC	43.5

Table 3: Percentage of convective bursts in tropical cyclones undergoing eyewall formation.

As illustrated for the case of STY Damrey (Section 2.5), convective hot towers contained within the burst cloud mass frequently begin to consolidate and form partial eyewall arcs or segments. While an exploration of mechanisms promoting eyewall spinup are beyond the scope of this paper, it seems likely that the process generally involves the co-location of regions of intense upward motion with one or more mesoscale centers of vorticity; such an arrangement may lead to vertical stretching and amplification of spin.

2.6.4.2 Duration of convective bursts

Figure 16 illustrates the frequency distribution of convective burst duration for the global sample of burst events. On average, bursts are long-lived in terms of a convective phenomenon (as measured from initiation time to dissipation time), with a mean lifespan of 28 hours. The average lifespan was generally 24-28 hours for all basins except the Indian Ocean, where the mean was 42 hours. (Initiation time was recorded as the first appearance

of the convective burst in the satellite imagery. Dissipation time is in actuality the time stamp of the last image in which the burst appears. The actual "dissipation time" is sometime between this time recorded and the time stamp of the next image in the database in which no convective burst appears.)

The relatively long duration of burst events underscores the persistence of their mesoscale circulations, and this persistence may be important for promoting intensification through the development of secondary circulations within the inner core. The Pearson correlation coefficient between burst duration and value of intensity change is r = 0.508 for the global population of convective bursts. The correlation coefficients for individual basins are found in Table 4.

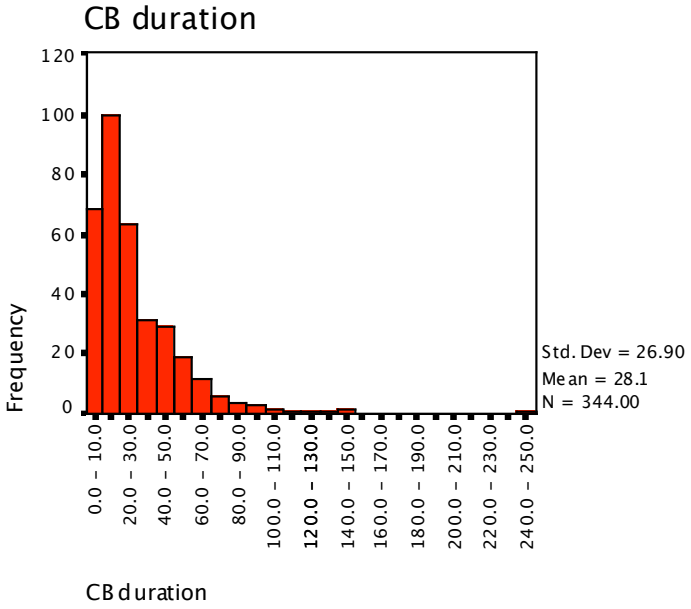

Figure 16: For N = 344 convective burst events, the frequency distribution of convective burst duration.

Basin	Pearson's r
ATL	0.29
EPAC	0.27
IO	0.52
SHEM	0.68
WPAC	0.39

Table 4: Basin-by-basin correlation coefficient between CB duration and storm intensity change (wind speed) during the burst event.

Thus the positive association is stronger for some basins than others, but suggests that the longer a burst is active, the greater the magnitude of ensuing intensification (as assessed during the lifespan of the burst). The global mean "lag time" between convective burst initiation and the storm peak MSW is 47 hours, with basin-specific values ranging from 22 to 58 hours. The likely mechanism for these lags relates to the timescale required for subsidence of air from high levels, generated by detrainment of convective outflow from the tops of hot tower turrets. For mean values of subsidence on the order of 10 cm/s, and descending from a height of 16 km, the time required for air to settle 10 km and warm the column adiabatically is on the order of 27-28 hours. The height of 16 km represents the climatological location of the deep tropical tropopause, and a column 10 km deep below this height represents the typical depth over which the warm anomaly in the hurricane eye becomes established. Thus, it seems plausible that a day or more may be required for the central pressure reduction to fully develop hydrostatically in response to subsidence-induced warming. However, in many cases intensification proceeds much more rapidly. The duration of a storm's total intensification need not track one-for-one with the duration of its convective burst, since many factors other than bursts influence intensification. For instance, there are small-scale effects that influence the efficiency of subsidence-induced warming (i.e. subsidence may be irregular and initiate from varying heights, the air may not descend the full 10 km, and adiabatic warming may be countered by lateral detrainment and mixing from the eyewall), and typically more than one burst occurs as part of a sequence of events during the storm deepening process.

2.6.4.3 Storm category versus magnitude of intensity change

One of the most intriguing results (Figure 17) is that of storm intensity category, in terms of the average amount of intensification (Δ MSW) that occurs during bursts. For instance, bursts occurring during the intensification of a Category 5 storm engender on average a 44 kt MSW change, while bursts occurring in a Category 2 only produce only a 12 kt change in MSW. These observations are in line with the work by Rodgers et al. (1998) (2001), who determined that as a storm became more inertially stable, the lag time between onset of the convective burst and subsequent peak in MSW lessened. Similarly here, as a storm becomes more inertially stable, the coupling between the energy released in the burst and its upscale assimilation into the storm's rotational kinetic energy becomes more efficient. In essence, more of the burst energy is captured, rather than dissipated in the form of gravity waves that advect energy away from the core (Ritchie, 2003).

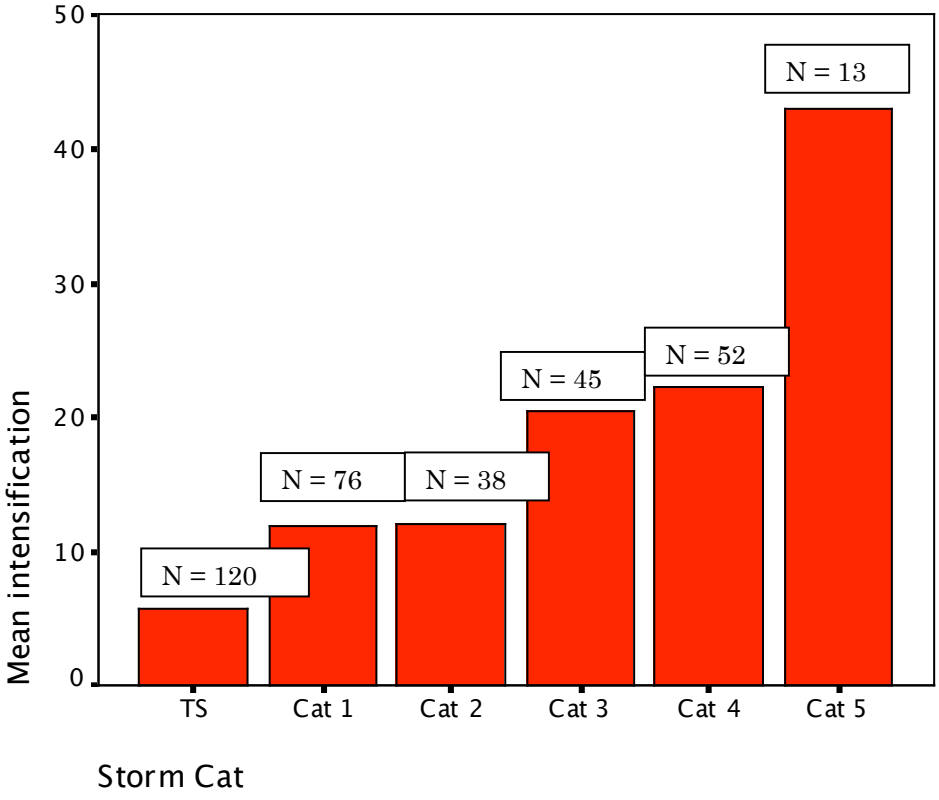

Figure 17 : For N = 344 convective burst events, the mean wind speed intensification (in kt.) based on category of storm on the Safir-Simpson Scale.

2.7 Summary

This chapter examined the natural history of convective bursts by examining descriptive statistics from the global census for the years 1999 – 2001. Convective bursts are present in the intensifying stage of 80% of tropical cyclones around the world and are typically associated with a moderate increase in intensity. The incidence of convective bursts peaks as summer progresses and as the moist static energy content of the ocean planetary boundary layer rises with increasing reservoirs of ocean heat content. The convective burst in most storms initiate within 1° of the tropical cyclone center. A convective burst in this region, within the vortical Rossby radius of deformation, should efficiently sustain upper-level latent heat release and subsidence-induced warming of the eye.

The next chapter, Chapter 3, presents a statistical examination of the atmospheric and oceanographic forcing mechanisms of convective burst initiation in an attempt to identify the characteristics typical of convective burst time periods. The following chapters in this dissertation explore the energetics of the processes by which a convective burst might influence tropical cyclone intensity from the ocean upward through the development and sustenance of the tropical cyclone warm core (as illustrated in Figure 2.)

CHAPTER 3
KINEMATIC, THERMODYNAMIC, AND OCEANOGRAPHIC INTERPLAY

3.1 Examining the forcing mechanisms of convective burst initiation

The objective of this section of the study is to examine the known forcing mechanisms of tropical deep convection in an attempt to assess the contribution of these factors to convective burst initiation and persistence. This objective is addressed through the development of an ensemble of statistical classification procedures, discriminant analyses, designed to test the relationships among atmospheric and oceanic variables suggested by the relevant literature and the previous census of convective burst initiation. In this study the discriminant analyses are being used as exploratory data analysis tools rather than inferential predictive models. The purpose is to highlight the empirically useful variables and to find a combination of variables that maximally discriminates between times of convective burst occurrence and non-burst events.

Since a main objective of this study is to assess the *relative* importance of the ocean versus the atmosphere, the oceanic variables are initially segregated from the atmospheric variables. The first discriminant analysis procedure in the ensemble examines the ability of the atmospheric variables to predict convective burst events. A second discriminant analysis uses exclusively the oceanic variables. Finally, the significant variables from both the atmosphere and the ocean are combined in an attempt to assess their cooperative classification abilities.

The basis of the study is the global set of named tropical storms and cyclones as recorded in the Best-Track files by the National Hurricane Center (ATL and EPAC) and the Navy Joint Typhoon Warning Center (IO, CPAC, WPAC, and SH) for the years 1999 – 2001 (Jarvinen, Neumann et al. 1984). The sample consists of observations calculated at the beginning of each six-hour interval of time at the Best-Track positions of each tropical storm and tropical cyclone (n = 3,702 observed times). The dependent variable is binary: convective burst existence/no convective burst existence during the six hour time period as recorded in

the convective burst survey from Chapter 2. Of these 3,702 observation times, 69% (2,556) are periods with no convective burst present. The other 31% (1,146) are convective burst times. The independent variables tested for their importance in convective burst initiation are included in Table 5 and Table 6 and will be discussed in further detail in the appropriate sections of this chapter. The statistical tests in the following sections are performed using SPSS 11 for Mac OS X.

3.2 Discriminant analysis

Discriminant analysis can be thought of as a special form of multiple regression that uses a matrix of the pooled variances and covariances of the variables instead of a correlation matrix. The point is to classify an unknown case, W, into one of k groups, W_1, W_2, … ,W_k on the basis of some variables X_1, X_2, …, X_p. Just like regression analysis, the procedure results in a set of coefficients α_1 … α_p which yields a set of "discriminant functions":

$$d = \alpha_1 X_1 + \alpha_2 X_2 + \cdots + \alpha_p X_p ,$$

that maximize the separation between groups. In this study the dependent variable is a dichotomy, convective burst/no convective burst, so the number of groups is 2 (k=2). The number of variables in the model, p, varies as focus shifts from the atmosphere to the ocean. In each analysis, a single discriminant function is produced to separate the two groups. The results of the discriminant analysis procedure are judged for significance using three statistical tests. The first tests for the number of significant discriminant functions by ranking Wilk's Lambda.

Since this study uses only two groups, the result is always a single discriminant function. The second test is a test for the significance of the discriminant coefficients. The results are achieved by standardizing the coefficients to assess their contribution to the function's value. A "ranking" of the discriminant function coefficients shows the relative importance of the variables. The final test examines the degree to which the discriminant function correlates with the groups using the Canonical Correlation. The square of the Canonical Correlation indicates the percentage of variation in the dependent variable that is "discriminated" by the independent variables in the analysis. In all procedures in this study, this "predictive" ability was low (< 20%), probably indicating that the relationships between the included variables and convective burst occurrence are really more of a non-linear

Description	Significance	Method of Computation	Units
1-min sustained 10-meter wind speed	storm intensity	Best-track file	$m\ s^{-1}$
storm translation speed	determines interaction timescale between ocean and atmosphere	Best-track file	$m\ s^{-1}$
coriolis parameter	inertial stability	Calculated from Best-track file: $f_0=2\Omega\sin(\phi)$	s^{-1}
850 mb wind divergence	Low-level wind flow	Storm-centered areal average	s^{-1}
150 mb wind divergence	Upper-level outflow	Storm-centered areal average	s^{-1}
150 mb Geopotential Height	Height of convective influence	Storm-centered areal average	m
850 mb Moisture divergence	Low-level moisture inflow	Storm-centered areal average	s^{-1}
Columnar Precipitable Water	Available moisture	Column average	$kg\ m^{-2}$
1000 – 850 mb layer average of θ_e	Low-level moist static energy	Storm-centered areal average	K
700 – 300 mb layer average of θ_e	Mid-level moist static energy	Storm-centered areal average	K
200 – 850 mb wind difference	Wind shear inhibits convective growth	Storm-centered areal average	$m\ s^{-1}$
925 mb wind divergence	Low-level inflow	Storm-centered areal average	s^{-1}
700 mb wind divergence	Mid-level inflow	Storm-centered areal average	s^{-1}
925 – 850 mb moisture divergence (difference)	Low-level inflow	Storm-centered areal average	s^{-1}
700 – 500 mb moisture divergence (difference)	Mid-level inflow	Storm-centered areal average	s^{-1}
500 – 850 mb θ_e (difference)	Mid-troposphere moist static energy gradient	Storm-centered areal average	K
500 – 925 mb θ_e (difference)	Mid-low level moist static energy gradient	Storm-centered areal average	K
700 – 925 mb θ_e (difference)	Low level moist static energy gradient	Storm-centered areal average	K
925 mb θ_e	Low level moist static energy	Storm-centered areal average	K

Table 5: Atmospheric predictor variables for the discriminant analysis procedure

Description	Significance	Method of Computation	Units
SSTcore	Minimum SST value within 60 km of storm core	Azimuthal radial average	°C
SSTahead	Mean SST from front two quadrants 222-444 km ahead of storm	Azimuthal annuli average	°C
SSTwake	Mean SST from rear two quadrants within 222 km of storm center	Azimuthal annuli average	°C
SSTclim	Mean SST from pixels <= 500 km from storm center	Azimuthal radial average	°C
Core–Front	SSTcore – SSTahead gradient	Difference	°C
Wake-Front	SSTwake – SSTahead gradient	Difference	°C
Hurricane Heat Content	Upper ocean energy available for TC	Azimuthal radial average	$(x10^8)$ J m^{-2}

Table 6: Oceanic variables for the discriminant analysis procedure.

process than the discriminant analysis can handle. The results are still enlightening as they do highlight the variables with the most linear (and understandable!) relationships to the convective burst events. The results of both relevant tests of significance are reported in the appropriate sections of this chapter.

Since discriminant analysis is based on the inverse of the within-groups variance-covariance matrix, the technique is sensitive to variables with large variances. If the two groups to discern are functionally very close together it will be difficult to distinguish between them, especially if the variable's within-groups variances are large. If the means of the variables for each group are quite different, and the variances are small, group classification will be easier. This was not often the case in this analysis.

Discriminant analysis is based on the General Linear Model (as is linear regression) and many of the same assumptions regarding the variables hold true. The model requires linearly independent homoscedastic relationships, multivariate normality of predictor variables, and a well-specified model. That being said some deviation of these assumptions is allowed as discriminant analysis is a very robust technique (Klecka 1980). In the following brief sections the conformance of this study to these assumptions is addressed. After that, each of the three discriminant analysis models used in the ensemble is presented, including specific analysis of the variables included in that model.

3.2.1 Independence of cases

Cases are said to be independent if the occurrence or nonoccurrence of one does not affect the probability of another. However atmospheric and oceanic variables are apt to exhibit positive serial dependence (persistence) with their own past or future values. Each "snapshot", consisting of multiple variables describing the state of the atmosphere or ocean at a given moment in time, may also show persistence throughout a given event as well. In the case of this study, does the presence of a convective burst in one 6-hour time period affect the probability that a burst will be present in the following six hours? Maybe. If the wind speed and the ocean temperature are high in one six hour time period of a tropical cyclone, will observations in the next six hours be as high or even higher? Perhaps.

The phenomena being examined in this study are not climatological – they are actually highly variable and rare weather events. Persistence should be extremely short-lived. However, to guard against any violation of this assumption, the discriminant analyses were performed using a "leave-one-out" classification scheme. Commonly known as "cross-validation" or the "jackknife" procedure, the discriminant function is derived for all of the cases (6-hr time periods) except one. The "left-out" case is then classified as an independent trial against the discriminant function. The procedure iterates in this fashion through all of the cases in the dataset. The final result is a complete set of independent results.

3.2.2. Multivariate normality of predictor variables

Meeting the multivariate normal assumption of discriminant analysis is required only when tests of significance are to be performed (i. e. when the minimization of committing a Type I error is necessary in hypothesis testing (Clark and Hosking 1986).) In this study, discriminant analysis is not being used primarily as a forecasting tool so hypothesis testing is unnecessary. However, the One-sample Kolmogorov-Smirnov test results that indicate the deviation of a sample variable's distribution from a specified distribution (in this case, the normal distribution) were not statistically significant in the case of any variable.

3.2.3 Equal within-group variance/covariance matrices across groups

The requirement of homoscedasticity is of prime importance to the quality of the discriminant function produced by the discriminant analysis procedure. SPSS performs two separate tests: 1) it computes and compares the natural logarithms of the determinants of the group covariance matrices and 2) it tests the null hypothesis of equal population covariance matrices using Box's M statistic. In all of the following procedures there were

slight differences between the variance/covariance matrices between groups. The log determinants are of the same magnitude indicating the differences are not very sizeable however. In each case Box's M statistic was found to be significant. Box's M statistic is very sensitive to non-normality and with large sample sizes, as is the case here with n=3,702, small deviations from homogeneity will look significant.

3.2.4 Group membership is mutually exclusive, collectively exhaustive, and truly categorical

In this study, a new variable (CB) was created for every case (6-hr time period). The variable is binary – it was assigned a value of "1" for time periods that include a convective burst episode and a null value of "0" for time periods with no burst. Every case was assigned one and only one value. No cases were excluded. The model is well-defined.

3.2.5 Summary of the statistical procedure

The objectives of the discriminant analysis procedures in the following sections of this chapter are to explore the influences of important atmospheric and oceanic variables on convective burst occurrence. The first discriminant analysis procedure investigates solely the atmospheric forcings. The next analysis focuses on the ocean's value as a predictor of convective tendencies. And finally a joint analysis of the atmosphere and the ocean is performed. The assumptions of the statistical methodology have been addressed. Details on the variables used in each procedure are contained in the appropriate sections below.

3.3 Can atmospheric factors affecting deep convection predict convective burst incidence?

The previously referenced studies by Rodgers et al. of Hurricane Opal (Rodgers, Olson et al. 1998) and Supertyphoon Paka (Rodgers, Olson et al. 2000) suggest the following environmental conditions are necessary (or at least sufficient) for initiating and maintaining inner-core convective bursts:

- warm SSTs (>26° C)
- cold tropopause temperatures
- a moist troposphere
- low vertical wind shear
- strong horizontal moisture flux.

To attempt to capture these characteristics the following atmospheric variables have been chosen for this study:

Kinematic Variables

- 925 mb, 850 mb, 700 mb, and 150 mb wind divergence
- 150 mb geopotential height
- 850 mb moisture divergence
- 925 mb – 850 mb difference in moisture divergence
- 700 mb – 500 mb difference in moisture divergence
- Difference in wind speed at 200 mb – 850 mb (as a proxy for wind shear)
- Best-track wind speed
- Storm translation speed

Thermodynamic Variables

- Precipitable water
- 1000 mb – 850 mb difference in θ_e
- 700 mb – 300 mb difference in θ_e
- 500 mb – 850 mb difference in θ_e
- 500 mb – 925 mb difference in θ_e
- 700 mb – 925 mb difference in θ_e
- 925 mb difference in θ_e.

These atmospheric variables were computed from the NCEP/NCAR reanalysis data (Kalnay 1996) that is freely available from multiple data repositories on the internet (the data for this study was downloaded from the Climate Diagnostics Center website (CDC 2005)). The reanalysis data are available at four measurement times during each day of the storm at 17 pressure levels from 1000 mb to 10 mb. The data are archived on a regular 2.5º latitude-longitude grid in GRIB file format that is easily read using GEMPAK 5.6.

The values of the variables were computed using this regular 2.5º latitude-longitude grid for each of the 3,702 6-hour time periods in the Best-track file at the latitude and longitude of a given storm's center point. For each time period a storm-centered azimuthal areal average was computed for radii of 200 km, 300 km, 400 km, 500 km, and 600 km. At 200 km only the storm's inner processes are captured, whereas at 600 km the ambient environment is included in the average as well. Table 5 contains an inclusive list of all of the variables used the atmospheric analysis, their significance, the data source, method of computation, and units.

3.3.1 Results of discriminant analysis using atmospheric predictors

3.3.2 Initial results

The first step in exploring the atmospheric variables and their relationship to convective burst events was to run the discriminant analysis procedure with each of the variables listed in Table 5 computed for all radii. Of these 87 variables, 10 variables were found to contribute significantly enough to be assigned coefficients in the discriminant function. The discriminant function coefficients for this test are found in Table 7. Ranking the coefficients by the magnitude of their absolute value displays their relative contribution to the process of discriminating between convective burst time periods and non-convective burst time periods. The coefficients are "partial" coefficients, reflecting the controlled association of the independent variables with the criterion variable. In other words, they represent the order of importance by unique contribution of each variable.

Variable	Coefficient (absolute value)
precipitable water (200 km)	1.416
precipitable water (500 km)	1.325
150 mb wind divergence (600 km)	.743
10 meter wind speed	.609
200 mb – 850 mb wind shear (600 km)	.482
850 mb moisture divergence (200 km)	.382
200 mb – 850 mb wind shear (300 km)	.370
Storm translation speed	.337
850 mb moisture divergence (600 km)	.251
500 mb – 850 mb difference in θ_e (600 km)	.234

Table 7: Standardized discriminant function coefficients for the atmosphere (complete variable set).

The atmospheric variables with little or no discriminating power were excluded from the function because the difference in the group mean value for a variable is too small to assist with group assignment. A conceptually easy way to analyze and discuss the rankings

of the variables of importance in the discriminant results is to examine descriptive statistics broken down by group membership. The SPSS output of means and standard deviations for the variables of importance in the atmospheric procedure is reproduced in Figure 18.

3.3.3 Discussion of "important" variables for the initial procedure

3.3.3.1 Precipitable water (200 km = 1.416, 500 km = 1.325)

The variables with the two highest rankings in this discriminant function, "precipitable water" for 200 and 500 km seem to dominate the function. The mean "precipitable water" averaged over the column for 200 km for convective burst time periods is .68 kg m^{-2} more (1% to 2%) than for non-convective burst times. The difference for 500 km is 1.37619 kg m^{-2} higher for convective burst periods.

3.3.3.2 150 mb wind divergence (600 km = .743)

The "150 mb wind divergence" at 600 km for the convective burst group is approximately 1-1/2 times that of the non-burst group. Given the intensity of the convection, the increased mass flux during a convective burst is to be expected. It is important to note that the convective burst itself is creating this divergence aloft. It is not necessarily a pre-cursor to burst formation.

3.3.3.3 10 meter wind speed (.609) and wind shear (600 km = .482, 300 km = .370)

The mean average wind speed for the group of null cases is about 5 m s^{-1} higher than for the convective burst group (34 m s^{-1} versus 29 m s^{-1}). The standard deviation of this variable is almost 14 m s^{-1} for the non-burst cases (10 m s^{-1} for the burst cases), which is too wide of a spread for valid interpretation. The same is true for "200 mb – 850 mb wind shear" at 600 km and 300 km. The difference in wind shear between the two groups is .61 m s^{-1} at the 300 km radius and .71 m s^{-1} at 600 km with a standard deviation of about 6.0.

Group Statistics

cb or no cb		Mean	Std. Deviation	Valid N (listwise) Unweighted	Weighted
no cb	bt wind speed in m/s	34.08013	13.887202	2556	2556.000
	storm translation speed in m/s	5.87999	4.162317	2556	2556.000
	850 mb moisture divergence (200 km)	-.55725	5.147275	2556	2556.000
	columnar avg precipitable water (200 km)	49.78569	12.260089	2556	2556.000
	200-850 wind shear (300 km)	11.65645	6.872248	2556	2556.000
	columnar avg precipitable water (500 km)	46.96712	11.039488	2556	2556.000
	150 mb wind divergence (600 km)	.62840	.647401	2556	2556.000
	850 mb moisture divergence (600 km)	-.80094	2.674780	2556	2556.000
	200-850 wind shear (600 km)	14.07389	6.168306	2556	2556.000
	500 - 850 mb difference in theta-e (600 km)	.70431	8.881251	2556	2556.000
cb	bt wind speed in m/s	29.08856	9.510712	1146	1146.000
	storm translation speed in m/s	4.63835	2.318999	1146	1146.000
	850 mb moisture divergence (200 km)	-1.38421	4.797056	1146	1146.000
	columnar avg precipitable water (200 km)	50.46722	12.048548	1146	1146.000
	200-850 wind shear (300 km)	11.04555	6.135920	1146	1146.000
	columnar avg precipitable water (500 km)	48.34331	10.763080	1146	1146.000
	150 mb wind divergence (600 km)	.91927	.646094	1146	1146.000
	850 mb moisture divergence (600 km)	-1.20956	2.527576	1146	1146.000
	200-850 wind shear (600 km)	13.37380	5.285897	1146	1146.000
	500 - 850 mb difference in theta-e (600 km)	1.89861	6.117657	1146	1146.000
Total	bt wind speed in m/s	32.53493	12.901502	3702	3702.000
	storm translation speed in m/s	5.49562	3.735457	3702	3702.000
	850 mb moisture divergence (200 km)	-.81324	5.055297	3702	3702.000
	columnar avg precipitable water (200 km)	49.99667	12.197441	3702	3702.000
	200-850 wind shear (300 km)	11.46734	6.658193	3702	3702.000
	columnar avg precipitable water (500 km)	47.39314	10.971684	3702	3702.000
	150 mb wind divergence (600 km)	.71844	.660741	3702	3702.000
	850 mb moisture divergence (600 km)	-.92743	2.636530	3702	3702.000
	200-850 wind shear (600 km)	13.85717	5.917394	3702	3702.000
	500 - 850 mb difference in theta-e (600 km)	1.07402	8.144713	3702	3702.000

Figure 18: Descriptive statistics of atmospheric variables important to initial discriminant function.

3.3.3.4 500 mb – 850 mb difference in θ_e (600 km = .234)

The most striking difference in group means is in "500 mb – 850 mb difference in θ_e" at 600 km. The mean environmental difference between the mid and lower tropospheric θ_e (the convective instability) for the convective burst cases is more than 2-1/2 times the non-burst cases. This implies that convective bursts are more apt to form in areas with higher mid-tropospheric background concentrations of moist static energy (note again the wide variability expressed in the standard deviation however.) Another interpretation may be that this elevated value is actually a "self-measure" showing that the mid-levels are moist enough and contain many undiluted convective clouds that penetrate upward through the troposphere.

3.3.3.5 850 mb moisture divergence (200 km = .382, 600 km = .370)

"850 mb moisture divergence" near the core (200 km) and at 600 km were approximately 1-1/2 to 2 times larger in the convective burst cases than the null cases. The forced low-level convergence necessary to initiate and maintain intense convection is apparent. Low-level moisture is readily available. Strong horizontal moisture flux was found to be a necessary characteristic of convective burst development by Rodgers et al. as cited earlier in this section.

3.3.4 Discrimination results- initial atmospheric model

The discriminant function discussed above had a Wilks' Lambda = .865 which, once converted into a Chi-square statistic, can be used to test the null hypothesis that "There is no discriminating power in the variables." In this case the df=10 ($P\ \chi^2 \leq 537$) with $p \leq .001$ so we reject the null hypothesis and conclude that the variables have some ability to discriminate. The Canonical Correlation is .368. Its square implies that only 13.5% of the variance in the dependent variables is explained by the independent variables. The result matrix is presented in Table 8. A variety of error or accuracy measures can be computed from the result matrix. Common measures are included in Table 9.

This initial exploratory discriminant analysis procedure was meant to narrow down the atmospheric variables especially with regard to which radii presented the most "classifying power" for which variables. The rather poor discriminant analysis results suggest that, as expected, the model is probably over-specified. A careful look at the correlation matrix including all 87 variables in the initial analysis revealed that the variables "precipitable water" and "850 mb moisture divergence" are highly positively

correlated with numerous other atmospheric variables. In an effort to uncover as much underlying structure as possible in the data, the procedure was run again without "precipitable water" and "850 mb moisture divergence" at any radii. These results are presented in the next section.

	CB or no CB	no CB	CB	Total
Count	no CB	1677 (a)	879 (b)	2556
	CB	362 (c)	784 (d)	1146
%	no CB	65.6	34.4	100.0
	CB	31.6	68.4	100.0

Table 8: Results of initial atmospheric discriminant analysis

Measure		Percent
Correct classification rate	(a+d)/n	66%
False Positive Rate	b/(b+d)	53%
False Negative Rate	c/(a+c)	18%
Misclassification Rate	(b+c)/n	36%

Table 9: Accuracy measures initial atmospheric discriminant analysis.

3.3.5 Atmospheric variable discriminant analysis with no precipitable water or moisture divergence

The second discriminant analysis procedure to explore the atmospheric variables that may influence convective burst occurrence yielded three new "important" variables to consider: "700 mb – 500 mb difference in moisture divergence" at 200km and 600km and the "500 mb – 925 mb difference in θ_e" at 300 km. The group statistics, the mean and standard deviations, are found in Table 10.

Variable	Mean	Std. Dev.
no CB		
700 mb – 500 mb difference in moisture divergence (200 km)	.08064	4.082580
700 mb – 500 mb difference in moisture divergence (600 km)	.11399	1.959737
500 mb – 925 mb difference in θ_e (300 km)	-4.71836	11.811601
CB		
700 mb – 500 mb difference in moisture divergence (200 km)	.13931	2.736088
700 mb – 500 mb difference in moisture divergence (600 km)	.29786	1.457338
500 mb – 925 mb difference in θ_e (300 km)	-4.37425	7.105356
Total		
700 mb – 500 mb difference in moisture divergence (200 km)	.09880	3.717960
700 mb – 500 mb difference in moisture divergence (600 km)	1.07402	8.144713
500 mb – 925 mb difference in θ_e (300 km)	-4.61184	10.581043

Table 10: Descriptive statistics for new variables in the atmospheric discriminant analysis

3.3.6 Final results for the atmospheric discriminant analysis

The absolute values of the discriminant function coefficients for the entire set of atmospheric variables except "precipitable water" and "850 mb moisture divergence" are presented in Table 11. Having removed these two dominating variables from the model's set of independent variables, more identifiable structure may now be apparent. In fact, the emergence of "700 mb – 500 mb difference in moisture divergence" at 200 km and 600 km as variables suggests stratification of the mid-troposphere with regard to moisture and wind divergence to be important. A second measure of θ_e, "500 mb – 925 mb difference in θ_e" closer to the storm environment (300 km) has also appeared as important.

Variable	Coefficient (absolute value)
150 mb wind divergence (600 km)	.758
10 meter windspeed	.665
200 mb – 850 mb wind shear (600 km)	.602
200 mb – 850 mb wind shear (300 km)	.468
500 mb – 850 mb difference in θ_e (600 km)	.398
500 mb – 925 mb difference in θ_e (300 km)	.321
storm translation speed	.344
700 mb – 500 mb difference in moisture divergence (600 km)	.217
700 mb – 500 mb difference in moisture divergence (200 km)	.163

Table 11: Discriminant function coefficients for atmospheric discriminant analysis without "precipitable water" and "850 mb moisture divergence".

Measure		Percent
Correct classification rate	(a+d)/n	66%
False Positive Rate	b/(b+d)	54%
False Negative Rate	c/(a+c)	18%
Misclassification Rate	(b+c)/n	34%

Table 12: Accuracy measures for atmospheric discriminant analysis without "precipitable water" and "850 mb moisture divergence".

The removal of the precipitable water variables and the moisture divergence variables and the replacement of these by mid-tropospheric moisture divergence stratification resulted in little to no increase in classification ability with the new discriminant function. The new model is still statistically significant. In this case the df=9 ($p\chi^2 \leq 492$) with $p \leq .001$. The Canonical Correlation = .353. Only 12.5% of the variance in the function's ability to classify a convective burst event is explained by the independent atmospheric variables. It is interesting to note that when the discriminant analysis procedure is run using only these nine significant variables (instead of all 77 remaining) identical results are produced.

3.3.7 Summary

In this section of Chapter 3, the following atmospheric variables have emerged as useful in discriminating periods of convective burst activity:

Kinematic variables

- increased 150 mb wind divergence (600 km)
- lower 10 meter wind speed
- slightly lower 200 mb – 850 mb wind shear at 300 km and 600 km
- increased 850 mb moisture divergence at 200 km and 600 km
- slightly slower storm translation speed
- an increased difference in 700 mb – 500 mb moisture divergence at 200 km and 600 km (with higher divergence levels at 700 mb)

Thermodynamic Variables

- more precipitable water in the column for a 200 km and 500 km radius
- a significantly larger 500 mb – 850 mb difference in θ_e (600 km)
- slightly less negative difference in 500 mb – 925 mb difference in θ_e closer to the storm (300 km), but outside the typical radius of 34-kt winds.

These variables will be revisited in the case studies presented in Chapter 7. In the next section the discriminant analysis procedure is presented for the oceanic variables.

3.4 Can oceanic factors predict convective burst incidence?

The upper-ocean thermal structure can help to maintain or modify tropical cyclone structure and intensity. The impacts of changes in the ocean on tropical cyclone structure, including local convective tendencies, and ultimately, tropical cyclone intensity change are not well understood.

Although deemed important, research on the ocean's role in modulating tropical cyclone intensity was postponed, as oceanic data, especially near storm centers, was scarce. As observations became available, tropical cyclone researchers attempted to use pre-storm SST data as an estimate of the average temperature of the ocean's mixed layer. Although researchers have known using SST alone oversimplifies a complex air-sea interaction problem, SST is routinely used as a proxy for more accurate measures of the heat content of the ocean. New tools have only recently become available allowing detailed analysis of the ocean's thermal structure, even in adverse conditions.

The pre-storm SST by itself is an inadequate predictor of tropical cyclone intensity (Evans 1993). Investigation of the relationship between SST and the minimum sea level

pressure in the storm suggests SST does provide a realistic upper bound on storm intensity (Holland 1997) (DeMaria and Kaplan 1994), (Emanuel 1988), (Miller 1958). The energy released by an air parcel ascending within a tropical cyclone eyewall is limited by two factors: the initial equivalent potential temperature of the inflowing air and the prevailing lapse rate (the degree to which the air temperature changes with height.) The temperature of the underlying layer of water directly affects the moisture content of the inflowing air and the surface temperature. Through these mechanisms, the boundary layer temperature of the ocean regulates the energy available for tropical cyclone formation, maintenance, and intensification.

The SST as represented by satellite remote temperature sensors is representative of the upper few meters (or in the case of TMI, centimeters) of the ocean. Minimal tropical storm winds can cause enough vertical mixing to cool these top meters of the ocean within an hour of onset (Shay, Goni et al. 1998). A more useful measurement of ocean temperature is that of the well-mixed layer of the ocean called the oceanic planetary boundary layer (OPBL). There are, however, no direct or proxy measurements of the OPBL except for scattered buoys and dropsonde experiments. Instead, a number of remotely sensed and climatological parameters can be combined to derive measurements of the upper ocean vertical structure and heat content (Shay, Goni et al. 1998). The lack of in situ measurements of other upper ocean processes, such as the effects of ocean currents, advection, and shear at the base of the OPBL, complicate any attempt to estimate the magnitude of observed oceanic heat content flux to the atmosphere. Previous observational and modeling results estimate only about 10% to 15% of the cooling in the upper ocean is due to surface latent and sensible energy fluxes (Black 1983), (Hong, Chang et al. 2000), (Chang and Miller 1977). No objective measurement tool can be designed without more frequent direct observations.

3.4.1 Sea surface temperature as a forcing mechanism of TC intensity

A warm ocean ($\geq 26^{\circ}$ C) has been considered a necessary environmental condition for tropical cyclogenesis for a long time (Riehl 1950). Current research suggests that tropical cyclone intensity/ocean interaction occurs on many scales. Both negative and positive feedbacks have been identified. For example, the effects of the cold wake of a TC in the warm ocean has been recognized since the 1960's (Leipper 1967), but received little attention until the last decade. Inter-storm interaction is in fact possible as was the case with Hurricane Danielle (1998) as it crossed Hurricane Bonnie's cold wake and showed a marked decrease in

intensity. Once Danielle left the pre-cooled wake area wind speeds increased once again. Figure 19 illustrates this example using satellite imagery.

The effects of localized warm anomalies are also important to storm intensity. Two recent studies employed newer remote sensing technologies to detect and measure the positive feedback interaction between the ocean and the hurricane. In both cases the storm crossed a particularly warm deep oceanic feature known as a warm core ring (WCR), shed from the Loop Current in the Gulf of Mexico. Shay et al. used upper-ocean heat measurements derived from Advanced Very High Resolution Radiometer (AVHRR) and TOPEX/Poseidon altimeter data to examine the strong effects of this warm core ring on the intensity of Hurricane Opal (1995) (Shay, Goni et al. 2000). The warm core ring (See Figure 20) was not detected using pre-storm SSTs alone. Only examination of the sea-height anomalies from the altimeter data showed its existence. One ocean buoy (42001) and the AVHRR suggested the change in SST to be 0.5 -- 1°C in the warm core ring area and 2° -- 3°C in the cold wake of Hurricane Opal. This evidence suggests that the ocean lost a significant amount of energy during Opal's intensification. Abundant oceanic heating was available for the storm, especially from the WCR. This energy loss occurred during a period of intensification from 965 to 916 mb when Opal's translation speed was greater than 8 ms^{-1} (Shay, Goni et al. 2000). The second study -- of Hurricane Gilbert (1988) by Jacob et al. -- was undertaken from the perspective of the oceanic mixed layer response to the tropical cyclone (Jacob, Marks et al. 2000). NOAA airborne expendable bathythermograph (AXBT) and airborne expendable current profiler (AXCP) data from before, during, and after passage of the hurricane were used to compute upper ocean heat and mass budgets. The authors found that entrainment at the base of the OPBL and vertical mixing (upwelling/downwelling) dominated the mass fluxes in the ocean and that entrainment moderated the heat budget in the eddy region under the storm. Increased entrainment at the base of the warm oceanic feature implies a shallower warm layer with less fueling potential for the hurricane above. The dual perspectives of these studies, one focusing on the effects of the ocean structure on TC intensity, the other on the changes in the ocean resulting from TC passage, highlight the reciprocal nature of the air-sea interaction in the tropical cyclone.

Generally, small horizontal SST anomalies (< 100 km in radius, i.e. smaller than the typical tropical cyclone eye) impact a storm very little as the storm passes quickly over the anomaly. But a small cold anomaly induced by the storm itself propagates along with the storm and may impact storm intensity (Schade 2000).

In early research, Price suggested the tropical cyclone itself as a source for increased SST variability and attempted to quantify the energy production of the ocean (Price 1981). More recently, Schade and Emanuel modeled the interactions between the ocean mixed layer and the TC and showed the SST response to a TC can dramatically affect the intensity of the hurricane itself (Schade and Emanuel 1999). They postulate that the cooling itself is caused by enhanced surface winds that force cold water into the warm mixed layer of the ocean through vertical turbulent entrainment. This small cold pool moves along with the storm, providing and increased sea-air contrast that ultimately negatively affects the intensification of the storm since this cold pool is located near the eyewall where most of the inflow occurs. Schade (1994) has also shown through modeling experiments that tropical cyclones are more sensitive to these small local reductions of SST near the eyewall than to the ambient SST. Some validation of these modeling results has been provided through a composite analysis of surface data (buoys and AXBTs) in 37 Atlantic basin tropical cyclones by Cione et al. (2000).

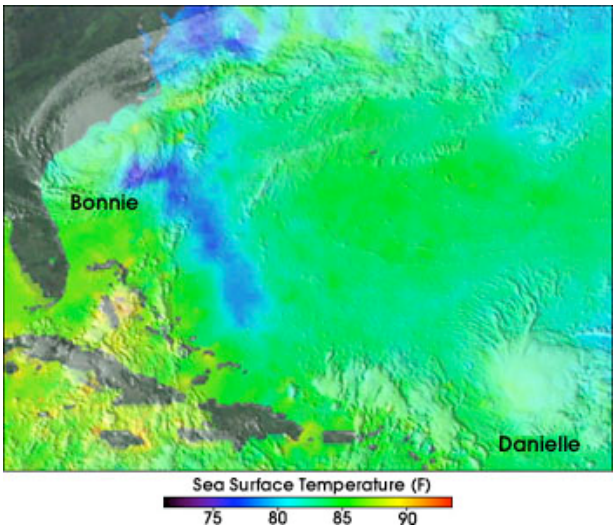

Figure 19: Satellite image of Hurricane Danielle approaching Hurricane Bonnie's cold ocean wake. (Image courtesy TRMM Project, Remote Sensing Systems, and Scientific Visualization Studio, NASA Goddard Space Flight Center.)

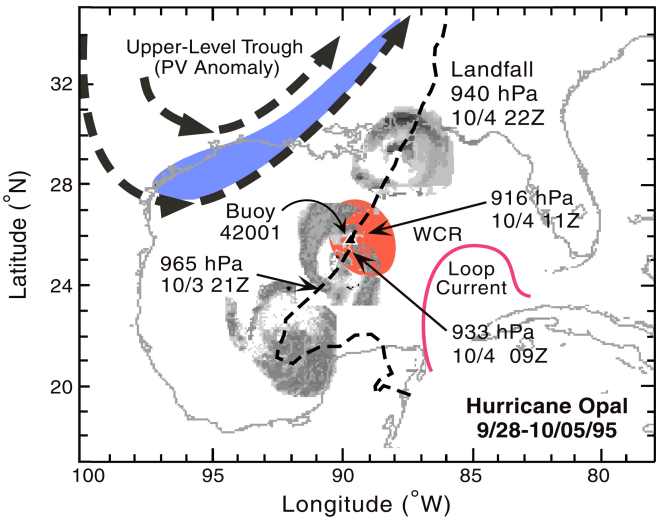

Figure 20: Tropical Cyclone Opal's encounter with a warm core ring in the Gulf of Mexico. From (Shay, Goni et al. 1998)

Their results show a statistically significant positive relationship between the difference in inner-core and ambient SST (of ~2°C) and tropical cyclone intensification. This cooling has come to be known in the research community as "SST feedback" and its mechanisms are still quite controversial.

All of these studies corroborate the argument that the oceanic background conditions should not be ignored in investigations of coupled ocean-atmosphere responses. New tools in meteorology and oceanography are making it possible to include interaction effects in research.

3.4.2 Oceanic variables for the discriminant analysis procedure

The ocean affects tropical cyclone intensity as the rate of evaporation increases with surface wind speeds and latent energy flux is enhanced. How well do convective bursts channel this flow of moist static energy from the ocean through the troposphere? This discriminant analysis procedure using solely oceanic variables attempts to address this question.

The potential oceanic forcing of convection in the tropical cyclone should have kinematic and thermodynamic components just like the atmosphere does. Since this study uses a total of 240 tropical storms and cyclones, no attempt has been made to focus on

localized ocean temperature anomalies such as warm core rings or cold wakes as forcing mechanisms. Therefore, the main ocean forcing mechanisms to be examined are the role of ambient SST and any self-perpetuating "SST feedback" cold pools. In his research on "SST feedback" Schade identifies these six variables that moderate its magnitude (Schade 1994):

1) thickness of the ocean's mixed layer
2) storm translation speed
3) areal extent of the storm
4) latitude of the storm
5) large-scale atmospheric conditions affecting TC intensity (shear, trough interaction, etc.)
6) oceanic structure below the mixed layer
7) relative humidity in the APBL.

The atmospheric conditions were addressed in the previous discriminant analysis and will be ignored until the next section where the ocean and atmosphere are re-united to see their combined effects. No variable has been chosen to deal with "the areal size of the storm" directly, as the effects of storm size are captured by other variables as the azimuthal averaging radii changes from 200 km to 600 km.

Once again, the magnitudes of the variables were computed for each of the 3,702 6-hour time periods in the best-track file at the latitude and longitude of a given storm's center point. The variables used in the ocean analysis, their significance, the data source, method of computation, and units are summarized in Table 6.

One variable to be included in this study is commonly known as "Hurricane Heat Content." In 1970, Leipper introduced the concept of upper ocean heat content defined as a measure of the integrated heat content in the part of the upper ocean above the 26°C isotherm:

$$Q_H(x,y,t) = \rho c_p \int_{z(T=26)}^{0} \Delta T(x,y,z,t)\, dz$$

where ρ is the average upper oceanic density (1026 kg m^{-3}), c_p is the specific heat of water at constant pressure (4178 J kg^{-1} K^{-1}), and ΔT is the temperature difference relative to the 26°C isotherm distributed over a depth interval dz. The units for Q_H are kJ cm^{-2} (Leipper 1967). Using thermal profiles from a series of asynoptic ship cruises in the Gulf of Mexico, Leipper

and Volgeneau found that during various times of the hurricane season, total heat exchanges fluctuated significantly (Leipper and Volgenau 1972). In other words, the ocean provides differing amounts of energy according to its upper ocean thermal structure. The 26°C isotherm was chosen as the reference temperature for two reasons: 1) Palmen found that SSTs of 26°C or higher are necessary for tropical cyclogenesis (Palmen 1948) and 2) 26°C is the mean surface air temperature for the tropical atmosphere during the times of most tropical cyclone development. (Malkus 1962).

For this study, global "hurricane heat content" (HHC) is acquired using satellite radar altimeter-derived vertical temperature profiles estimated from sea-surface height anomalies (SSHA). The Operational Global Ocean Analysis (Naval Research Lab, Stennis Space Center) uses SSHA deviations from TOPEX, ERS2, and GFO satellites as input to an optimal interpolation procedure to produce daily global 1/8° SSHA fields. They then use a "first guess" field and various SST observations in another optimal interpolation procedure to produce daily global 1/8° SST fields as well. Historical profiles of surface temperature and height anomalies are then used in a regression model to relate the remotely sensed temperatures and height anomalies to the subsurface temperatures. The profiles used are validated at the Fleet Numeric Meteorology and Oceanography Center (FNMOC) through a quality control check at all levels with 99% probability. A graphic illustrating this process is included as Figure 21.

The choice of oceanic variables to attempt to capture the persistent near/inner core-cold anomaly was taken from the work of Cione and Uhlhorn (2003). In their observational study of the hurricane environment they offer useful vocabulary for discussing the tropical cyclone-induced SST change. In their study, the ambient SST (SST_A) is located in either the right or left front quadrant (storm-relative) at least 2° in latitude ahead of the storm, well away from the storm center. The inner-core SST (SST_{IC}) is the minimum SST within a 60-km radius of the storm center. The inner-core wake (SST_{ICW}) is the minimum SST observed in either the right rear or left rear quadrant of the storm within 200 km radius of the center location. These definitions need to be modified for the purpose of this study since the data employed is remotely sensed. See Table 6.

The SST data used in this study to compute these variables are from an objectively interpolated SST tropical cyclone cold-wake climatology constructed from near real time global optimum interpolated microwave (TRMM) SSTs from NASA/Remote Sensing Systems Inc. All images cover a global region extending from 40S to 40N at a pixel resolution of 0.25 deg (~25 km).

3.4.3 Results of discriminant analysis using oceanic predictors

The first step in exploring the oceanic variables and their relationship to convective burst events was to run the discriminant analysis procedure with each of the variables listed in Figure 22. Of these 10 variables, 5 variables were found to be useful enough to be assigned coefficients in the discriminant function. The discriminant function coefficients for this test are found in Table 13. The SPSS output of the group-by-group descriptive statistics is in Figure 22. The model is statistically significant. In this case the df=5 (p $\chi^2 \leq 623$) with $p \leq .001$. The Canonical Correlation = .394. Only 15.5% of the variance in the function's ability to classify a convective burst event is explained by the independent ocean variables.

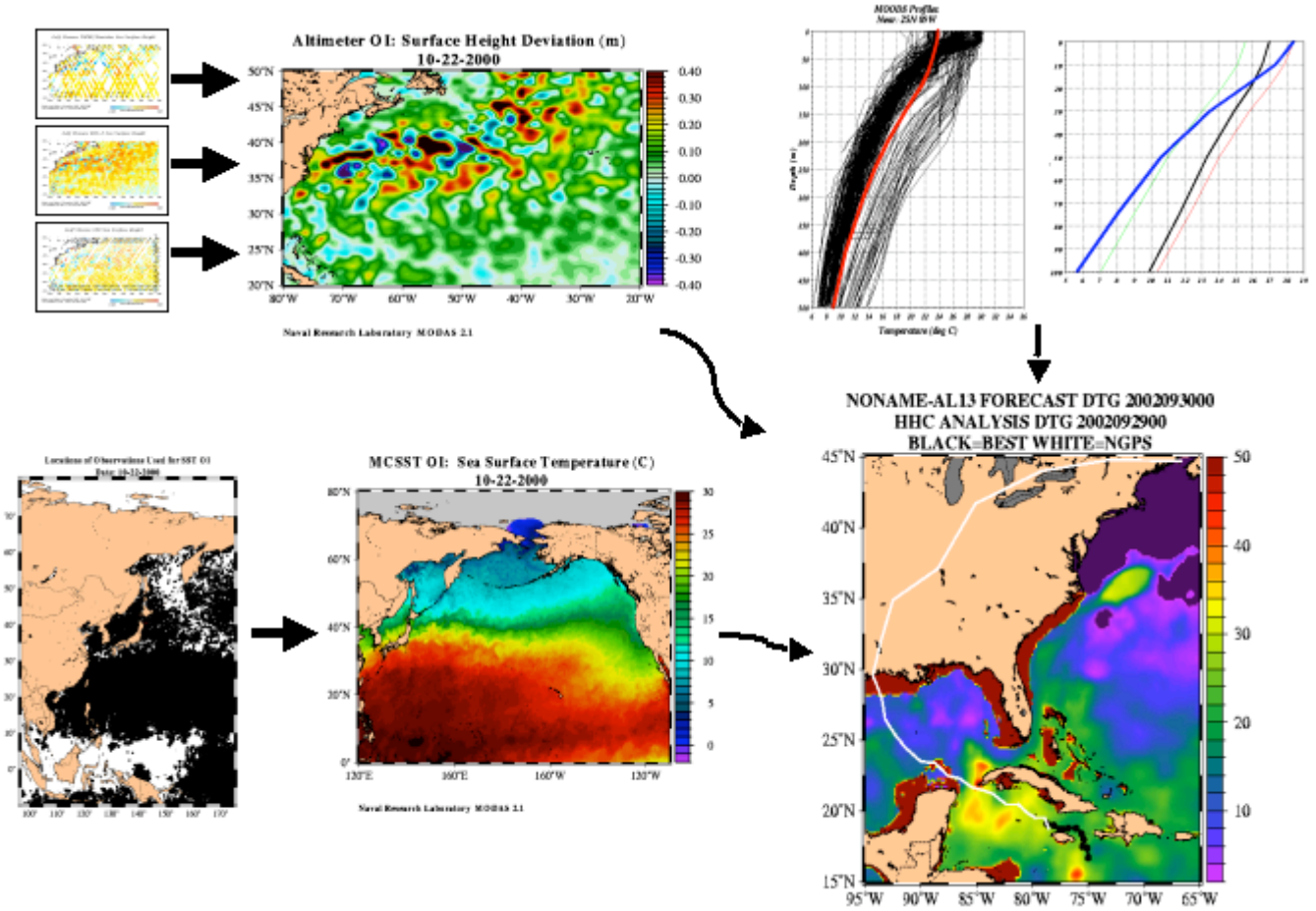

Figure 21: Operational global daily analysis of SSHA, climatology, SST, and HHC (J m^{-2}). (Naval Research Lab, Stennis Space Center, courtesy Clark Rowley.)

3.4.4 Discussion of the significant variables for the initial procedure

3.4.4.1 Climatological SST (.637)

The large area mean SST dominates the discriminant function having two times more discriminating power than the HHC and almost three times any other variable. By the nature of the computation, this SST incorporates all of the other SST variables in its average, and therefore is very highly correlated. The mean SST for the convective burst cases is 1.25°C higher than for the non-burst cases. All of the other SST variables also have higher

Variable	Coefficient (absolute value)
mean SST from pixels ≤ 500 km from storm center	.637
hurricane heat content	.381
sea-surface height anomaly	.259
SST_{ICW}-SST_A	.218
storm translation speed	.123

Table 13: Standardized discriminant function coefficients for the ocean (complete variable set).

Group Statistics

cb or no cb		Mean	Std. Deviation	Valid N (listwise) Unweighted	Valid N (listwise) Weighted
no cb	storm translation speed in m/s	5.87998713871	4.16231656428	2556	2556
	coriolis parameter	.00009330411	.000044973520	2556	2556
	min sst value within 60 km of storm core	27.04272300469	1.85771145195	2556	2556
	mean sst from front 2 quadrants 222–444 km ahead of storm	27.29956103286	1.85714890922	2556	2556
	mean sst from rear 2 quadrants within 222 km of storm center	26.46518701095	1.86624921732	2556	2556
	meant sst from pixels <= 500 km from storm center	27.45360993740	1.65964672285	2556	2556
	SSTinnercore minus SSTahead	-.25672065728	.873238172936	2556	2556
	SSTicw minus SSTahead	-.83431533646	1.06393302870	2556	2556
	sea-surface height anomaly	.00512323944	.088358884320	2556	2556
	along track hurricane heat content	6.85748200313	7.31384832090	2556	2556
cb	storm translation speed in m/s	4.63835311811	2.31899884756	1146	1146
	coriolis parameter	.00009577464	.000043777957	1146	1146
	min sst value within 60 km of storm core	28.39895287958	1.11395622262	1146	1146
	mean sst from front 2 quadrants 222–444 km ahead of storm	28.60993455497	1.12693761644	1146	1146
	mean sst from rear 2 quadrants within 222 km of storm center	27.85903141361	1.31632312596	1146	1146
	meant sst from pixels <= 500 km from storm center	28.69910994764	.987886536872	1146	1146
	SSTinnercore minus SSTahead	-.21098167539	.613944657489	1146	1146
	SSTicw minus SSTahead	-.75090314136	.888710895195	1146	1146
	sea-surface height anomaly	-.01001047120	.079372010479	1146	1146
	along track hurricane heat content	12.49071815009	7.82896392895	1146	1146
Total	storm translation speed in m/s	5.49562393298	3.73545700115	3702	3702
	coriolis parameter	.00009406890	.000044615564	3702	3702
	min sst value within 60 km of storm core	27.46256077796	1.77753141196	3702	3702
	mean sst from front 2 quadrants 222–444 km ahead of storm	27.70520340357	1.77229580316	3702	3702
	mean sst from rear 2 quadrants within 222 km of storm center	26.89666882766	1.83189408729	3702	3702
	meant sst from pixels <= 500 km from storm center	27.83916990816	1.59220093244	3702	3702
	SSTinnercore minus SSTahead	-.24256158833	.802175535125	3702	3702
	SSTicw minus SSTahead	-.80849405727	1.01354983585	3702	3702
	sea-surface height anomaly	.00043841167	.085952321253	3702	3702
	along track hurricane heat content	8.60132009724	7.91678349674	3702	3702

Figure 22: Group Means and standard deviations for the entire set of ocean variables

mean values for the convective burst cases than the null cases. Since the climatological SST variable is so robust, it will be dropped from the next procedure so as to try to discover which SST regions are worthy of further research.

3.4.4.2 Hurricane heat content (.381)

The mean hurricane heat content for the convective burst cases (12.5 J m^{-2}) is almost double the HHC for the non-burst cases (6.9 J m^{-2}). High hurricane heat content does act to force convective tendencies. Further analysis regarding the temporal and spatial scales is necessary to discern the true nature of this relationship.

3.4.4.3 Sea-surface height anomaly (.259)

Satellite radar altimetry observations of SSHA are valuable for understanding and detecting mesoscale eddies and for describing variations in the mixed layer depth. In order to better understand the role of the SSHA in this discriminant analysis procedure, an explanation of its derivation is in order. As noted in Goni et al. (Goni, Shay et al. 2000) the derived SSHA is:

$$\eta'(x,y,t) = \eta(x,y,t) - \bar{\eta}(x,y),$$

where $\bar{\eta}$ is the mean sea height. The dataset used in this analysis expresses this time series of sea-level deviations (in meters) relative to a 5-year mean, averaged along 0.2 degree ground track segments. The data are produced using linear differences, correcting for solid and ocean tides, local and non-local inverse barometer, sea-state bias, and geoid to reduce errors. The data for a particular 6-hr time period is computed by calculating a150 km azimuthal average centered on the storm location as identified in the best-track data set.

Mesoscale ocean features only move a few km day^{-1} so this altimeter measurement can provide the surface data needed to detect and locate warm dynamical mesoscale oceanic features, usually identified as positive SSHA values (Shay, Goni et al. 1998). Large scale SST cooling patterns induced by tropical cyclones can be identified by surface depressions in the wake of the storm (Shay, Goni et al. 2000). A region of oceanic upwelling generally dominates the near-eye region beneath a tropical cyclone. Oceanic upwelling areas in the thermocline tend to be associated with baroclinic processes that will take place in areas associated with convective downdrafts at the sea surface due to the wind-forced mixed current divergence

and convergence. The isopycnal displacement is scaled by a function of wind speed and storm motion. Stronger wind stress or slower storm motion results in higher values of isopycnal displacement. Upwelling areas are regions of divergence of surface water. In this case, the mean SSHA for the convective burst time periods tends to be negative (mean = -.01 m) while the anomaly for the non-burst cases is slightly more positive (mean = .005 m). The standard deviation is ~0.08 m for both groups. The tendency to exist amidst a slightly exaggerated surface depression (over a 350 km^2 area) may indicate a relationship between convective bursts and enhanced upwelling. Or convective downdrafts may be enhancing surface water divergence to enhance the depression.

3.4.4.4 SST_{ICW}-SST_A (.218)

The mean difference between the SST_{ICW} and the ambient SST (SST_A) has a tendency to increase (in a negative direction) more for the non-burst cases than for the convective burst cases. This implies that either the SSTs ahead of the storm are getting warmer while the inner-core wake SSTs remain the same or vice-versa. A likely scenario is that the warm layer is mixed out, there is, perhaps, more upwelling and the reservoir of oceanic energy available to the storm – the hurricane heat content—decreases. In other words, storms with no CB event have a colder inner-core wake than storms with CBs. Since convective bursts seem to persist in warmer waters than storms with no burst, this result implies that the energy reservoir over the depth of the layer of warm water, the thermal structure of the ocean's mixed layer, is exhausted more quickly for storms with no convective burst

3.4.4.5 Storm translation speed (.123)

The mean storm translation speed for the convective burst cases was once again slightly lower (by 1 m s^{-1}) than for the null cases. Perhaps "dwell rate" of the storm in the enhanced "hurricane heat content" water is a convective forcing? Linear discriminant analysis cannot answer this question.

3.4.4.6 Classification results of the first discriminant analysis for the ocean.

The result matrix for the first oceanic discriminant analysis is presented in Table 14. Accuracy measures for this analysis are presented in Table 15. It is interesting to note that the oceanic variables seem at first glance to have slightly better "predictive power" than the atmospheric variables did alone. This may in fact be the case. It might also be true that the horizontal scale of the data for the ocean (1/8° latitude) was better at detecting the

	CB or no CB	no CB	CB	Total
Count	no CB	1632	924	2556
	CB	298	848	1146
%	no CB	63.8	36.2	100.0
	CB	26.0	74.0	100.0

Table 14: Results of initial oceanic discriminant analysis

Measure		Percent
Correct classification rate	(a+d)/n	67%
False Positive Rate	b/(b+d)	52%
False Negative Rate	c/(a+c)	15%
Misclassification Rate	(b+c)/n	33%

Table 15: Accuracy measures from initial oceanic discriminant analysis.

mechanisms of convective burst forcing (mesoscale processes?) than the 2.5° grid of the atmospheric variables.

3.4.5 Oceanic discriminant analysis with no climatological SST

The discriminant analysis procedure was re-run without the highly correlated "mean SST from pixels ≤ 500 km from storm center" variable. The resulting discriminant function coefficients are presented in Table 16 The group means and standard deviations were previously included in Figure 22 earlier in this section. The new variables to emerge were SSTs in two regions: SST_{ICW} and SST_{IC}. Both variables showed an approximately 1.4°C warmer region for the convective burst cases. The SST_{ICW} emerged as having slightly more classifying ability than both SSHA and SST_{IC} in this analysis. This result highlights the need to study the ways that the convective burst can modify its environment more fully.

The results of the new oceanic discriminant analysis (Table 16, Table 17, and Table 18) are practically unchanged from those of the initial run. This seems to imply that the climatological SST variable in the initial model was in fact obscuring or incorporating some detail regarding regional SST values shown to be important in the second analysis. Once again the ability of the variables to classify was statistically significant (df=5 (p $\chi^2 \leq$ 621) with

$p \leq .001$). The Canonical Correlation was .393, implying that 15.4% of the variability in the dependent variable was explained by the predictor variables in the model. These results once again highlight the relationships, probably nonlinear ones, at work in convective burst generation and persistence.

Variable	Coefficient (absolute value)
hurricane heat content	.412
SST_{ICW}	.364
sea-surface height anomaly	.281
SST_{IC}	.277
storm translation speed	.127

Table 16: Standardized discriminant function coefficients for the ocean (climatological SST removed).

	CB or no CB	no CB	CB	Total
Count	no CB	1650	906	2556
	CB	293	853	1146
%	no CB	64.6	35.4	100.0
	CB	25.6	74.4	100.0

Table 17: Results of final oceanic discriminant analysis

Measure		Percent
Correct classification rate	(a+d)/n	68%
False Positive Rate	b/(b+d)	52%
False Negative Rate	c/(a+c)	15%
Misclassification Rate	(b+c)/n	32%

Table 18: Accuracy measures: final oceanic discriminant analysis.

3.4.5.1 Summary of the oceanic discriminant analysis section

In this section, the oceanic discriminant analysis procedures highlighted in the following characteristics as distinguishing time periods with a convective burst from periods with no convective burst:

- warmer mean SST from pixels ≤ 500 km from storm center
- almost two times the hurricane heat content
- a slightly more depressed SSH
- the temperature gradient from behind the storm to ahead of the storm (SST_{ICW}-SST_A) becomes more negative
- slightly slower storm translation speed
- warmer values for both SST_{ICW} and SST_{IC}.

In the next section the combined atmosphere/ocean discriminant analysis results are presented and discussed.

3.5 Can a combination of oceanic and atmospheric factors predict convective burst incidence?

3.5.1 Results of the combined ocean-atmosphere discriminant analysis

For the final discriminant analysis procedure the 21 variables deemed to have discriminating power by the previous analyses (not including the climatological ocean) were entered together into a combined model. The atmosphere and ocean may have some linear relationships detectable by the statistical process. In fact, the results were significantly improved – the Correct Classification Rate rose to 71%. The Misclassification Rate fell slightly to 29%. The discriminant function coefficients are presented in Table 19. The group mean values remain unchanged from their previous values so are not presented here. The classification results of the procedure are shown in Table 20 and Table 21.

The eleven predictor variables with influence on the discriminating function fall almost equally balanced between atmospheric predictors and ocean predictors. The number of thermodynamic variables is also basically equal to the kinematic variables (depending on which category SSHA falls in.) The most striking difference between this procedure and the others is seen by examining the variables the model did *not* find to be useful discriminators. These are:

- coriolis parameter (latitude)
- SST_{IC} - SST_{ICW}
- SST_{ICW} - SST_A

- SST_A
- 700 mb – 500 mb difference in moisture divergence(200 km, 500 km)
- precipitable water (200 km, 500 km)
- 850 mb moisture divergence (200 km, 600 km)

None of the moisture variables that dominated the initial atmospheric discriminant analysis were seen to have any discriminating power. Instead all of the moist static energy variables (θ_e) were included in the function.

Examining the variables included in the discriminant function suggests a few other conclusions. The convective burst time periods are characterized by warmer ocean measures than the non-burst times. The inclusion of SST_{ICW} and SST_{IC} seems to suggest that the storms with convective bursts more actively modify their own environments. This makes sense given the intensity of the convection and the amount of increased mass flux taking place during a convective burst event. Wind shear is important; the convective burst time periods are characterized by slightly less shear than the non-burst group. Finally, the 10-meter wind speed itself seems to be related to convective burst existence with the convective burst group having lower mean wind speeds (29 m s^{-1} versus 34 m s^{-1}) than the null group.

Variable	Coefficient (absolute value)
10 meter wind speed	.491
500 mb – 850 mb difference in θ_e (600 km)	.468
SST_{ICW}	.343
200 mb – 850 mb wind shear (600 km)	.308
hurricane heat content	.295
500 mb – 925 mb θ_e difference (300 km)	.260
SST_{IC}	.254
200 mb – 850 mb wind shear (300 km)	.221
150 mb wind divergence (600 km)	.211
sea-surface height anomaly	.168
storm translation speed	.099

Table 19: Standardized discriminant function coefficients for the combined atmosphere and ocean analysis.

	CB or no CB	no CB	CB	Total
Count	no CB	1759	797	2556
	CB	273	873	1146
%	no CB	68.8	31.2	100.0
	CB	23.8	76.2	100.0

Table 20: Results of the combined ocean and atmosphere discriminant analysis

Measure		Percent
Correct classification rate	(a+d)/n	71%
False Positive Rate	b/(b+d)	48%
False Negative Rate	c/(a+c)	13%
Misclassification Rate	(b+c)/n	29%

Table 21: Accuracy measures: combined atmosphere and ocean discriminant analysis.

3.5.2 Summary

The importance of the moist static energy variables and the warm ocean conditions to convective burst existence supports the hypothesized importance of the ocean on tropical cyclone eyewall convective tendencies. This study purports that the action of the boundary layer sea-air fluxes are the root of the upward energy cascade. The next chapter focuses on these sea-air fluxes by exploring a method to estimate the upper-ocean heat content "utilized" by a tropical cyclone.

CHAPTER 4
FROM THE BOTTOM UP: SEA-AIR FLUXES IN THE TROPICAL CYCLONE BOUNDARY LAYER

The important ocean processes affecting the upper ocean heat content available for a tropical cyclone are highlighted in Figure 23. The thickness of the ocean's mixed layer and the thermal structure of the upper ocean (both influenced by bathymetry, currents, shear, wind-induced waves, density, salinity, etc.) provide the reservoir of energy available to tropical cyclones. The tropical cyclone itself affects this reservoir by moderating the upwelling of cold water beneath the storm center, the mixing due to wind-driven waves, the sea-spray effects, and the convective downdrafts.

This chapter examines the net effects of these processes, the "ocean feedback", on the upper-ocean heat content reservoirs available to the tropical cyclone by using remotely sensed values, observed wind values, and bulk parameterized values to estimate sea-air fluxes.

4.1 Ocean feedback in the literature

In his classic textbook, Tropical Meteorology, Riehl (1954) described hurricanes as heat engines and showed that the inflowing air has to become appreciably warmer than that of the distant environment in order for the conversion from potential to kinetic energy to take place as air ascends in the eyewall. This inflowing air acquires enthalpy from the underlying surface – the ocean. Early in the 1960's Malkus and Riehl (1960) published a paper emphasizing, once again, that the horizontal temperature gradients that sustain tropical cyclones arise from heat transfer from the ocean. They use the hydrostatic relation to calculate a relationship between surface pressure fall and boundary layer moist static energy changes from the ambient environment to the inside edge of the eyewall:

$$\partial p_s = -2.5\partial\theta_{eb} \qquad (1)$$

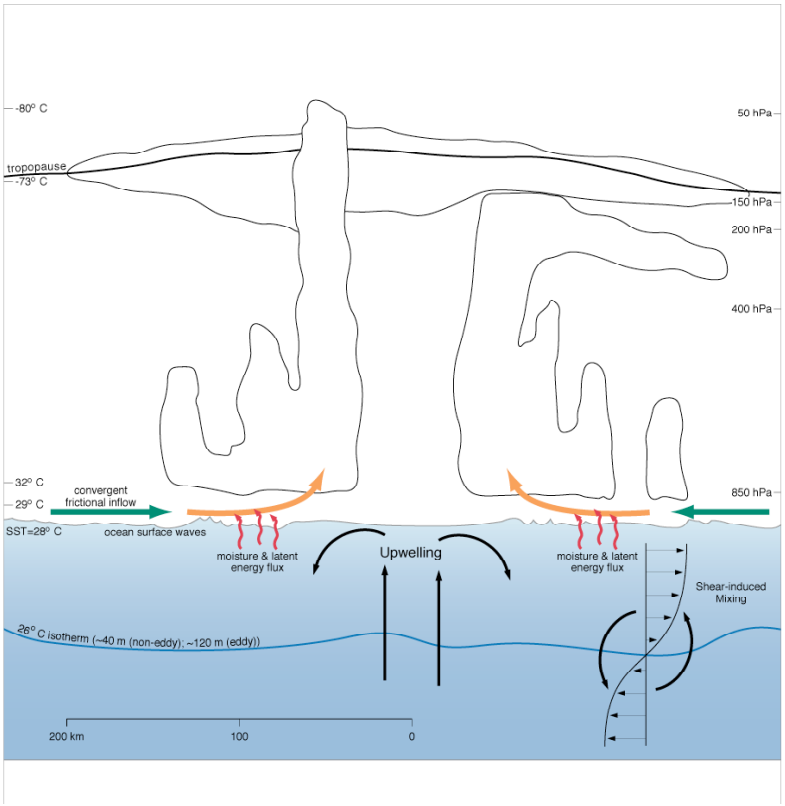

Figure 23: A warm ocean provides energy to the TC through the boundary layer sea-air fluxes.

where ∂p_s is the drop in surface pressure in millibars, and $\partial \theta_{eb}$ is the increase in equivalent potential temperature (in Kelvin) of a parcel lifted from the boundary layer. This relationship shows explicitly how hurricane intensity relates to the increase in boundary layer entropy that comes from sea-air enthalpy transfer. As the development of observational tools like dropsondes and measurement tools progressed it became known that hurricanes are warm core vortices. As illustrated in Hawkins and Imbembo (1976) aircraft data showed that the horizontal temperature gradient is concentrated in the eye and eyewall of the storm and that the temperature anomaly inside the eye can be as large as 15K warmer than the upper tropopausal air of the surrounding environment at the same pressure. (See Figure 24.) This pronounced increase in θ_e near the storm's eyewall made it clear that there must be a strong surface entropy source under the eyewall.

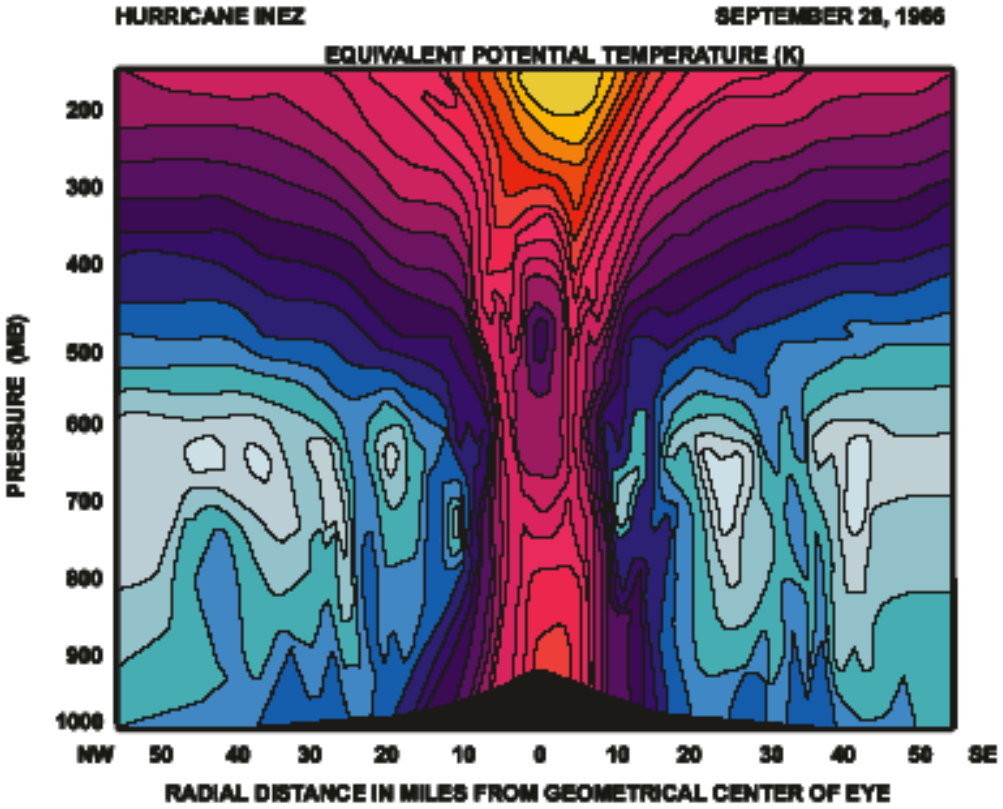

Figure 24: θ_e as a function of pressure and radius from the center of Hurricane Inez (1966) based on aircraft data at 5 flight levels. Contours have intervals of 2 K with a minimum value of 336 K (light blue) and a maximum value of 376 K (yellow). Updated by Emanuel, based on Hawkins and Imbembo (Hawkins and Imbembo 1976).

In the late 1960's, Ooyama (1969) published the results of the first successful numerical model simulation of a tropical cyclone showing, along with other things, that a storm's intensification relies heavily on surface enthalpy fluxes. In 1986 Emanuel published his air-sea interaction model for tropical cyclones (Emanuel 1986). In this paper he derives an expression for the maximum wind speed that connects the strong sensitivity of hurricane intensity to the boundary layer processes that drive the enthalpy and momentum exchanges between the air and the ocean. The maximum wind speed is:

$$v_{\max}^2 = \frac{T_{sst} - T_{out}}{T_{out}} \frac{C_k}{C_D} \left(k_{sst}^* - k \right), \qquad (2)$$

where T_{sst} and T_{out} are the absolute temperatures at the surface and near the top of the storm, C_k and C_D are surface exchange coefficients for enthalpy and momentum, and k_{sst}^* and

k are the specific enthalpies of air at saturation at sea-surface temperature and pressure, and boundary layer air, respectively. Emanuel explains this equation in terms of the Carnot Cycle where enthalpy is added to the system at the high ocean temperature and removed at the lower temperature of the storm's outflow near the tropopause.

Under average tropical conditions a local decrease in sea-surface temperatures of only 2.5° C will cause k_{sst}^{*}- k to zero out. So Emanuel's relationship is quite sensitive to local perturbations of sea surface temperature-- larger scale gradients of sea-surface temperature are accompanied by similar gradient in the specific enthalpy of the boundary layer air. The k_{sst}^{*}- k difference then remains relatively constant.

This sensitivity to local sea-surface temperature anomalies was largely ignored for twenty years because of the earlier publication of a paper by (Chang and Anthes 1979) simulating a hurricane with a coupled ocean-atmosphere model that showed little effect of ocean feedback on storm intensity. Other studies using more advanced coupled models such as (Khain, Ginis et al. 1997) (Bender and Ginis 2000) (Schade and Emanuel 1999) showed that ocean feedback has a first-order effect on hurricane intensity and interest in ocean feedback was renewed.

In his dissertation work Schade used Emanuel's coupled model to investigate the relative importance of two separate effects of sea-surface temperature on tropical cyclone intensity. (Schade 1994) (Schade and Emanuel 1999) (Schade 2000) The first effect is from the large-scale sea-surface temperature field (in equilibrium with the atmosphere). He found that higher ambient SSTs set the stage for the tropical cyclone and provide the potential for stronger intensity. But the second effect, the tropical cyclone induced reduction of SST directly under the eye, had much stronger effects on intensity. A diagram illustrating the change in tropical cyclone intensity change as a function of SST is included here as Figure 25 for reference. The mechanisms of this local reduction of SST are related to the surface wind field of the tropical cyclone, but the details are the subject of much heated debate running the gamut from undiluted convective downdrafts and boundary layer roll vortices to re-entrant sea spray. (Powell 1990) (Powell 1990) (Donelan, Drennan et al. 1997) (Cione, Black et al. 2000) (Andreas and Emanuel 2001) (Barnes and Bogner 2001) (Chan, Duan et al. 2001) (Giordani and Caniaux 2001) (Emanuel, DesAutels et al. 2004) (Wang, Kepert et al. 2001) (Ginis, Khain et al. 2004) (Bister 2001).

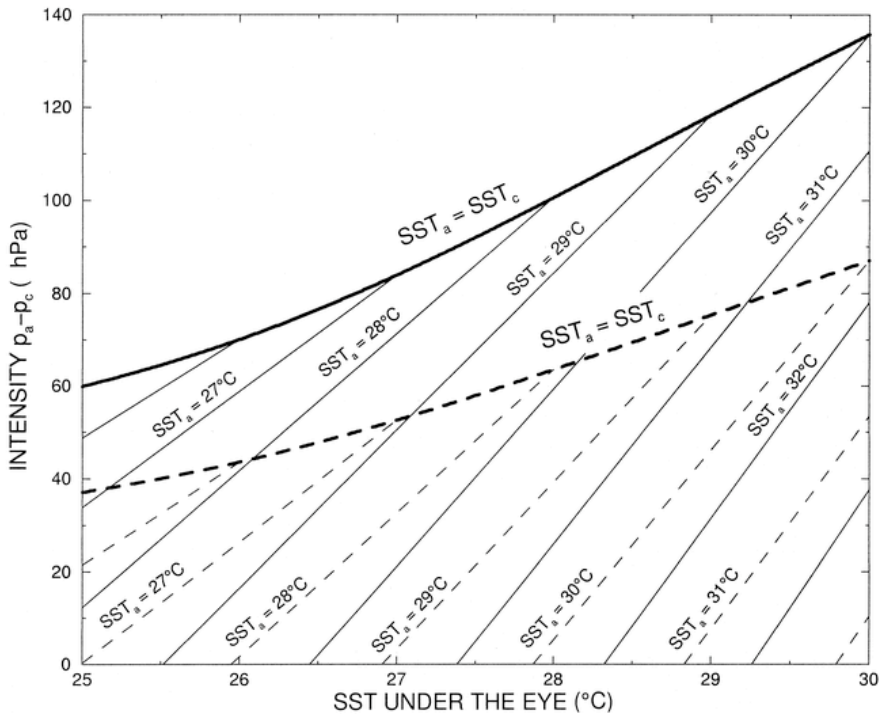

Figure 25: Tropical cyclone intensity change as a function of SST under the eye. The heavy solid and dashed lines correspond to the MPI that is realized without ocean feedback, when $SST_A = SST_{IC}$. The thinner solid and dashed lines correspond to ambient RH of 75% and 85% respectively. These thin lines connect points with the same ambient SST. (Schade, 2000.)

Cione et al. in their 2003 paper on sea surface temperature variability in hurricanes (referred to earlier in Chapter 3) used observational data from 23 Atlantic, Gulf and Caribbean hurricanes consisting of AXBT, drifting buoy observations, and HRD field campaign data to arrive at the following conclusions:

- The differences between SST_{IC} and SST_A (~0° to 2° C) are significantly less than the horizontal changes typically observed in the post-storm tropical cyclone wake environment (4° to 5° C)
- Relatively small changes in SST_{IC} can greatly alter the sea-air fluxes within the inner core region. SST changes of 1° C can lead to surface enthalpy changes of ~ 40%.
- For the observations in their study, the magnitude of the SST change ($SST_{IC} - SST_A$) is statistically linked to tropical cyclone intensity change. Storm that experience

lower levels of SST_{IC} cooling experience an increase in surface enthalpy flux and are more likely to intensify.

This paper (and its predecessor in 2000) present the most comprehensive observational study of the tropical cyclone boundary layer to date, although the results have been subject to much controversy regarding buoy sensor failure under high speeds and spray conditions. Barnes and Bogner (Barnes and Bogner 2001) substantiated the Cione et al. results with a study using 130 Omega dropwindsondes within 500 km of six Atlantic hurricanes. Three other very important (and controversial) results emerged from both of these observational studies. Inside of a 3.25° radius the observed low-level inflow:

- is not isothermal
- is not constant with respect to surface specific humidity
- is not in thermodynamic near-equilibrium with the sea.

These results are slowly being incorporated into the newer coupled atmosphere-ocean models.

In the same paper, Cione, Black, and Houston use the storm speeds, storm intensities, and upper-ocean thermal profiles from the observations to estimate the upper-ocean heat content (HHC), the energy extracted by the storm (Q_{H_ext}) as a function of tropical cyclone transit time, and the percentage of this energy utilized by the storm (Q_{H_util}).

4.2 Basis of flux calculations

In this study, the same measures of sea-air interaction will be calculated using the Cione et al. algorithm, incorporating remotely sensed values, observed values, and bulk parameterized values. The intent is to roughly estimate flux values for the case studies that follow in Chapter 7, in order to determine if ocean-atmosphere fluxes increase in convective burst time periods as compared to non-burst time periods. Although there is little hope of achieving exact magnitudes given the data input, fluxes should be estimated such that they will be comparable in a relative sense – "convective burst: more flux", "no convective burst: less flux."

There exist few precedent articles for using this approach. Miller and Katsaros (1992) estimated SSM/I derived surface latent heat fluxes in a study near a cyclone just before its period of rapid deepening. Mack and Wylie (1982) estimated the convective mass flux in three severe storm systems over Oklahoma. A few climate budget studies have estimated basin-wide or global fluxes (Kelly and Qiu 1995) (Bentamy, Katsaros et al. 2003). More recently, Pan et al. (Pan, Yan et al. 2004) have used combined satellite wind vectors, SSM/I, and AVHRR observations to estimate sensible heat flux in an ocean region east of Japan

where atmospheric convergence appears year-round. They use a relationship between wind convergence and sea level humidity and sea surface temperature to make the estimate. Their estimates compared favorably with fluxes in the same area retrieved from NCEP/NCAR Reanalysis data and the Goddard Satellite-Based Turbulent Flux.

The main difficulty in estimating these fluxes using remotely sensed data lies in the inability to adequately measure the sea level air temperature. In the previously mentioned paper by Cione et al. (2000) the authors fit a curve to their observed measurements of the sea-air contrast (SST_{IC}- T_A) given a radial distance, x:

$$SST_{IC} - T_A = 0.033x^3 - 0.114x^2 - 0.911x + 3.025\,, \qquad (3)$$

This polynomial best-fit curve has an R^2=0.401 and is valid for SST's of at least 27° C and surface wind speeds >13 m s^{-1} outside 0.75° radius of the storm center or >17.5 m s^{-1} inside 0.75° radius. This relationship is used as appropriate to estimate the sea-air contrast and to arrive at a value for the surface air temperature T_A in this study.

The 10-meter wind data used to calculate the fluxes herein was courteously provided by Christopher Hennon from a surface wind analysis system from HRD known as H*Wind (Powell 1990). The wind analysis incorporates all available surface weather observations (ship reports, buoys, coastal platforms, surface aviation reports, reconnaissance aircraft data adjusted to the surface etc.) This includes data sent by NOAA P3 and G4 research aircraft, the Stepped Frequency Microwave Radiometer (SFMR) measurements, all U. S. Air Force Reserves C-130 reconnaissance aircraft, and remotely sensed winds from SSM/I, ERS, QuickScat, TRMM and GOES. The data are composited relative to the storm center over a 4-6 hour period. The final product of the processed data is a gridded 10-m surface file with 6 km horizontal resolution. The output of two analyses from Hurricane Floyd (ATL 1999) is in Figure 31 and Figure 32 as examples.

For each storm for which H*Wind analyses are available, the fluxes are calculated as an annular average, centered on the storm center and at 0 - 0.5°, 0.5° - 1°, 1° - 1.5° and 1.5° - 2° radii.

4.3 Flux calculation algorithm

Given the storm speed, storm initial intensity, an SST and a radius – x, start with (3) above and rearrange to solve for T_A:

$$T_A = SST - 0.033x^3 + 0.114x^2 + 0.911x - 3.025 \quad (4)$$

Compute the inner-core enthalpy flux, Q_{core} using the standard bulk aerodynamic formulas:

$$\begin{aligned} Q_{core} &= Q_s + Q_L \\ &= \rho U\{c_p C_h (SST - T_A) + L_v C_e (r_{sst} - r_A)\} \end{aligned} \quad (5)$$

where ρ is the density of air, T_A is the air temperature at 10m, c_p is the specific heat of air at constant pressure, L_v is the latent heat of vaporization at a given T_A. U represents the 1-minute wind speed at 10 m. And r_{sst} and r_A are the saturation mixing ratio at the SST and the actual mixing ratio of the air at 10m, respectively. C_h and C_e are the dimensionless coefficients of heat exchange and moisture exchange at 10 m given by:

$$C_{H10} = C_{E10} = (a + bU_{10}) \times 10^{-3}. \quad (6)$$

The constants a and b are empirically determined constants that were derived under relatively high wind conditions (>20 m s^{-1}) where a=0.75 and b=0.067 (Garratt 1977) (Black, Elsberry et al. 1988). Q_{core} has units of Wm^{-2}.

Next estimate the upper ocean heat content (HHC) extracted by the storm, Q_{H_ext}, and the amount of upper-ocean heat content available to the system that is "utilized" by the storm, Q_{H_util}.

$$Q_{H\_ext} = Q_{core} TC_{transit-time} \quad (7)$$

$$Q_{H\_util} = Q_{H\_ext} / Q_H, \quad (8),$$

where $TC_{transit\text{-}time}$ is the time in seconds for a storm to travel the inner-core diameter (120 km). Q_H is the upper-ocean heat content as defined in Chapter 3 by Leiper and Volgenau and provided by the same source as in the previous chapter, the U.S. Naval Research Lab at Stennis Flight Center.

The analyses and estimates for this study focus on conditions near the inner-core region (0 – 60 km from the storm center) however the fluxes were calculated for each of four

annuli around the tropical cyclone: 0° to 0.5°, 0.5° to 1°, 1° to 1.5°, and 1.5° to 2° radial distances.

4.4 A numerical example

In this example calculation the following conditions are given:

SST_{IC} = 28° C = 301.15 K

T_A = 25.5° C = 298.65 K

Q_H = 7.5 x 10^8 J m^{-2}

p = 980 mb – 98,000 h Pa

U_{10} = 35 m s^{-1}

storm speed = 5 m s^{-1}

radius of interest, x = 0.5°.

First, calculate the surface air temperature, T_A:

$$T_A = SST - 0.033x^3 + 0.114x^2 + 0.911x - 3.025$$

$$T_A = SST - 0.033(.5)^3 + 0.114(.5)^2 + 0.911(.5) - 3.025$$

$$= 2.55° \text{ C} = \underline{275.7 \text{ K}}$$

Now estimate the heat and moisture exchange coefficients:

$$C_{H10} = C_{E10} = (.75 + 0.067U) \text{ x } 10^{-3}$$

$$= \underline{3.095 \text{ x } 10^{-3}}$$

Estimate L_v at T_A:

$$L_v = 2.501 - (2.361 \text{ x } 10^{-3})\ T_A$$

$$= 2.501 - (2.361 \text{ x } 10^{-3})\ (25.5)$$

$$= \underline{2.44 \text{ x } 10^6 \text{ J kg}^{-1}}$$

Calculate r_{sst} and r_A using the water vapor pressure for the SST and then for T_A:

$$e_{sst} = 610.7Pa \times e^{-\frac{L_v}{R_v}\left(\frac{1}{SST} - \frac{1}{273.16K}\right)}$$

where R_v is the gas constant for water vapor = 461.5 J kg^{-1} K^{-1}.

$$e_{sst} = 610.7Pa \times e^{-\frac{2.44x10^6}{461.5}\left(\frac{1}{301.15K} - \frac{1}{273.16K}\right)}$$

$$e_{sst} = \underline{\underline{3{,}685.72\,Pa}}$$

and

$$e_{T_A} = 610.7\,Pa \times e^{-\frac{2.44\,x10^6}{461.5}\left(\frac{1}{298.65\,K}-\frac{1}{273.16\,K}\right)}$$

$$e_{sst} = \underline{\underline{2{,}983.15\,Pa}}$$

then

$$r_{SST} = 0.622 \times \frac{3{,}685.72}{98{,}000 - 3{,}685.72} = \underline{\underline{.0243}}$$

and

$$r_{T_A} = 0.622 \times \frac{2{,}983.15}{98{,}000 - 2{,}983.15} = \underline{\underline{.0195}}$$

now calculate Q_s and Q_L:

$Q_s = \rho\ U_{10}(c_p\ C_{H10}(SST\text{-}T_A))$

ρ = air density = 1.22 kg m^{-3}

c_p = 1,850 J kg^{-1} K^{-1}

Q_s= (1.22)(35)(1,850)(3.095 x 10^{-3})(2.5)

= <u>611.22 W m^{-2}</u>

and

$Q_L = \rho\ U_{10}(L_v\ C_{E10}(r_{sst}\text{-}r_{TA}))$

= (1.22)(35)(2.44 x 10^6)(3.095 x 10^{-3})(.0048)

= <u>1,547.8 W m^{-2}</u>

Finally,

$Q_{core} = Q_s + Q_L$ = <u>2,159.02 W m^{-2}</u>

$TC_{transit\text{-}time}$ = distance/rate = 120,000 m / 5 m s^{-1} = <u>24,000 s</u>

$Q_{H\_ext} = Q_{core}$ x $TC_{transit\text{-}time}$ = 2,159 x 24,000 = <u>5.18 x 10^7 J m^{-2}</u>

$Q_{H\_util} = Q_{H\_ext}/Q_H$ = 5.18 x 10^7/ 7.5 x 10^8 = .0691 x 100 = <u>6.91%</u>.

In other words, the magnitude of the upper-ocean energy extracted by the storm in the inner core region (5.18×10^7 J m^{-2}) is about 7% of the upper-ocean energy available to it. Most hurricanes utilize less than 10% of the available energy. (Cione et al., 2003) The mean Q_{H_util} of the time periods in this study for which it was calculated (n=92) was 8.6%.

4.5 Results of the flux calculations.

Figure 26 shows the mean flux values for all time periods in the study when the H*Winds analysis was available. Agreement is tolerable with the observational data set of Cione et al. Their mean latent heat flux from 0° to 0.75° latitude was 1108 W m^{-2} (std. dev = 482) and sensible heat flux for the same region was 220 W m^{-2} (std dev. = 139). The summary statistics for Q_L, Q_S, Q_{core}, Q_{H_ext}, and Q_{H_util} are given in Figure 30. The magnitudes seem to fall in the appropriate ranges but with high variability and compare with those of Cione as in Figure 29.

The mean Q_{h_util}, also shown in Figure 26, is 8.6% near the inner-core of the tropical cyclone. This percentage of the total enthalpy utilized by the tropical cyclone decreases to about 3.1% at 2° radius from the storm center. This distribution of energy utilization is consistent with the hypothesized importance of convective bursts and inner-core boundary layer fluxes. These results agree with the results of Cione et al. (2003) that most tropical cyclones utilize less than 10% of the energy available to them.

For the hypothesized energy flow to be validated, the enthalpy flux during convective burst event should be greater than during a non-convective burst event. A comparison of Figure 27 and Figure 28 show this to be the case. Both the total enthalpy flux and the energy utilization percentage (Q_{H_util}) are at least double for the time periods with a convective burst. In fact, the Q_{H_util} for the convective burst time periods averages 11.7% while the utilization is only 2.7% for the non-convective burst time periods.

These flux calculations are highly dependent on the surface wind speed and the surface air temperature. The tropical cyclone's translation speed, in effect the "dwell rate" of

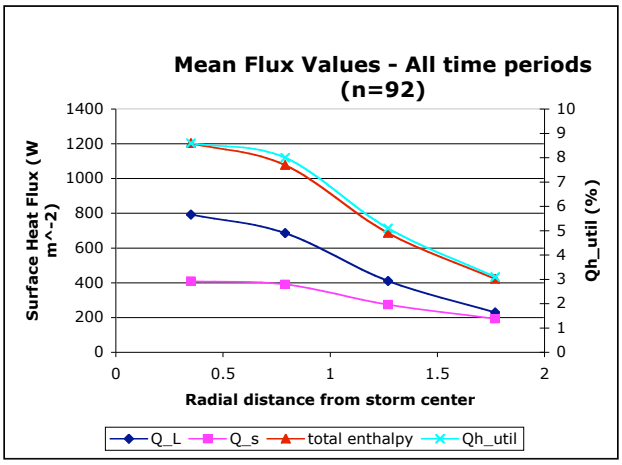

Figure 26: Mean flux values calculated for all time periods, CB and non-CB.

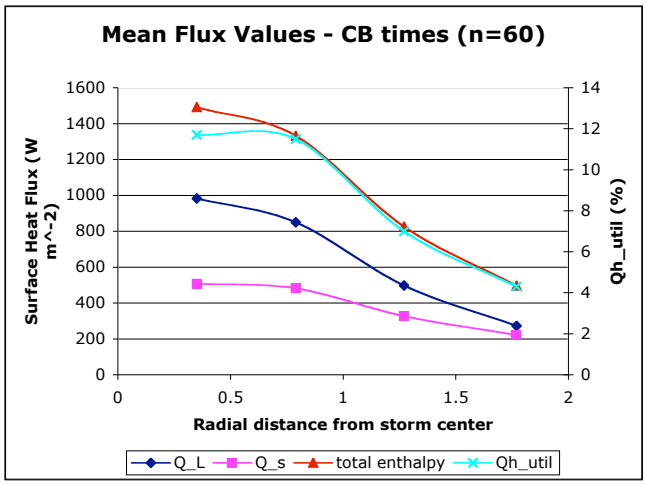

Figure 27: Flux calculations for the time periods with a convective burst.

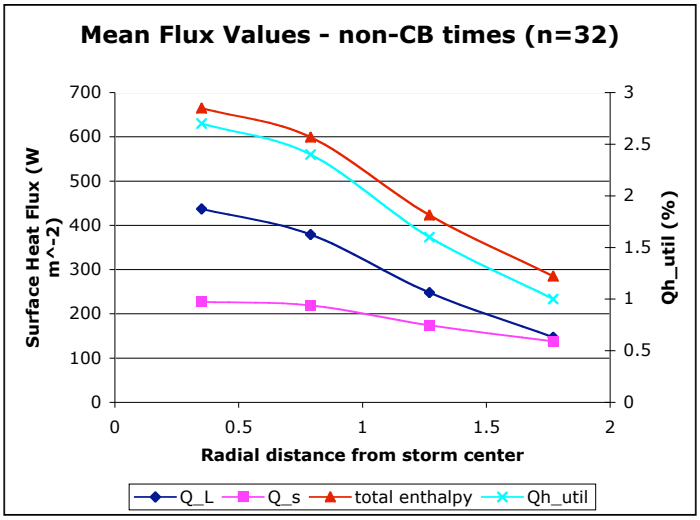

Figure 28: Mean flux values for time periods with no convective burst present.

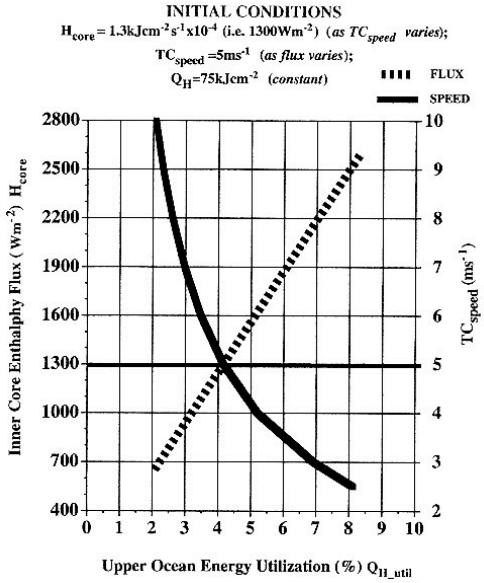

Figure 29: Example flux calculation results from the observational study of Cione et al. (2003).

Descriptive Statistics

	N	Minimum	Maximum	Mean	Std. Deviation
1Ql	92	28.33221773989	3367.716264 29	793.5171775853 39	592.9788455256 430
1Qs	92	15.46985957922	1688.435343 90	410.5042 56001391	295.113222 4939322
1Qcore	92	43.80207731911	5056.15160818	1204.021 43358673	887.7736264193670
1Qh_ext	92	300528.8323781	18723 6002.74 7	38710170.4845257	390 03248.24276 321
1Qh_util	92	.000340532867	.553784819941	.085 87027394189	.1080654 3582 3779
2Ql	92	63.95214472497	1706.0 2136424	686.5823 14660896	433.7859994761 260
2Qs	92	41.21172228376	908.47 1108926	391.0005 71982108	222.1924943915615
2Qcore	92	105.1638670087	2539.2 0358066	1077.582 88664300	653.0396655623440
2Qh_ext	92	627268.6526901	19128 4364.524	33169601.6634671	296 15142.56582872
2Qh_util	92	.000541924849	.929173999500	.08047765658654	.1252710 7428 8231
3Ql	92	62.85640661589	1018.1 7259161	411.7281 30853112	251.2514577550 116
3Qs	92	51.42524411682	778.04 2664741	274.4308 00264688	154.7370917955609
3Qcore	92	114.2816507327	1796.2 1525635	686.1589 31117800	395.5779539907394
3Qh_ext	92	605309.4977568	10766 4044.994	20458591.6552819	171 70003.56350568
3Qh_util	92	.0005229 5337	.5229 8383895	.0514754399443	.07622364194831
4Ql	92	45.30467282145	575.73 4612263	229.7410 23195738	139.2754909098563
4Qs	92	51.70165049239	614.74 7705153	193.4133 82774644	115.0692058845116
4Qcore	92	97.00632331384	1190.4 8231742	423.1544 05970382	236.0976109678812
4Qh_ext	92	936563.7097990	60256095.710 8	12326714.8588229	100 74740.85435521
4Qh_util	92	.000809138389	.292697197627	.03148130946667	.0457372 0801 2412
Valid N (listwise)	92				

Figure 30: Descriptive statistics of the flux calculations in this study. The prefix "1"stands for 0°-0.5° radius, "2" for 0.5°-1°, "3" for 1°-1.5°, "4" for 1.5°-2°.

4.6 Summary

The discriminant analysis procedures in the previous chapter emphasized the importance of a comparatively warmer ocean for convective burst existence. In particular, the mean HHC was double for the convective burst time periods. Given the results of the flux calculations in this chapter, that any given storm utilized only 8% on average of the available energy, the existence of twice the HHC during convective burst times seems contradictory. However, the storms with no convective burst experienced increased inner-core wake cooling, presumably from increased mixing, upwelling, etc. Thus, the thermal structure (i. e. depth) of the mixed layer, not just the "amount" of energy contained in the pool of warm water seems to be relevant. In their 2003 study, Cione et al. found that storms that experience lower levels of inner-core SST cooling experience an increase in surface enthalpy flux and are more likely to intensify. The results of this study corroborate their results.

The flux calculations in this chapter show that time periods in tropical cyclones experiencing a convective burst event do in fact exhibit enhanced surface energy fluxes. Convective burst time periods have total enthalpy fluxes two times the magnitude than the fluxes during non-burst time periods. The convective burst periods also show twice the energy utilization (Q_{H_util}) than storm periods without convective bursts.

The flux calculations computed in this section will be used in the case study analyses in Chapter 7. Although the magnitudes of the fluxes themselves may be over-dependent on the assumed values of the surface air temperature and the mean surface wind speeds used in the estimation process, comparison of their relative magnitudes should be sufficient for the case study analysis.

The inner-core energetics of tropical cyclones with convective bursts are compared with the energetics of tropical cyclones without convective bursts in the next chapter. The vertical profiles of latent energy release from TRMM overpasses provide estimates of the magnitudes of the differences. The energy flow hypothesized by this study purports the enhanced sea-air fluxes calculated using the methods of this chapter should be apparent in the case studies presented in Chapter 7 whenever a convective burst occurs. These enhanced fluxes should be associated with enhanced latent energy release and perhaps with an increased temperature anomaly in the tropical cyclone eye (as examined in Chapter 6.) The influence of enhanced fluxes may or may not be immediately apparent in the case study time series analyses, but should appear within the convective timescale of 12 to 36 hours.

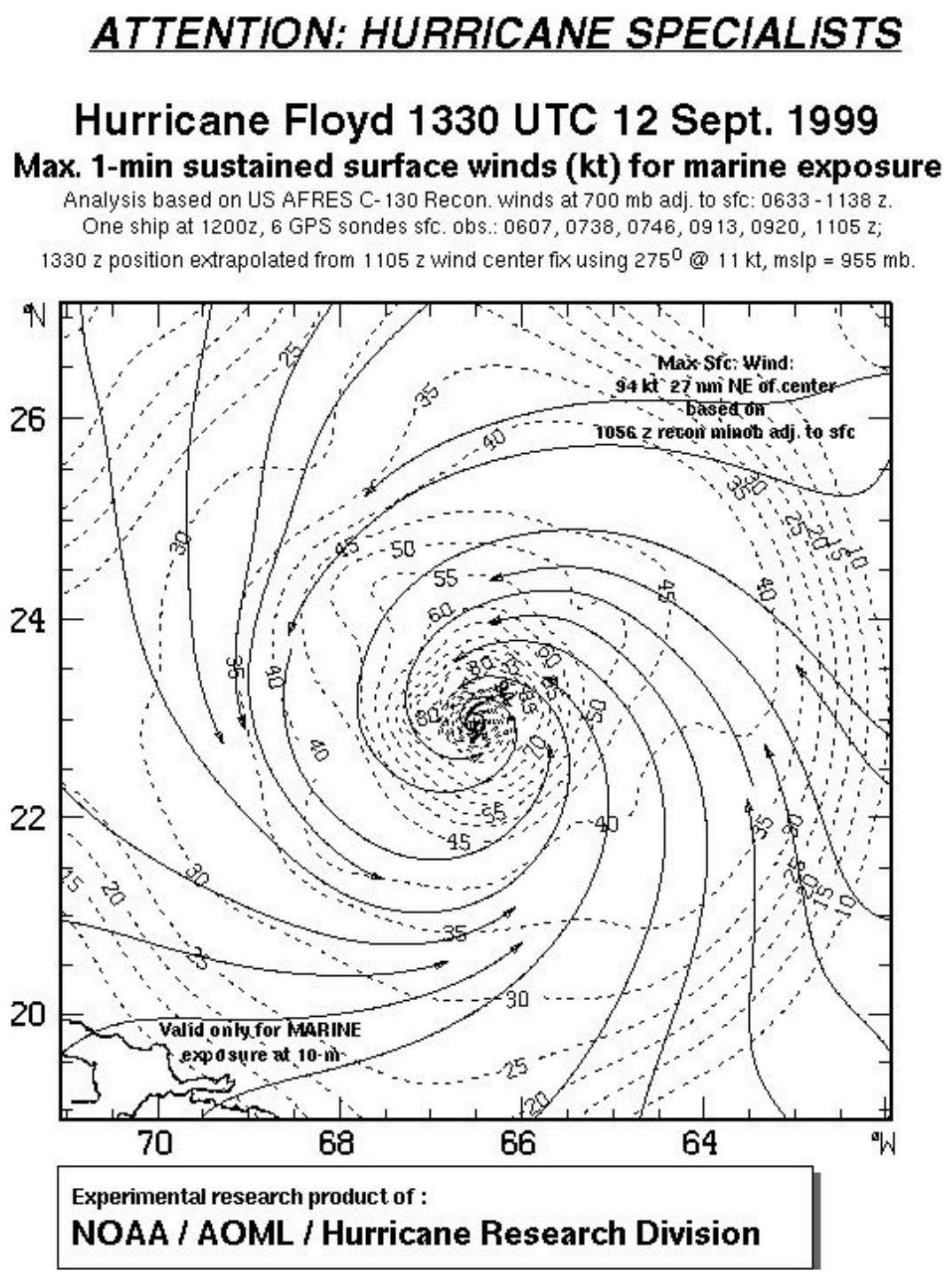

Figure 31: Final H*Wind analysis of Hurricane Floyd (ATL 1999) 9/12/1999.

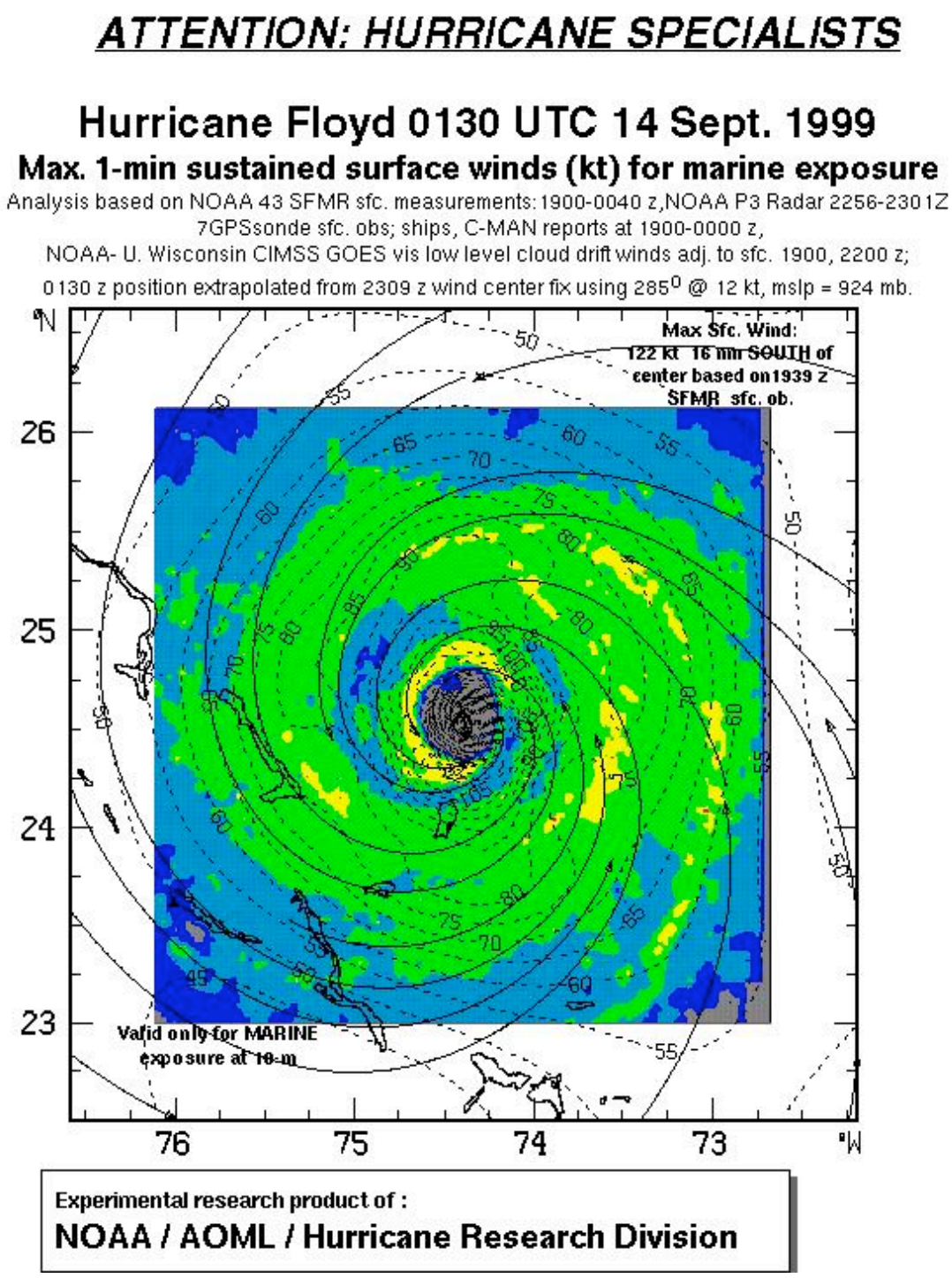

Figure 32: Final H*Wind analysis of Hurricane Floyd (ATL 1999) on 9/14/1999 during an eyewall replacement cycle.

CHAPTER 5
CONVECTIVE BURST ENERGETICS

Any enhancement of sea-air fluxes, as estimated in the previous chapter, should be apparent as enhanced upper-level latent energy release if the hypothesized energy chain in Figure 33 is viable. To test this hypothesis vertical profiles of latent energy release from TRMM are examined by building composite profiles based on convective burst activity. Three composite profiles are constructed:

- time periods with a convective burst with concurrent wind speed increase of at least 15 kt.
- time periods with a convective burst with little concurrent wind speed increase of 0 to 15 kt.
- time periods with no convective burst present.

The non-convective burst time periods occur during the intensification phase of the storm (where a convective burst event is most likely to occur.) These profiles are compared and presented at the end of this chapter.

5.1 Storm energetics

Rodgers et al. (Rodgers et al. 1998, Rodgers and Pierce 1995, Rodgers et al. 1994 a, b) and Heymsfield et al. (2001) have documented the cloud microphysics and energetics of several tropical cyclones from satellite data in case studies. Results from these case studies suggest that an increase in eyewall/inner-core latent heat can be enhanced by either 1) the inward propagation of convective rainband cycles or 2) the generation of a convective burst. The presence of either of these phenomena may spur a period of tropical cyclone intensification as long as the low to mid-troposphere is inertially stable enough to resist gravity waves that would carry the increased latent energy away from the storm center.

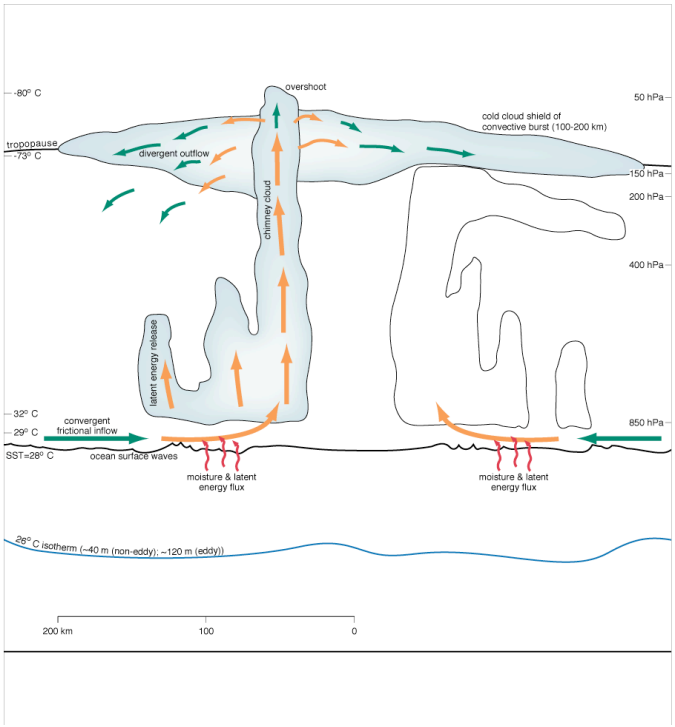

Figure 33: The convective burst may be efficient at mining the enhanced boundary layer fluxes and channeling this increased energy into the mid-upper tropospheric levels, eventually seen as increased latent heat of condensation.

In 2000, Rodgers et al. (Rodgers et al. 2001) studied the environmental forcing mechanisms of Supertyphoon Paka's latent heat structure using rain rate and latent heat release observations from SSM/I and TRMM imagery. The authors detected the following inner-core conditions during convective burst events:

- increased rain rates
- convective processes dominated the latent heat production
- large amounts of latent heating penetrated deeper layers of the troposphere
- the eyewall became more symmetric, propagated inward, and had more lightning.

In an attempt to generalize these observations from convective bursts in a single storm, Paka, to characteristics of any typical convective burst event, this study examines the vertical latent heating profiles from many time periods from the 31 storms listed in Table 22.

Name	Category	Basin	Year	Burst?
Alberto	3	ATL	2000	no
Nadine	TS	ATL	2000	no
Flossie	2	EPAC	2001	no
Olga	1	ATL	2001	no
Karen	1	ATL	2001	no
Alda	1	SHEM	1999	no
Beatriz	3	EPAC	1999	no
Cindy	4	ATL	1999	yes +15
Floyd	4	ATL	1999	yes +15
Gert	4	ATL	1999	yes +15
Lenny	4	ATL	1999	yes +15
Isaac	4	ATL	2000	yes +15
Carlotta	4	EPAC	2000	yes +15
Damrey	5	WPAC	2000	yes +15
Saomai	5	WPAC	2000	yes +15
Erin	3	ATL	2001	yes +15
Bilis	5	WPAC	2000	yes +15
Jose	2	ATL	1999	yes <15
Florence	1	ATL	2000	yes <15
Hilary	1	EPAC	1999	yes <15
Aletta	2	EPAC	2000	yes <15
Chantal	TS	ATL	2001	yes <15
Kate	1	WPAC	1999	yes <15
Wukong	2	WPAC	2000	yes <15
Dalila	1	EPAC	2001	yes <15
Gil	2	EPAC	2001	yes <15
Ana	TS	ATL	2003	no
Cristobal	TS	ATL	2002	no
Keith	4	ATL	2000	yes +15
Isidore	3	ATL	2002	yes +15
Lili	2	ATL	2002	yes +15

Table 22: Storms used in the compositing process to build typical latent heating profiles for convective burst and non-convective burst cases. The last column “Burst?” indicates whether or not a storm had at least one convective burst episode, and the degree of intensification (in knots) that took place concurrently.

Of the 118 observed time periods in these 31 storms, 25 were time periods in storms with no convective burst event, 58 observations were during a storm with a convective burst with significant concurrent intensification (wind speed increase of ≥ 15 kt), and 35 observations occurred during a storm with a burst event that did not precede significant intensity increase (wind speed change < 15 kt). The individual vertical latent heating profile for each storm for each time period that data is available is calculated. The TRMM overpass closest to the time of a convective burst was chosen (typically no lag was longer than 15 minutes.) Since most tropical cyclones have at least one convective burst event, the composite profile of non-convective burst events includes TRMM overpasses in tropical cyclones that have had a convective burst event either very early or very late in the storm life cycle. This convective burst period must not have occurred within 72 hours of the TRMM overpass being included as a non-burst period. From these individual profiles, a composite for each of the three groups (no convective burst, burst with little change, burst with intensification) is presented. A comprehensive list of the storms included in the composites, the date and time of the TRMM overpass, and the group membership of that overpass is included in the Appendix.

5.2 SSM/I latent heating profiles from GPROF

The latent heating profiles themselves are derived from TRMM passive microwave observations using a combined radar-radiometer (TRMM precipitation radar (PR) and thematic-mapper imagery-(TMI)) retrieval algorithm (Grecu and Olsen, 2005). The estimation of rain rates and latent heating based on satellite passive microwave observations is well established (Kummerow et al. 1996, 2001), Olsen et al. (1996, 1999, 2005) and Grecu and Olsen (2005, accepted). In a very simplified explanation, a TRMM swath like Figure 34 is processed in the following manner:

- A large set of brightness temperature observations are associated with precipitation profiles using coincident TMI-PR retrievals
- the PR precipitation profiles are associated to latent heating using cloud model simulations (from the Goddard Cumulus Ensemble.) which function like a look-up table.

The relationship between the precipitation total and the latent heating vertical profile is:

$$\int_0^{Z_{top}} \rho LH \, dz = \frac{L_v}{c_p} \frac{rr}{3600},$$

where Z_{top} is the highest cloud top height, ρ is the density of air, LH is the latent heating, L_v is the latent heat of vaporization, c_p the specific heat of air at constant pressure, and rr is the estimated rain rate. (Bill Olsen, personal communication). Figure 35 illustrates this estimation process in a basic way.

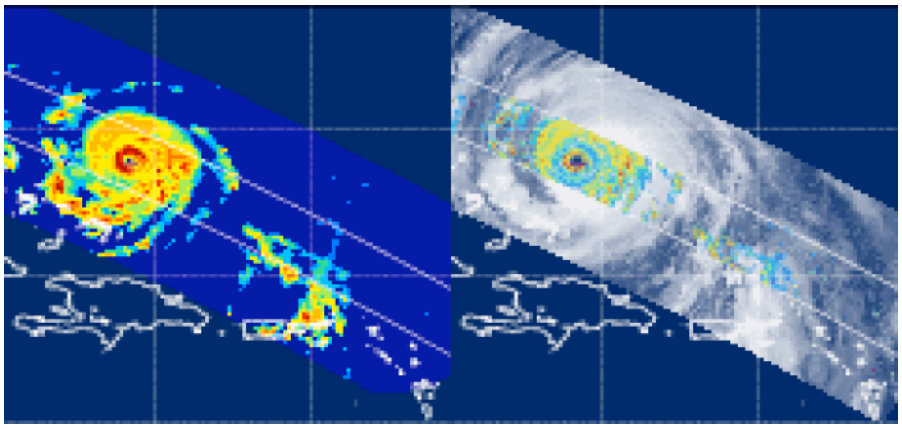

Figure 34: TRMM TMI IR image (left) and PR image (right) for Hurricane Floyd 09/13/1999 at 09:32z. The TMI sensor is passive and the precipitation radar is active.

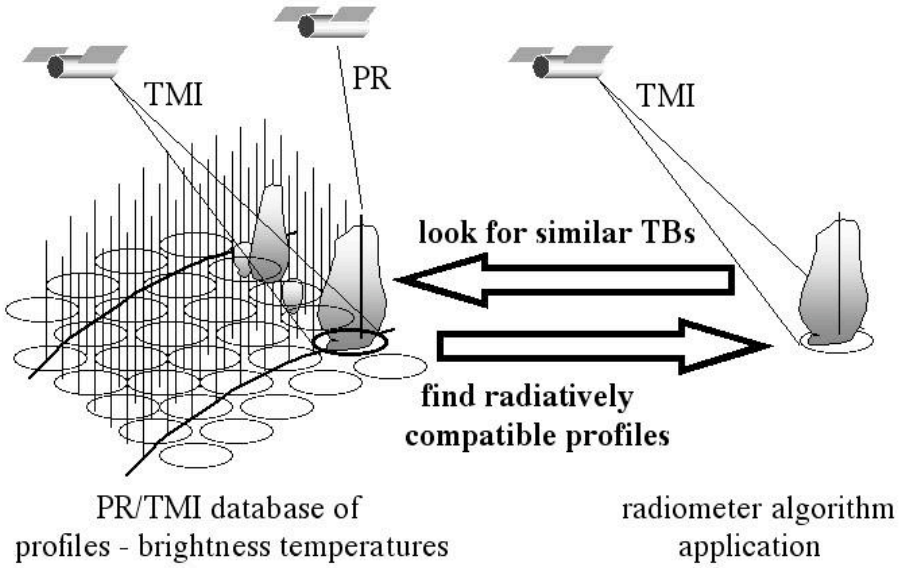

Figure 35: Basic explanation of the combined active-passive (PR-TMI) Bayesian methodology for estimating rain rates and latent heating. (Grecu and Olsen, 2005).

The latent heating profiles are calculated for the convective rainfall fraction of the pixels, the stratiform fraction of the pixels, and the total raining pixels. All three parameters are retrieved at a horizontal resolution of 12.5 km × 12.5 km. The sum of the "raining pixels" – technically a unitless index value of all of the brightness temperatures in any given overpass—will be used later in the case study section of this study as a proxy for "rain rate." Mirceau Grecu and Bill Olsen of NASA Goddard Space Flight Center graciously provided the algorithm output for the profiles presented below.

5.3 Composite profiles of latent heating

The composite profiles in Figure 36, Figure 37, and Figure 38 show a two-fold increase in energy release for the storms with convective burst events compared to storms with no convective burst event. In each case, the storms with convective bursts but very little change in storm intensity are also significantly more energetic than those with no burst event. The magnitude of the latent heating for this group is only slightly less than for the "convective burst with significant strengthening" group. This latent heat release enhancement seen in the convective burst cases implies increased buoyancy and upward vertical motions in the

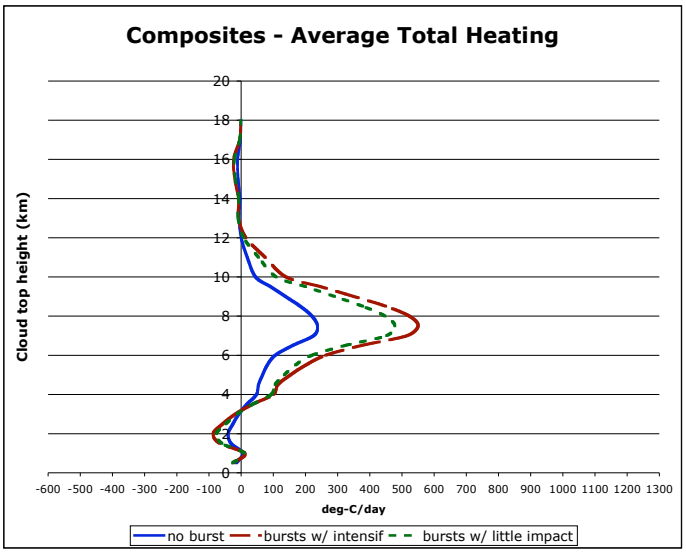

Figure 36: Composite latent heating profile for total heating.

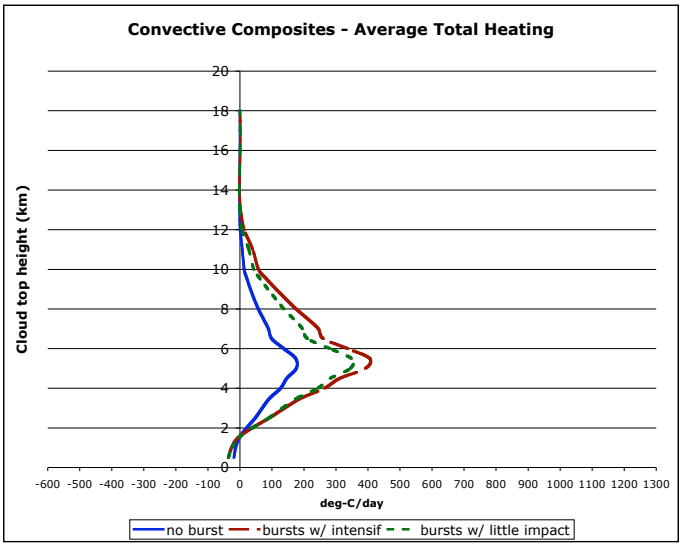

Figure 37:Composite latent heating profile for the convective fraction of the pixels in the TRMM observation. The convective rain fraction is associated with significant cloud updrafts and downdrafts like those in hot towers throughout the eyewall region or in intense rainband convection.

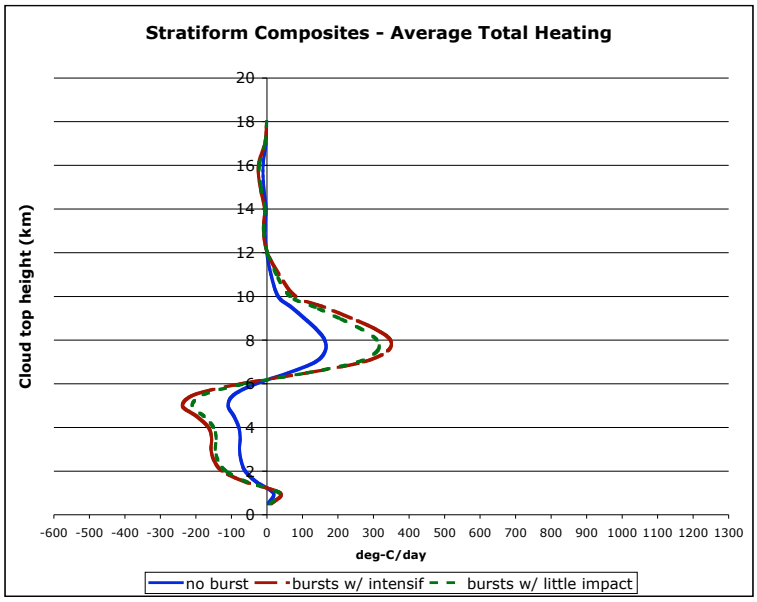

Figure 38: Composite latent heating profile for the stratiform convective fraction – typically outside the eyewall region.

mid- upper-tropospheric eyewall regions perhaps in response to increasing ice microphysical processes (Rodgers, 1998, 2000).

The distribution of this enhanced latent heating may help tropical storm intensification by enhancing the secondary circulation by generating enough upward motion to compensate for the cyclonic angular momentum lost to surface friction and tropospheric outflow. This enhanced buoyancy and upward vertical motion increases the ability for subsidence warming into the eye to occur as more energetic air reaches higher levels inside the eyewall. The enhanced energy of the upward moving air should increase the magnitude of the energy released in subsidence and converted to warming through the latent heat of condensation as well.

5.4 Summary

The composite vertical profiles of latent energy demonstrated the large magnitude increase (double the magnitude) in energy that accompanies convective burst events. Prior to this study, this observed enhancement in latent energy had been shown for only a handful of time periods in tropical cyclones.

The doubling of latent energy release seen in the profiles of convective burst time periods most probably reflects the twofold total enthalpy flux calculated for time periods with convective bursts as calculated in Chapter 4. The increased fluxes provide increased moist static energy which powers the hurricane heat engine through a series of transformations involving latent energy, increase in geopotential and sensible heating in adiabatic processes.

As discussed in the beginning of this chapter, convective rainband cycles may be another mechanism for enhancing rain rates and latent energy transfer. Convective bursts and convective rainband cycles do not necessarily exist in opposition. Both are vehicles for strengthening inertial stability by decreasing the Rossby radius of deformation so the increased latent heating can impact the storm.

The next chapter will investigate the fate of the enhanced latent energy generation. Can it be transformed into warming which subsides in the eye of the tropical cyclone to increase and maintain the warm anomaly?

CHAPTER 6
THE ENERGETICS: INSIDE THE EYE

Shortly after the NASA TRMM satellite was launched, its precipitation radar captured an intense convective burst episode in Hurricane Bonnie (ATL, 1998). The resulting imagery was astounding as this was the first time a satellite image was able to "see beneath" the cirrus shield and other clouds to reveal the precipitation structure of a hurricane. This "first image" of a convective burst from space-borne radar is shown in Figure 39.

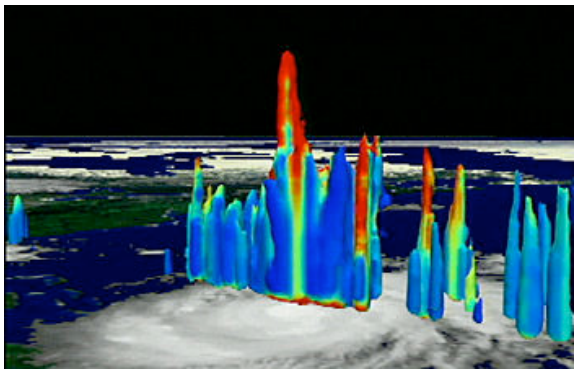

Figure 39: First visualization of a convective burst in Hurricane Bonnie (ATL 1998) from TRMM. The height of the convective towers in this image (max 18 km.) is exaggerated for clarity. Colors correspond to precipitation from blue (light) to red (heavy). (Image by Greg Shirah, NASA/GSFC Scientific Visualization Studio).

The vertical profiles of latent energy release used to build the composite profiles in the previous chapter were calculated for each TRMM overpass for each storm in Table 22 for which sufficient data existed. These individual profiles will be useful in the case study analyses to monitor the energetics of each stage in a particular storm's lifecycle. In an attempt to establish a link between the enhanced upper tropospheric latent energy release to the

enhancement of the warm anomaly in a tropical cyclone's eye, the Advanced Microwave Sounding Unit (AMSU) tropical cyclone temperature anomaly output will be examined for each case study. If an enhanced warm anomaly appears within a reasonable convective timeframe of 12 to 24 hours, this will lend credence to the hypothesized energetics chain pictured once again in Figure 40.

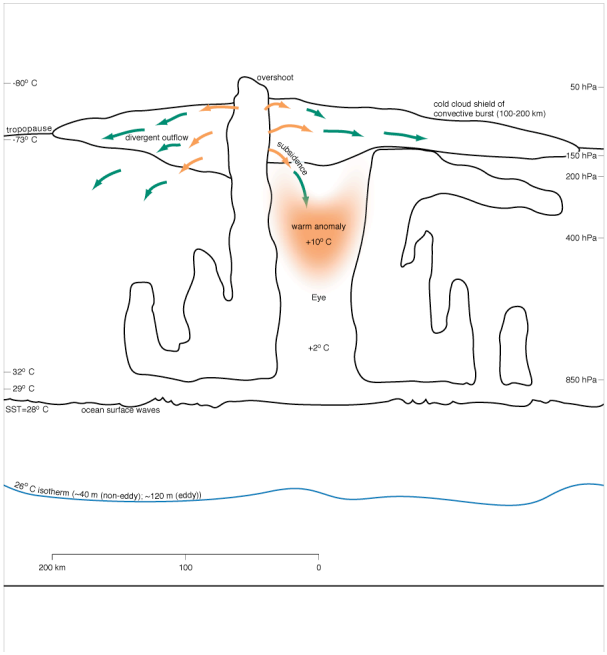

Figure 40: The enhanced upper tropospheric latent energy is transformed into adiabatic warming as the air slowly subsides in the eye of the tropical cyclone, increasing and maintaining the warm core of the tropical cyclone. This warming, drier subsiding air along the inside edge of the hurricane eyewall leads to surface pressure decrease and eventually an increase in tangential wind velocities.

6.1 Hurricane Bonnie

In a 2001 paper focusing on the convective burst in the eyewall of Hurricane Bonnie, Heymsfield et al. provided detailed observations from the 1998 Convection and Moisture Experiment-3 (CAMEX-3) on the structure of this convective burst including observations within the hot towers and the convective-scale updrafts and downdrafts. The authors found observational evidence of strong convective downdrafts, on the order of several meters per second, along the inside edge of the eyewall. This downward flow subsided approximately 10 km downward and 20 km horizontally into the eye of the hurricane. Observations from the NASA ER-2 Doppler Radar (EDOP), (Heymsfield et al., 2001,their Figure 7) emphasizing the inside of the upper eye in the area near the intense eyewall convection and the subsidence in this region is shown in Figure 41. In this figure white traces show vertical velocities, black traces are θ_e from the DC-8 flight level data. White reflectivities exceed 8 m s^{-1}. Black reflectivities are less than –8 m s^{-1}. The pennant wind barb stands for 25 m s^{-1}, the flag, 5 m s^{-1}, and a half flag, 2.5 m s^{-1}. The "S" indicates the subsidence region. The white dotted line in the top panel shows an area of low reflectivity stratospheric air intrusion. Note the strong (> 10 m s^{-1} vertical velocities) in the eyewall with high (> 50 dBZ, white) reflectivities in the lower panel. Upward motion this strong with high reflectivity suggests dense graupel or small hail are falling from about the freezing level down to about 6 km. The authors suggest that the stratospheric penetration of the vigorous convective tower initiated subsidence of dry air. This subsidence is then enhanced as it entrains moist cloudy air from the updraft down along the inner edge of the tropical cyclone eye. Malkus (1958) first proposed this detrainment from the convective updraft into the region of subsidence. Marks (1992) and Stossmeister and Barnes (1992) found other observations of downdrafts along the inner edge of the hurricane eyewall. Emanuel (1997) and Liu (1999) modeled the feedback effects from this subsidence/eyewall detrainment.

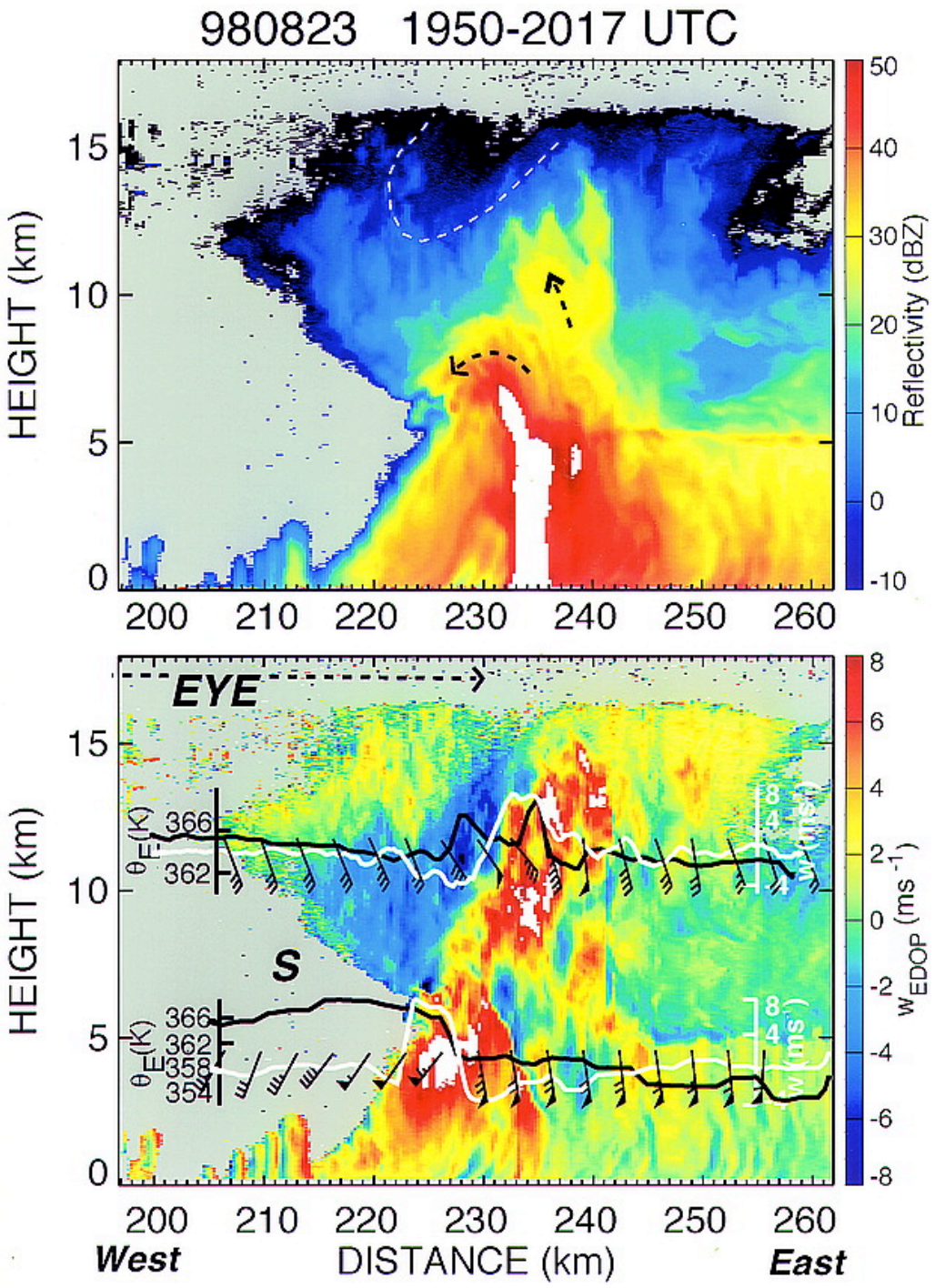

Figure 41: EDOP reflectivities and vertical velocities during a flight line sampling the upper portion of the "chimney cloud" in TC Bonnie's convective burst. (from Heymsfield et al, 2001, Figure 7).

6.2 Tropical cyclone eye temperature anomalies from AMSU

The existence of this region of subsidence and the plausibility of detrainment of the warm moist cloud air from the convective updraft supports the hypothesis that convective bursts are capable of mining the boundary layer fluxes and transferring energy deep into the troposphere. From there it can warm the upper levels through latent heats of condensation and subsidence-induced warming of the eye.

In fact, Velden et al. (1999) confirmed that significant warming took place through the deep layer of the eye of Hurricane Bonnie using data from the Advanced Microwave Sounding Unit (AMSU). See Figure 42. The AMSU temperature retrievals from Bonnie compare favorable with the flight level data from CAMEX-3.

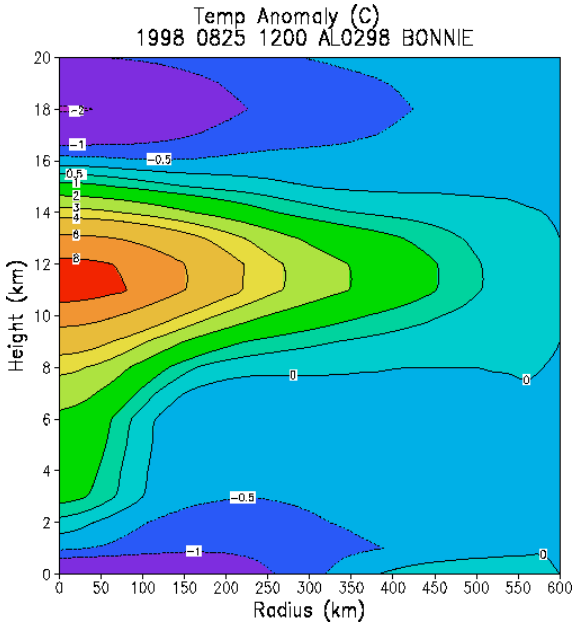

Figure 42: AMSU temperature anomaly showing 8° C of anomalous warming in the eye of Hurricane Bonnie (1998).

The NOAA-15, 16, and 17 Polar Orbiting Satellites carry AMSU instruments. The horizontal resolution is about 50 km near nadir and about 100 km on the limbs. Despite the limited resolution, AMSU provides structure information not available from any other platform. In addition to temperature anomalies, AMSU analyzes gradient winds, surface pressure, and cloud liquid water. Like the TRMM precipitation radar, clouds are nearly transparent to the microwave bands of AMSU. The temperature retrieval algorithm

(Goldberg, 1999) is used to determine the temperature at 40 pressure levels from .01to 1000 hPa. The temperatures at 23 levels from 50 to 920 hPa are used to generate the tropical cyclone temperature anomaly product. The retrieved temperatures are azimuthally averaged at each vertical level from 0 to 20 km, with a 600 km radius around the storm. The temperature at the radius of 600 km at each level is then subtracted to give the anomaly. Mark DeMaria of CIRA at Colorado State University courteously provided the AMSU data for these case studies.

6.3 Convective bursts and warm core temperature anomalies

The connection between convective burst events and tropical warm core sustenance/enhancement and subsequent intensification has been the subject of much research. The roles of subsidence, detrainment, and the effects of these mechanisms on the thermal structure of the tropical cyclone eye are still being debated. One very plausible hypothesis by Willoughby (1979, 1990, 1995) is readily applicable to the chain of energetics hypothesized by this study. Subsidence is distributed over a wide area outside of the eyewall but is concentrated in a small area inside the eye itself. As the air subsides, adiabatic warming takes place and the air dries. Detrainment of moist cloudy air from the eyewall convection may occur as well. Since the adiabatic warming is stronger inside the eye, a sharp contrast in pressure develops as the pressure inside the eye decreases. The tangential winds increase due to this increased pressure gradient.

In the case of a convective burst, the extreme height of the overshooting cloud tops and the upward motion necessary to maintain this convection may allow for even more adiabatic warming than usual to occur as air slowly subsides along the inside edge of the hurricane eyewall for a longer period of time. The subsiding air may slowly descend at an average rate of centimeters per second. Given the height of the convective towers present in a convective burst event – 12 to 18 km – the effects of the enhanced latent energy release may not be seen in a warm core temperature anomaly for 12, 18, 24 or even 36 hours. As such, a time lag between the convective burst's enhancement of energy delivery and tropical cyclone intensification may be observed.

In an attempt to relate the vertical profiles of latent energy from TRMM presented in the last chapter and the convectively induced eyewall subsidence discussed earlier in this chapter, timelines of imagery will be constructed for each of the case studies to be presented in the next chapter. Each timeline will juxtapose the latent energy profile with a near time coincident AMSU temperature anomaly. If time coincident warming accompanies the

increase in upper tropospheric latent heating, remembering that a lag may occur, the final link of the energetics hypothesis chain may be established.

CHAPTER 7
CASE STUDIES

7.1 The energy chain

The last four chapters introduced the major parts of the hypothesis chain this study attempts to link:

⇒ enhanced surface convergence and/or sea-air fluxes establish a favorable environment

⇒ a convective burst event occurs

⇒ sustained upper tropospheric energy release occurs

⇒ subsiding air leads to an upper level warm anomaly.

The rest of the chain will be linked when it can be shown that this warm anomaly leads to hydrostatic adjustment and surface pressure fall as the storm's intensity increases.

In the discriminant analysis section of this study the following characteristics typifying a convective burst environment emerged:

- a good supply of moist air in the ambient environment
- lower tropospheric convergence near the storm (200 km)
- warm ocean temperature structure
- low wind shear
- a larger scale (600 km radius) well mixed, fairly stable mid troposphere
- a slow moving storm with a longer dwell rate
- moderate wind speed
- a tendency to modify the near-storm ocean environment.

In this chapter of case studies, analysis will start from the bottom up – with the ocean. First a brief overview of the tropical cyclone in question will be presented. A graph showing the following variables for each case will follow:

- Best-track maximum sustained wind speed (WSpd in m s^{-1})
- hurricane heat content (HHC in J m^{-2})
- $SST_{ICW} - SST_A$ (°C)
- 500 mb – 850 mb θ_e difference averaged at 600 km radius (5850ted6 in K).

Convective burst time periods are shaded in red in the accompanying graphs.

Following this discussion of the most basic characteristic variables, the flux analysis for each case study will be presented. Fluxes do not exist for each time period in the storm record. Only times that would support a valid H*wind analysis were included in the flux calculations. The "rain rate proxy" variable discussed in the chapter on latent energy is also graphed on this analysis. Given the relationship presented earlier, a higher magnitude of "rain rate proxy" corresponds to increased latent energy release. Note that the "rain rate proxy" does not exist for all time periods in the storm record either. Not every TRMM orbit overpass captures the main circulation of the storm in question. Also, TRMM does not have a constant time frequency. Bad orbits are discarded leaving temporal gaps in coverage.

Finally, an imagery timeline of vertical profiles of latent heating and the AMSU warm core anomalies will be presented. The intent is to trace the energetics of the convective burst events from the ocean through the convective burst into the eyewall tropopause, and then perhaps into the subsidence warming region of the tropical cyclone eye.

7.2 Floyd (ATL, 1999)

Hurricane Floyd was a large and intense Cape Verde storm that threatened the Bahamas and Florida. The storm struck North Carolina before turning toward the northeast on Sept. 16. The storm's major intensification phase began on Sept. 13th as an eyewall replacement cycle started that lasted about three days. One contributor to Floyd's significant strengthening was enhanced upper ocean heat content along the storm track, just east of the Bahamas. Floyd caused major flooding especially in North Carolina.

7.2.1 Floyd: characteristic variables

Floyd's whole life span was spent in relatively warm waters, as can be seen from the HHC variable in Figure 43. The hurricane heat content was gradually increasing as the convective burst period (red shaded rectangle) began. A slight maximum of HHC was reached during the CB event, followed by a slight decrease most likely due to ocean mixing. It is interesting to note the signature of very intense mixing – large oscillations of $SST_{ICW} - SST_A$ beginning almost simultaneously with the onset of the storm's maximum wind speed on 9/12. The largest negative difference in the SSTs, a large cold wake, occurred about 18 hours after the peak storm intensity. As Floyd passed through the region of increased ocean heat content (noted earlier) the HHC increased sharply and the cold wake made a near simultaneous recovery as the storm crossed the Gulf Stream. The θ_e difference between the mid and lower troposphere is minimized just prior to the onset of the CB event.

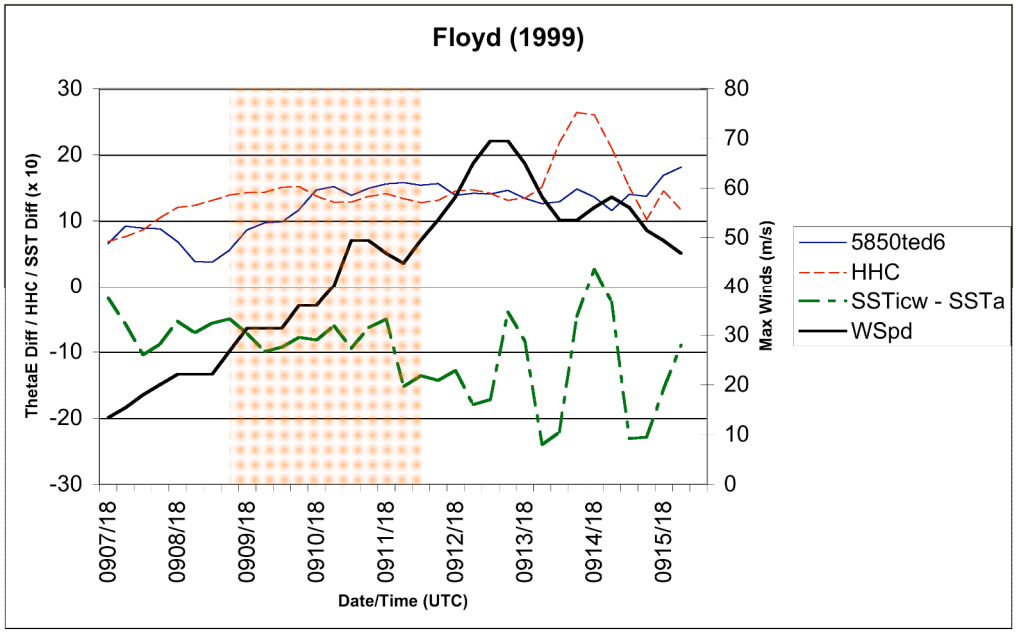

Figure 43: Characteristic variables of Hurricane Floyd (1999).

7.2.2 Floyd: flux analysis

The flux analysis of Hurricane Floyd, Figure 44, shows a secondary peak in fluxes mirroring the first small peak in intensity during the convective burst event on 9/11. A well-defined peak in the rain-rate proxy occurs during the CB. The peak Q_L (latent energy flux) occurs during the midst of the convective rainband cycle on 9/14. Note this also corresponds to a maximum difference in SSTs in Figure 43 when Floyd crossed the Gulf Stream.

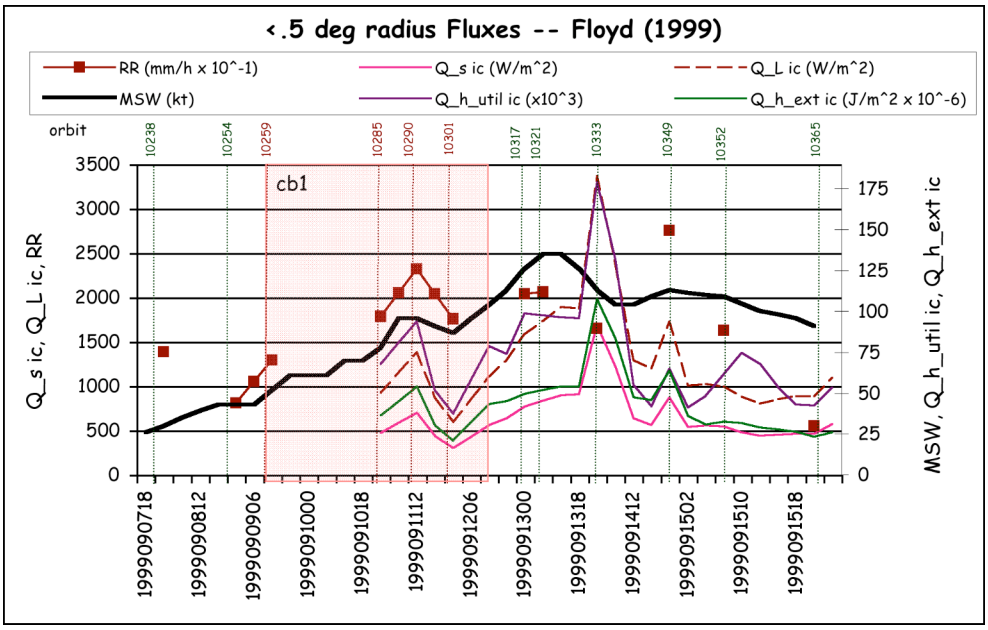

Figure 44: Flux calculations for Hurricane Floyd. Radius = 0 to 0.5°.

7.2.3 Floyd: energetics timeline

The vertical profiles of latent heating shown in Figure 45 illustrate the evolution of latent energy release throughout Hurricane Floyd's lifecycle. The first image (top left) occurs during the early intensification change just prior to the onset of the CB. The storm is over warm waters at this point. The second image (top middle) was observed during a small wind speed plateau early in the convective burst. The third profile (top right) shows enhanced latent energy release coincident with a secondary storm intensity maximum. The peak latent energy release, on 9/11 at 1019 UTC (bottom left) occurs near the end of the CB event. The next image (bottom middle) shows the storm near its peak intensity. In Figure 46 the peak latent heat release as seen in the profiles in Figure 45 occurs just prior to the AMSU temperature anomaly observation near 0000 UTC on 9/12 (top right image.) The wind speed maximum occurs just after this image. About 12 hours before the convective rainband cycle begins, a cold anomaly develops below 8 km. Once the convective rainband cycle begins, the cold anomaly spreads, and the elevated warming spreads out and down as far as 600 km from the storm center.

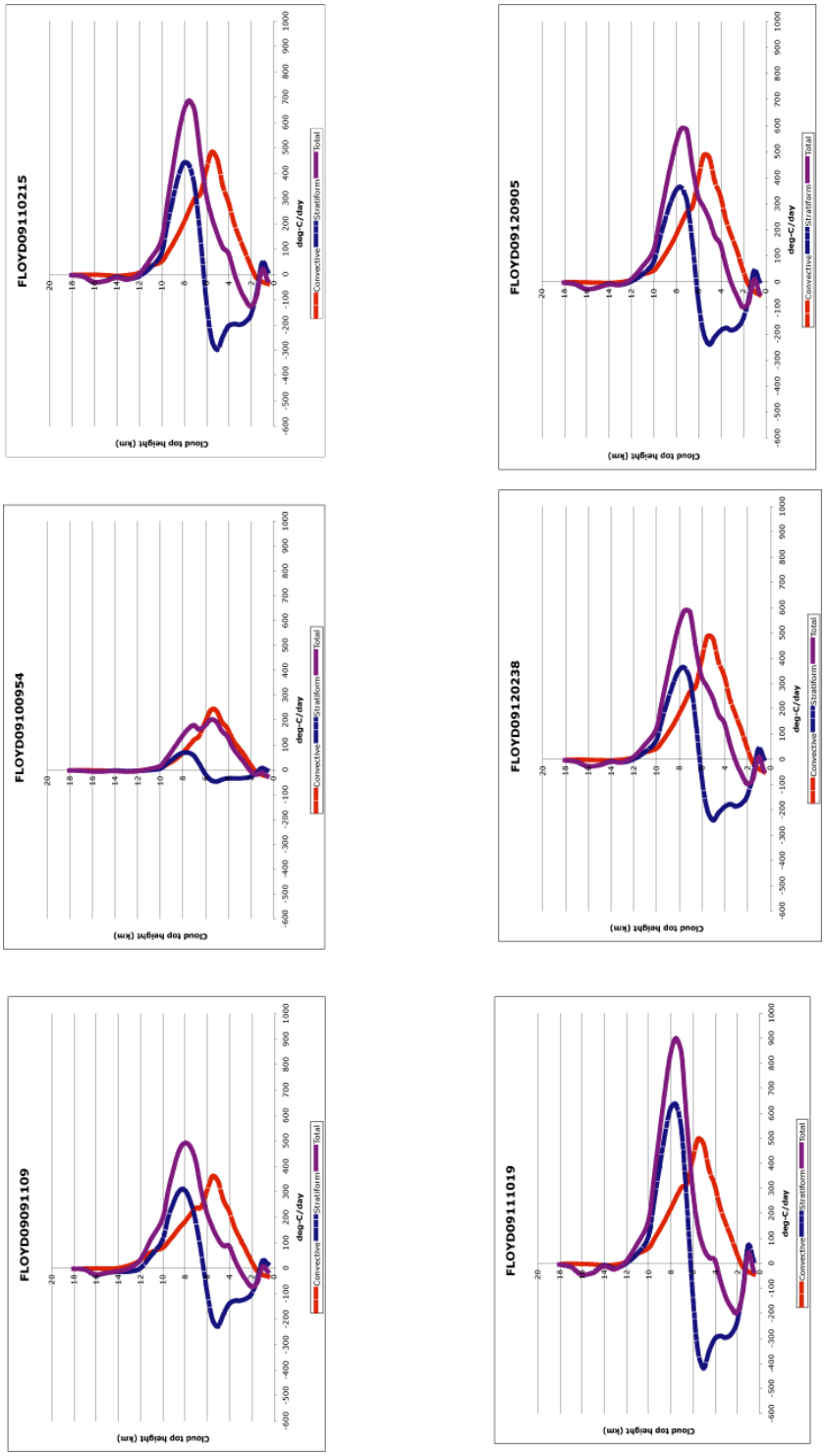

Figure 45: Vertical profiles of latent energy release, Hurricane Floyd (1999).

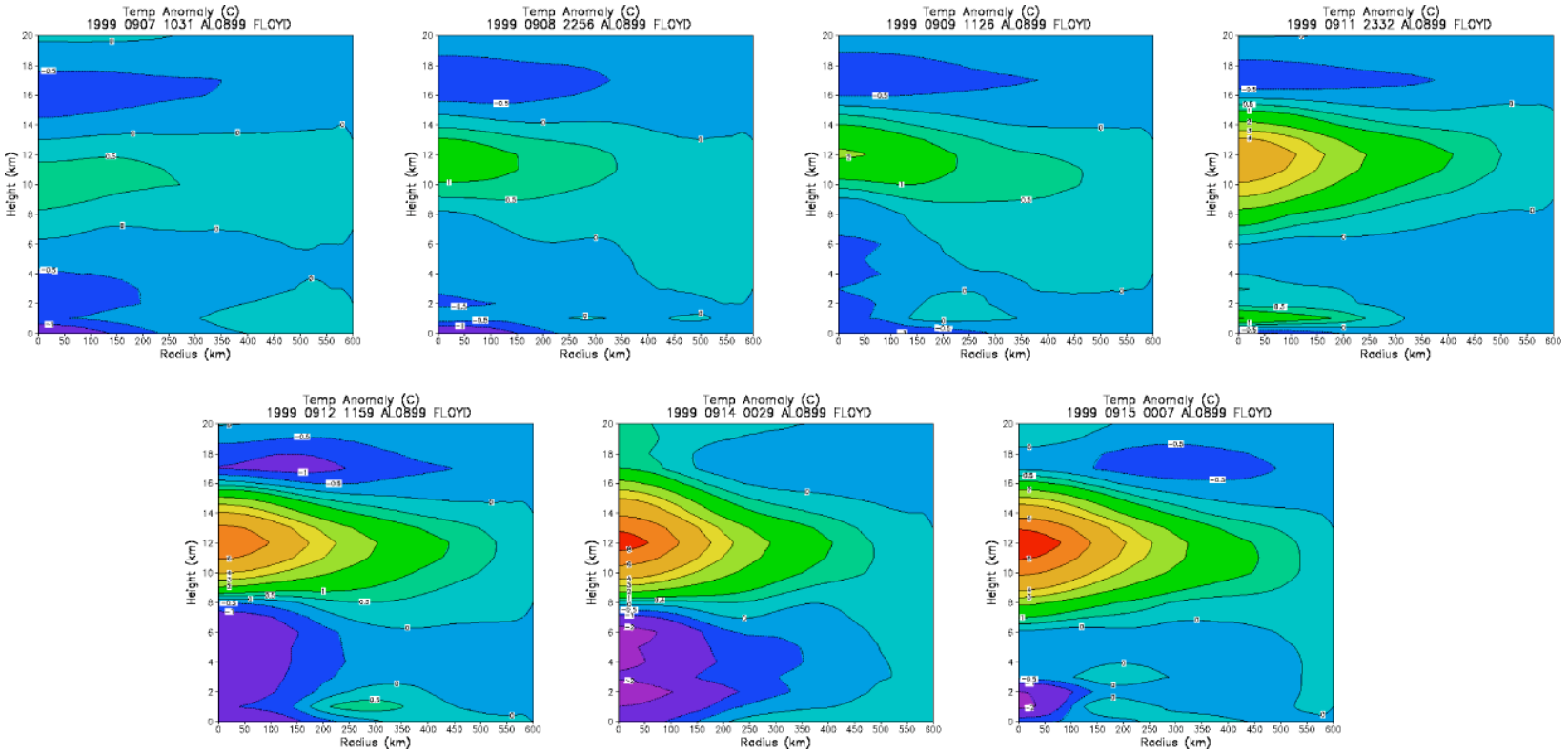

Figure 46: AMSU temperature anomalies for Hurricane Floyd (1999).

7.3 Gert (ATL, 1999)

Gert was a 130 kt central Atlantic hurricane generated from an African easterly wave. Gert affected Bermuda and caused high waves off Newfoundland. The storm crossed over an area where Floyd had just passed. The weakness in a ridge allowed Gert to move north-northeast on September 16th to the 21st.

7.3.1 Gert: characteristic variables

Gert was moving into an area with a warmer mixed as the convective burst event began on 9/13. The HHC maximum occurred about 12 hours after the storm reached its peak intensity on the 16th at 0000 UTC. A very erratic mixing signature occurs from the point of the storm's maximum intensity onward because the ocean mixed layer is already cooled by Floyd.

The θ_e difference increases slightly positively through the beginning of the burst event. During the period of maximum winds, the θ_e difference is slightly smaller (the layer is more well mixed) until the θ_e difference peaks almost coincident with the largest SST_{ICW} cooling on 9/19.

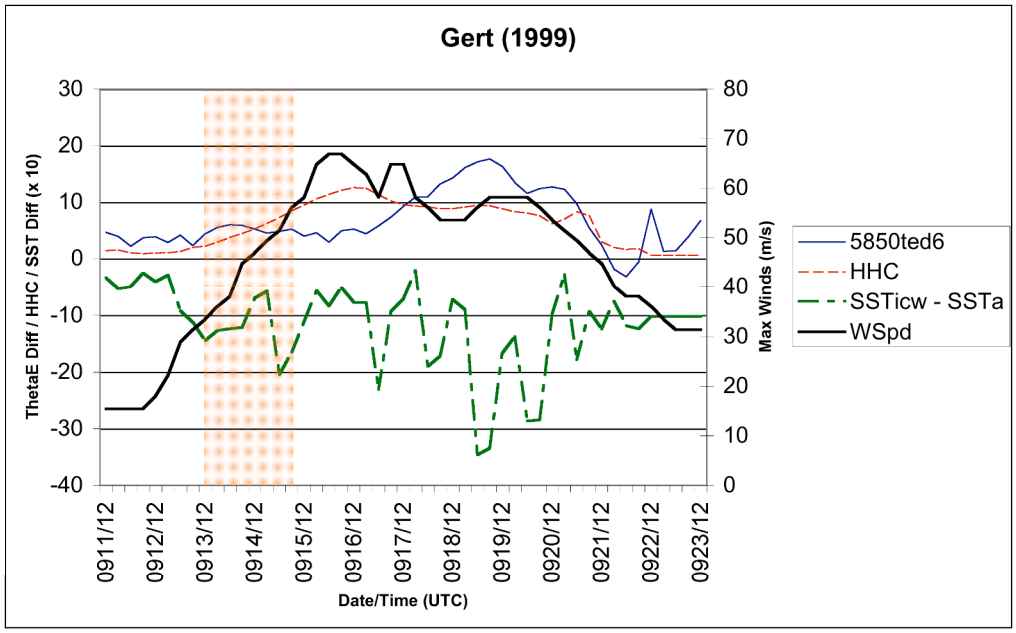

Figure 47: Characteristic variables for Hurricane Gert (1999).

7.3.2 Gert: flux analysis

H*wind analyses were not consistently available for Gert so the flux measurements are sporadic. See Figure 48. Even so, the maximum fluxes appear to have occurred on or around 9/16 at 0000 UTC, coincident with the storm maximum wind speed. A peak in Q_{h_util}, the percentage of energy used by the storm given what was available to it, occurs with the secondary maxima on 9/17 at 1200 UTC. Given the HHC on Figure 47, the observable peak in Q_{h_util} lags the max HHC by about 6 hours. The rainfall rate proxy makes a steady climb as the storm intensifies. Missing orbits make it impossible to tell where the maximum rainfall rate may be however.

7.3.3 Gert: energetics timeline

Both of the vertical latent heating profiles in Figure 49 were observed during the convective burst episode immediately preceding Gert's maximum intensity. The AMSU (Figure 50) temperature anomaly plots chronicle the latent energy development in the storm. The first two images (top left and top middle left) occur before the CB event has taken place. The convective burst-related latent heating profiles precede the next two AMSU images (top middle right and top right). The time of maximum sustained winds occurs coincident with the third image (on 9/15 at 1053 UTC). In this series of temperature anomaly plots it is interesting to see the storm begin to weaken on 9/20 at 1220 UTC. The warming subsides down into the low levels and eventually makes it to the surface.

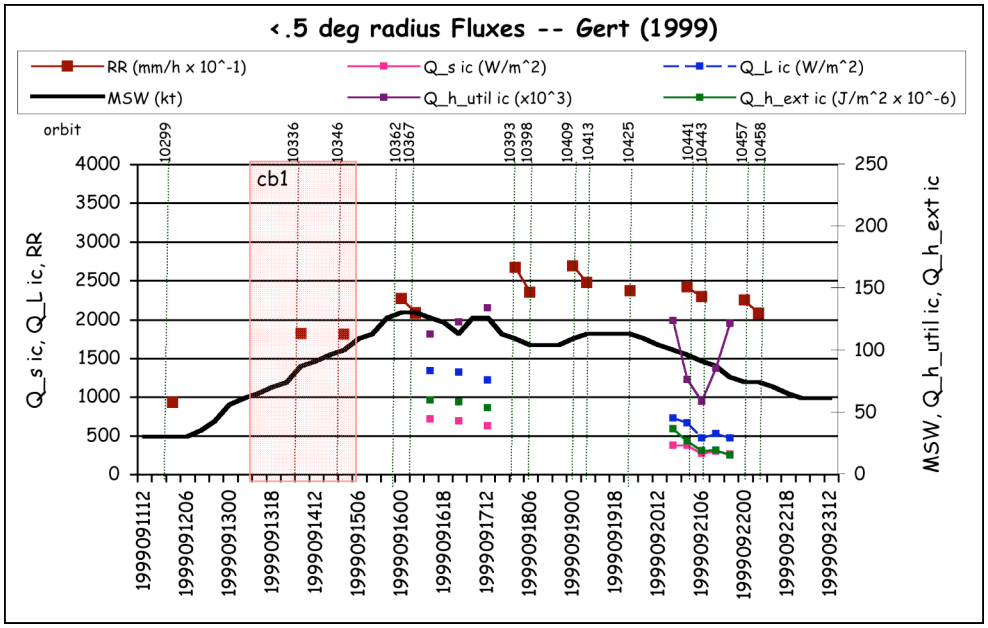

Figure 48: Flux calculations for Hurricane Gert. Radius = 0 to 0.5°.

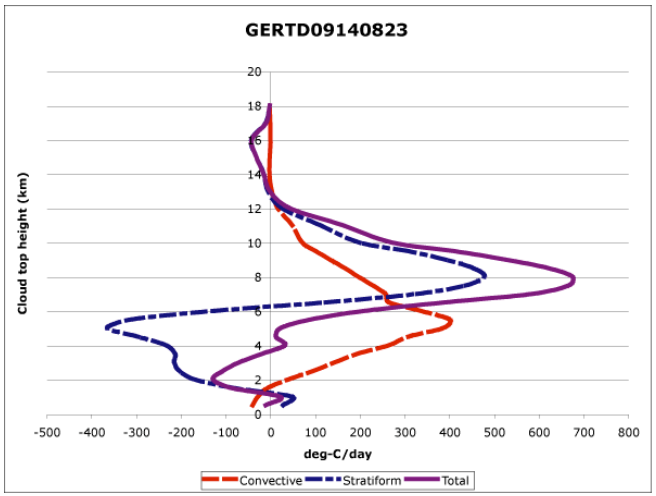

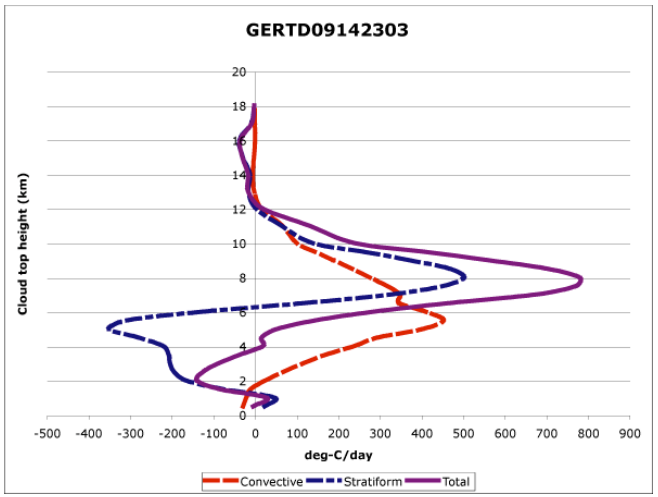

Figure 49: Vertical profiles of latent energy release, Hurricane Gert (1999).

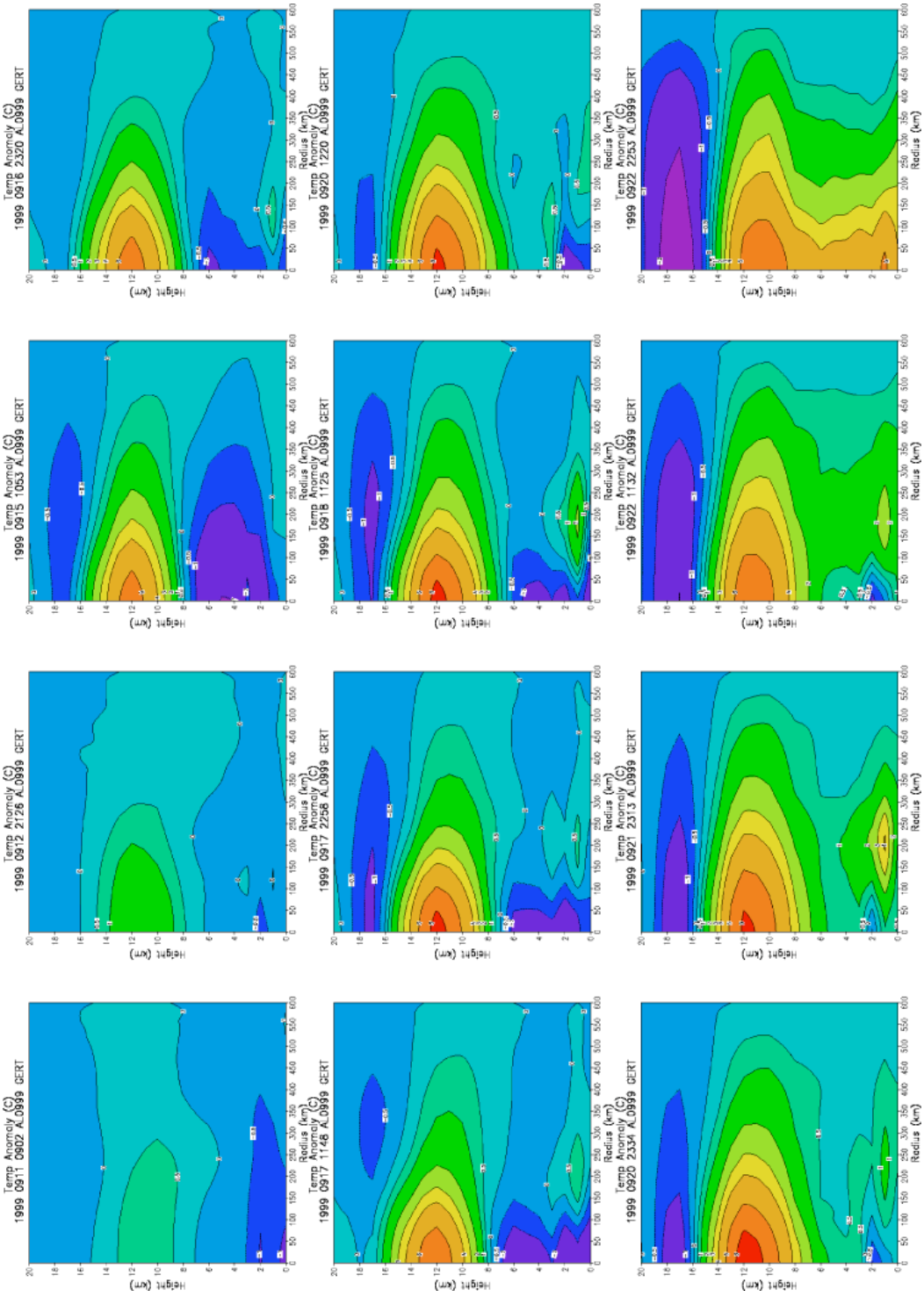

Figure 50: AMSU temperature anomalies for Hurricane Gert (1999).

7.4 Jose (ATL, 1999)

Hurricane Jose was a category 2 hurricane that began as an African easterly wave. It made landfall for a short time on Tortola and the British Virgin Islands. Jose experienced very strong vertical shear and became a tropical storm on 10/21. On 10/24 Jose re-strengthened and became a hurricane once again. The re-intensification was short-lived, however, and Hurricane Jose became Tropical Storm Jose again less than 24 hours later.

7.4.1 Jose: characteristic variables

One pattern that is apparent in Figure 51 is the shape of the θ_e difference curve. The minimum θ_e difference occurs at the same time as the peak wind speed. As the wind speed begins to decrease (after making a brief landfall) the θ_e difference becomes increasingly larger in the positive direction. Finally during the second convective burst, the SST difference goes from a cold wake condition to a positive spike, then back to cold. For a short period, the SST_A was colder that the SST_{ICW}. The point of the largest positive difference in SST occurs just after HHC drops off, and at the maximum positive 500 mb –850 mb θ_e difference.

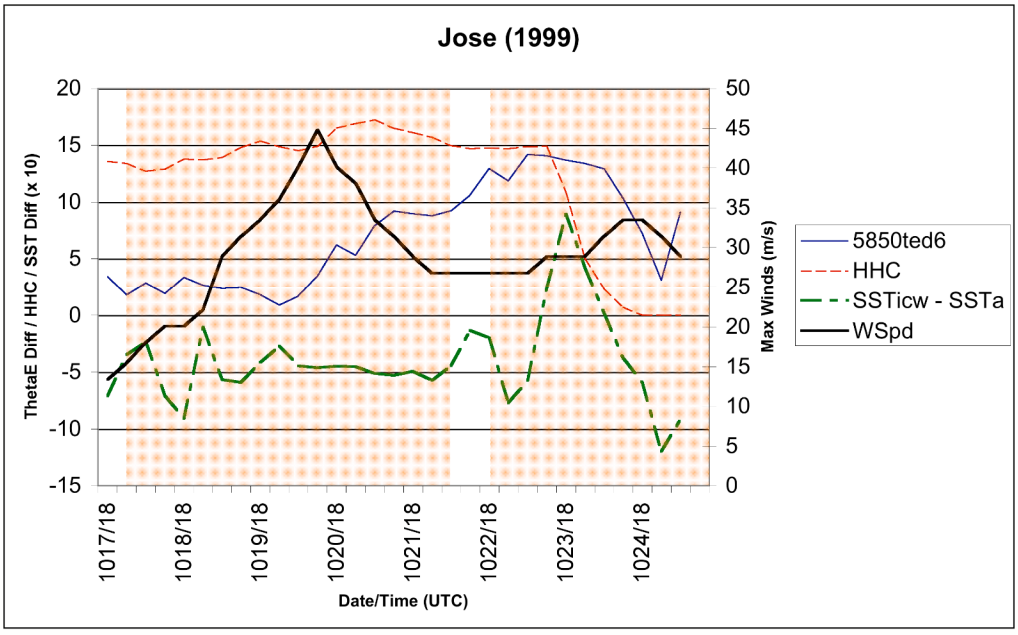

Figure 51: Characteristic variables of Hurricane Jose (1999).

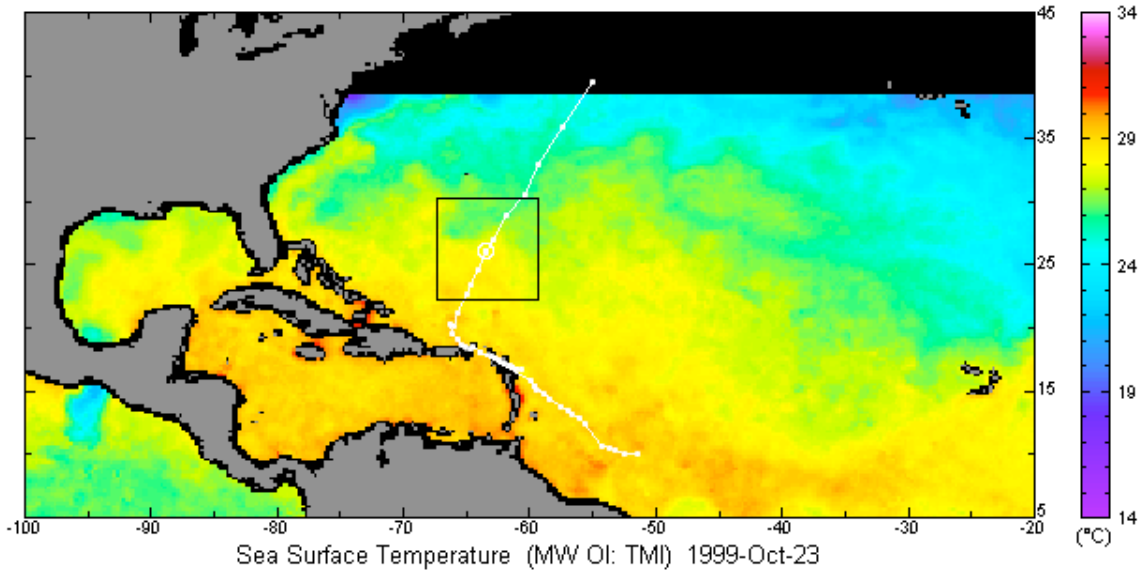

Figure 52: SST map of Hurricane Jose, 10/23/1999. Note colder water ahead of storm.

7.4.2 Jose: flux analysis

Both convective burst episodes in Jose had wind speed maxima coincident with either Q_L or rain rate proxy maxima. The rainfall rate proxy is missing between 10/19 and 10/21, the dates of maximum intensification and Jose's short landfall in the Southern Caribbean. Even though these rainfall rates are missing, one might assume they move in the same direction as the fluxes, in which case the rainfall rate proxy would have had its peak at the point of maximum sustained wind too. A second maxima in the rainfall rate proxy occurred during the second convective burst episode.

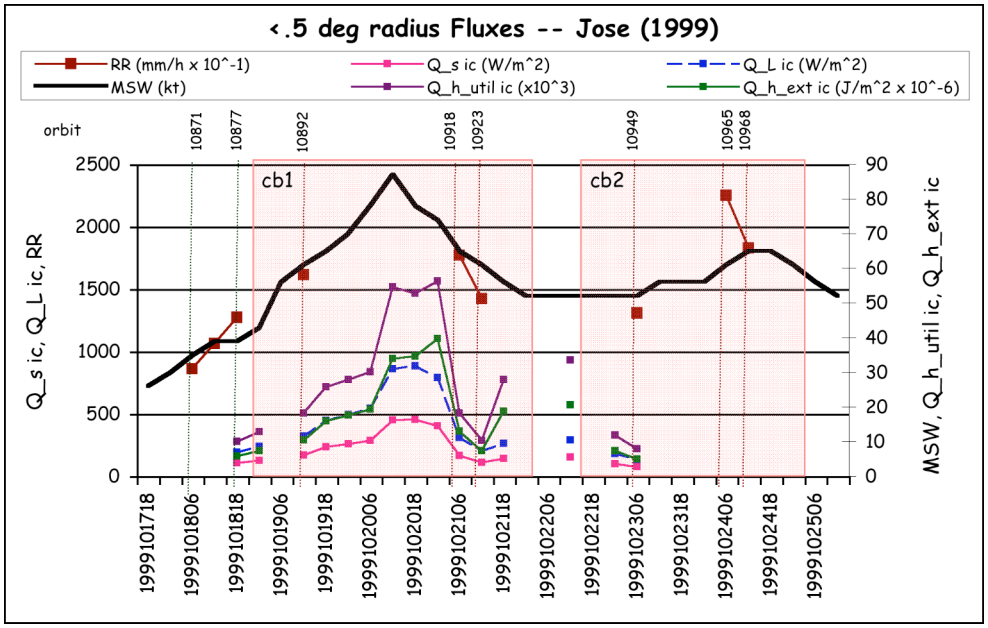

Figure 53: Flux calculations for Hurricane Jose. Radius = 0 to .5°.

7.4.3 Jose: energetics timeline

The latent heating profiles for Jose in Figure 54 are good illustrations of the magnitudes of the latent heating change that takes place in a convective burst incident. The first four panels (top row, left to right and middle row, left) illustrate one convective burst from early in its formation (10/19 1434 UTC) through its ending stage (10/21 1345 UTC). At first glance the profiles look very similar. But a look at the magnitudes on the x axis shows how the latent energy starts near 700 C° d^{-1}, wanes to 350 C° d^{-1}, then grows again to almost two times that level back to 700 C° d^{-1} and finally to around 500 C° d^{-1} at the end of the first burst. The second burst follows a similar latent heating pattern from 500 C° d^{-1} to 900 C° d^{-1}, and back to 400 C° d^{-1} before dissipating on 10/25. By analyzing the timing of this sequence more closely it becomes apparent that the changes in the latent heating profiles and the changes in the surface fluxes go hand in hand in this case. An examination of the AMSU temperature anomalies in Figure 55 clearly shows that the temperature structure of Jose never truly developed the upper level warm anomaly found in a strong hurricane. The period of peak wind speed occurs between the first and second images (top left and top middle left.) In the image from 10/21 2344 UTC the

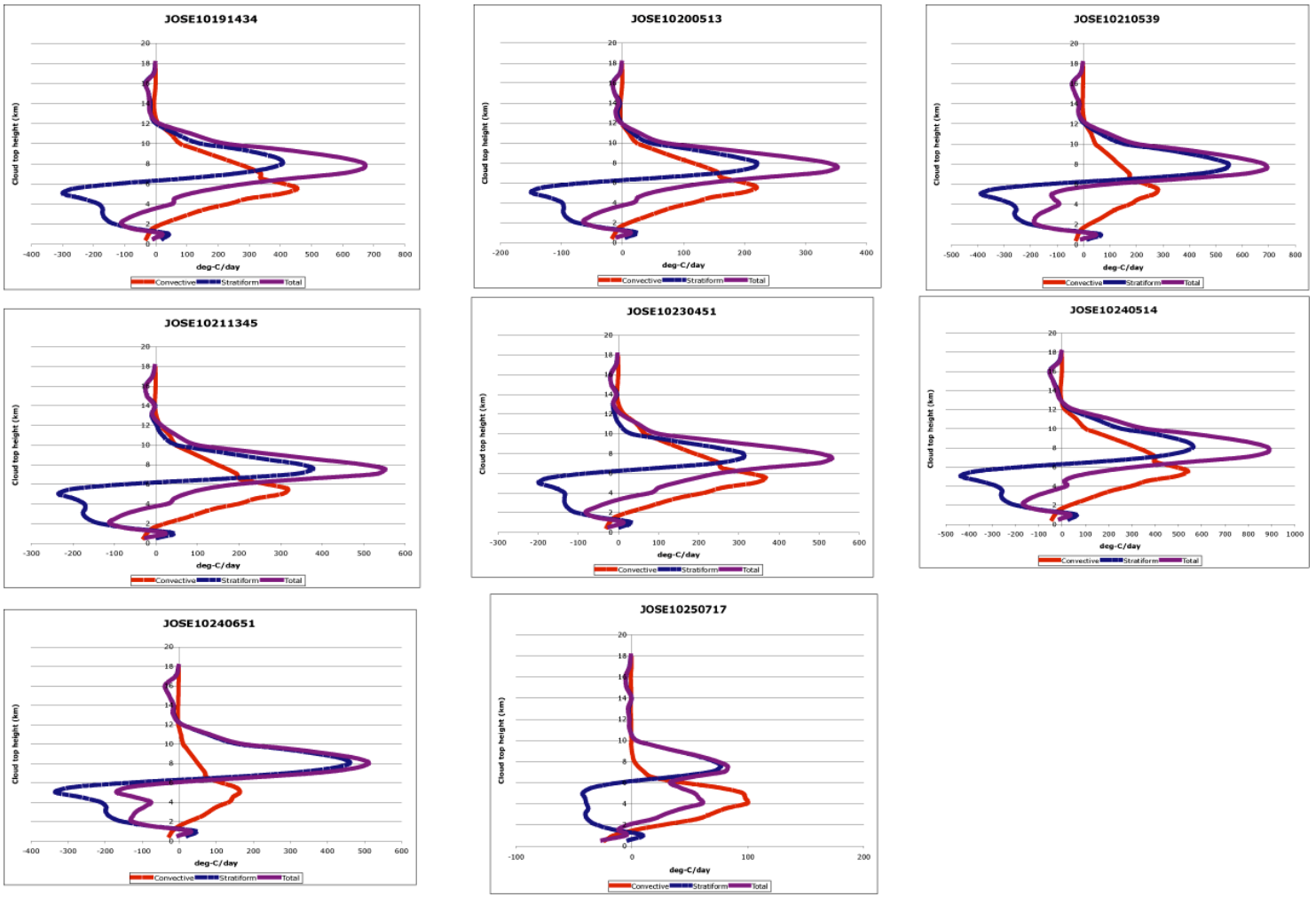

Figure 54: Vertical profiles of latent energy release, Hurricane Jose (1999).

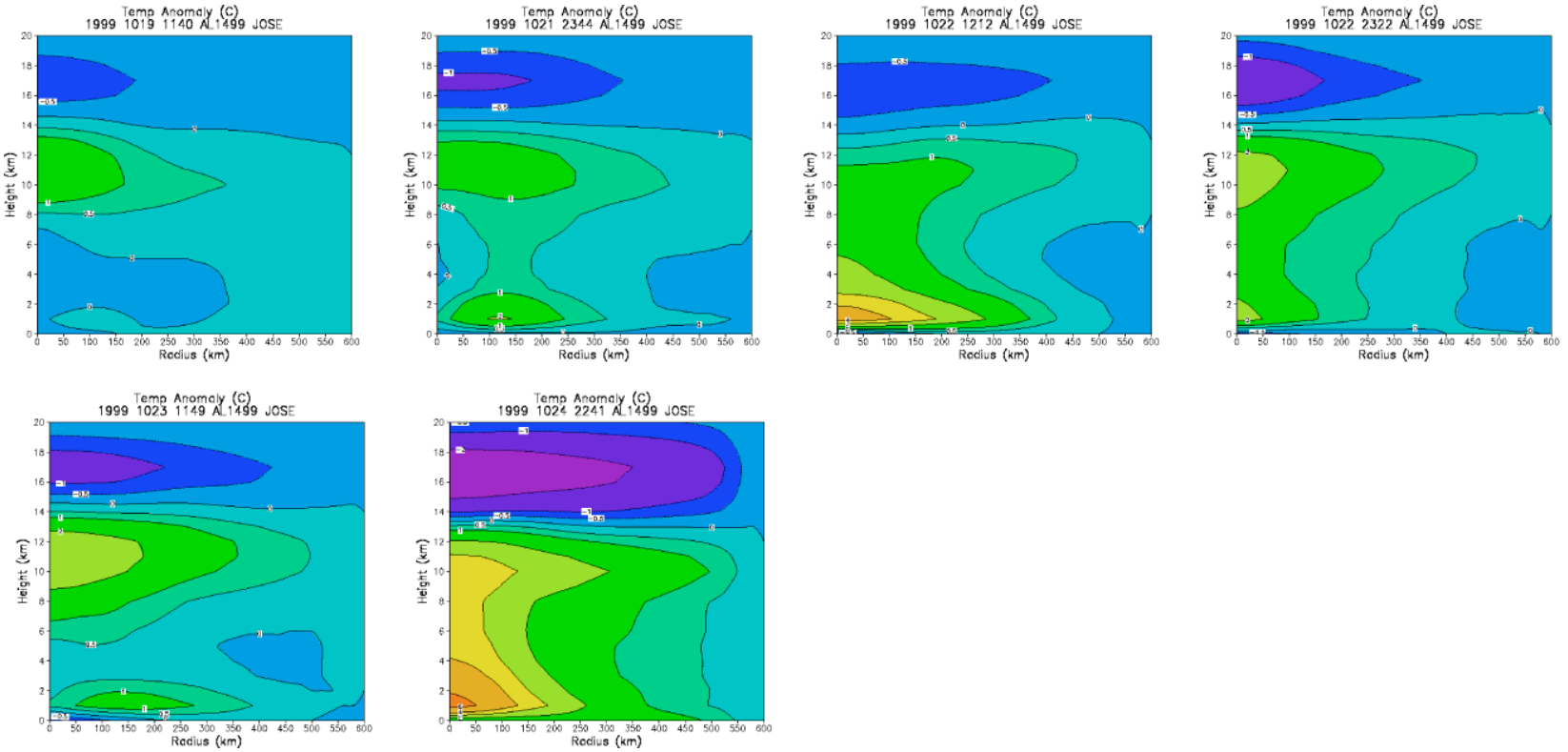

Figure 55: AMSU temperature anomalies for Hurricane Jose (1999).

upper level warming was never stratified from the lower levels and the upper level actually has a growing cool anomaly.

7.5 Lenny (ATL, 1999)

Hurricane Lenny has a reputation for being an outlier among the hurricane population. It was the first storm ever recorded to have a west-to-east track across the Caribbean Sea. Lenny became a hurricane about 150 miles southwest of Kingston, Jamaica on September 15th. Later that day, Lenny weakened only to rapidly re-intensify on the 16th as the central pressure dropped 34 mb. Lenny's motion slowed on the 17th due to trough interaction and eventually turned southeastward early on the 19th. Just before making landfall on St. Maarten, Lenny weakened due to oceanic upwelling..

7.5.1 Lenny: characteristic variables

As seen in Figure 56 Lenny experienced four separate episodes of convective burst. The first two were short-lived and early in the storm lifecycle. The first major convective burst event (CB #3) began on 11/15 at 1800 UTC and persisted until 11/17 at 1200 UTC. This burst period saw significant growth in surface wind speed. The SST_{ICW}-SST_A variable seems to follow the wind speed very closely for the entire storm. There are two small maxima in HHC that occur, one in each major convective burst event although the HHC is trending downward through the life of the storm. As in Jose, the minimum θ_e difference (in this case almost equals zero) occurs at the same time as the peak wind speed. In Lenny this time period also corresponds to a minimum difference in SSTs (about zero).

7.5.2 Lenny: flux analysis

The flux analysis of Lenny is especially rich – many H*Wind analyses were available for this storm. At first glance a pattern between the surface fluxes and the wind speed is apparent. In this case the surface wind speed seems to be driven directly by the latent energy flux, Q_L,in the inner core region of the storm (<.5° radius). The maximum rainfall rate proxy leads the Q_L maximum by about 24 hours.

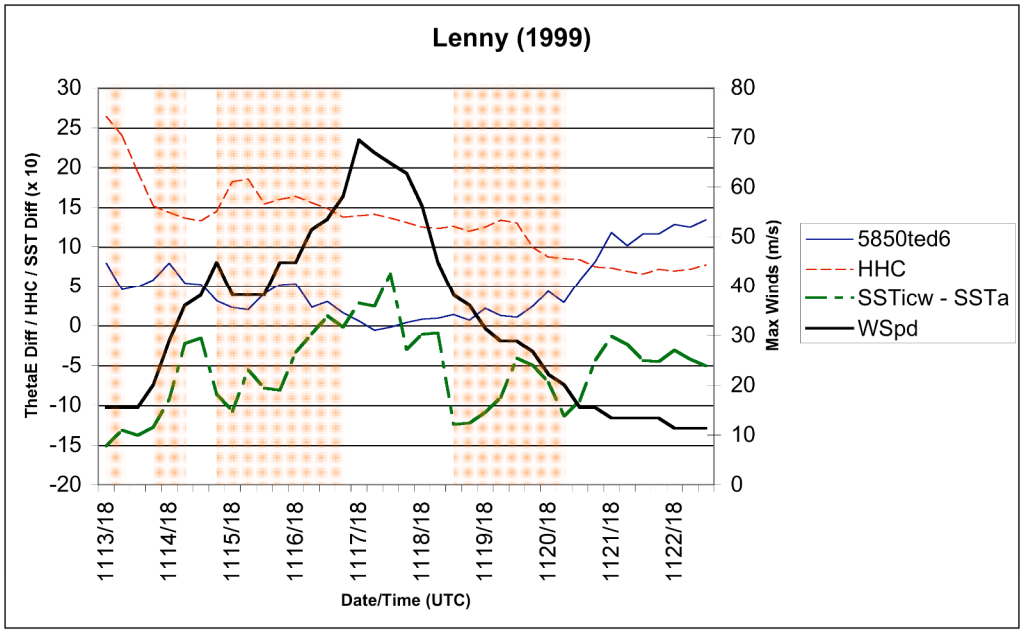

Figure 56: Characteristic variables of Hurricane Lenny (1999).

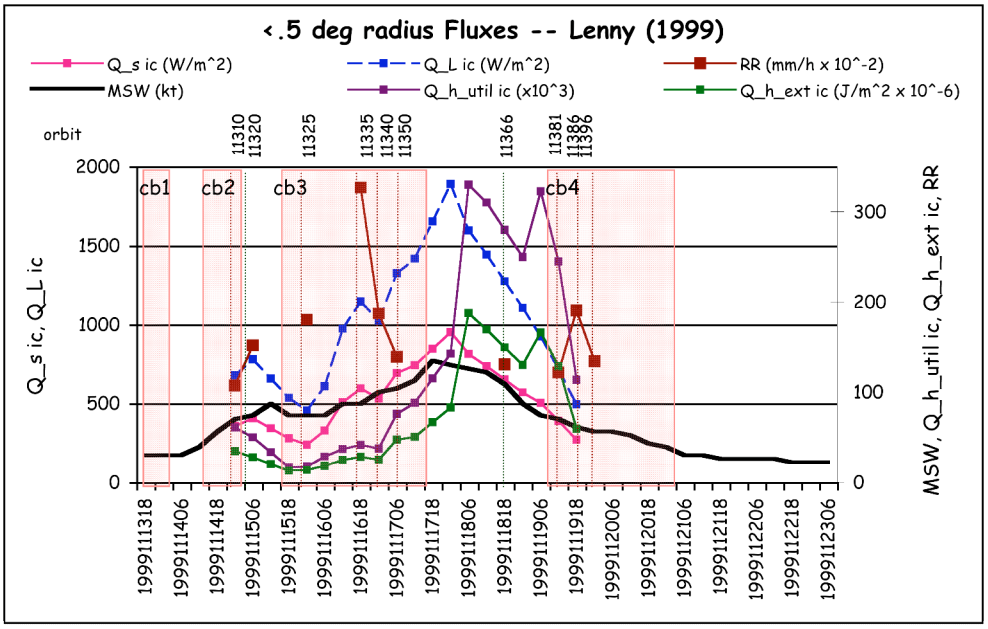

Figure 57: Flux calculations for Hurricane Lenny. Radius = 0 to 0.5°.

In the discussion the SST_{ICW}-SST_A difference seemed highly correlated with the surface wind speed. This seems to relate to a direct link to the surface fluxes as well. Once again, and it is quite evident in this storm, this SST_{ICW}-SST_A difference seems to increase temporarily in the negative direction at the beginning of each convective burst. This seems to imply that the onset of the extreme convection causes increased inner-core wake cooling, "mixing out" of a relatively shallow warm mixed ocean layer, or helps to intensify upwelling beneath the storm.

7.5.3 Lenny: energetics timeline

The time series of profiles of vertical latent heating (Figure 58) provides a good overview of the storm's energetics. The first major convective burst in Lenny, from 11/15 through 11/17, is well represented. Using the magnitude of total heating (stratiform fraction + convective fraction) as an indicator, the profile from 11/14 at 0222 UTC (before the burst) shows 200 °C d^{-1}. The next profile (top middle) shows the observed magnitude increased to 300 °C d^{-1}, then an increase to 600 °C d^{-1} by 11/15 at 1730 UTC. November 16th at 0136 UTC has a total heating magnitude of approximately 700 °C d^{-1} and finally on 11/16 at 1615 UTC, the total heating hit a maximum value of 1200 °C d^{-1}. This observed profile (middle row, center) corresponds in time to the maximum rainfall rate proxy examined in Figure 57 in the previous section. From this point in time forward in the storm the total heating decreases time period by time period until on 11/20 at 1306 UTC (during the second major CB) the total heating is approximately 600°C d^{-1} (last plot).

The period of maximum latent heating, the center image in Figure 58, when the energy profile peaked at 1200 °C d^{-1} corresponds to the observation of the maximum temperature anomaly of +4°C from the AMSU soundings (center row, middle, left) in Figure 59. The rainfall rate proxy maximum on 11/16 (discussed earlier) corresponds to the AMSU anomaly plot on 11/16 at 0028 UTC (middle row, left) showing a +3°C warm anomaly. In the case of this storm, the rainfall rate proxy maximum seems to lead the flux maximum, with the net result being an increased warm anomaly aloft.

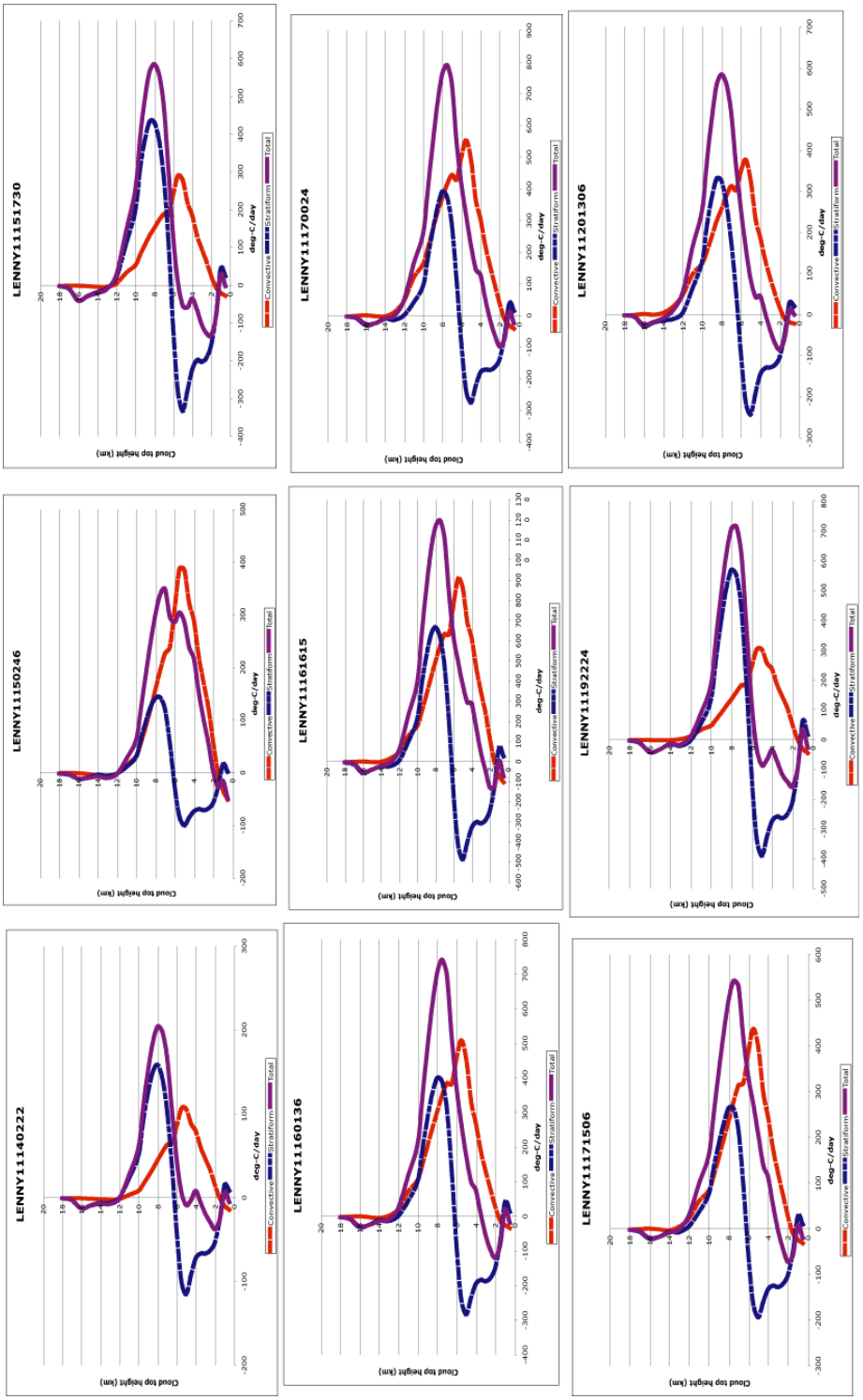

Figure 58: Vertical profiles of latent energy release, Hurricane Lenny (1999).

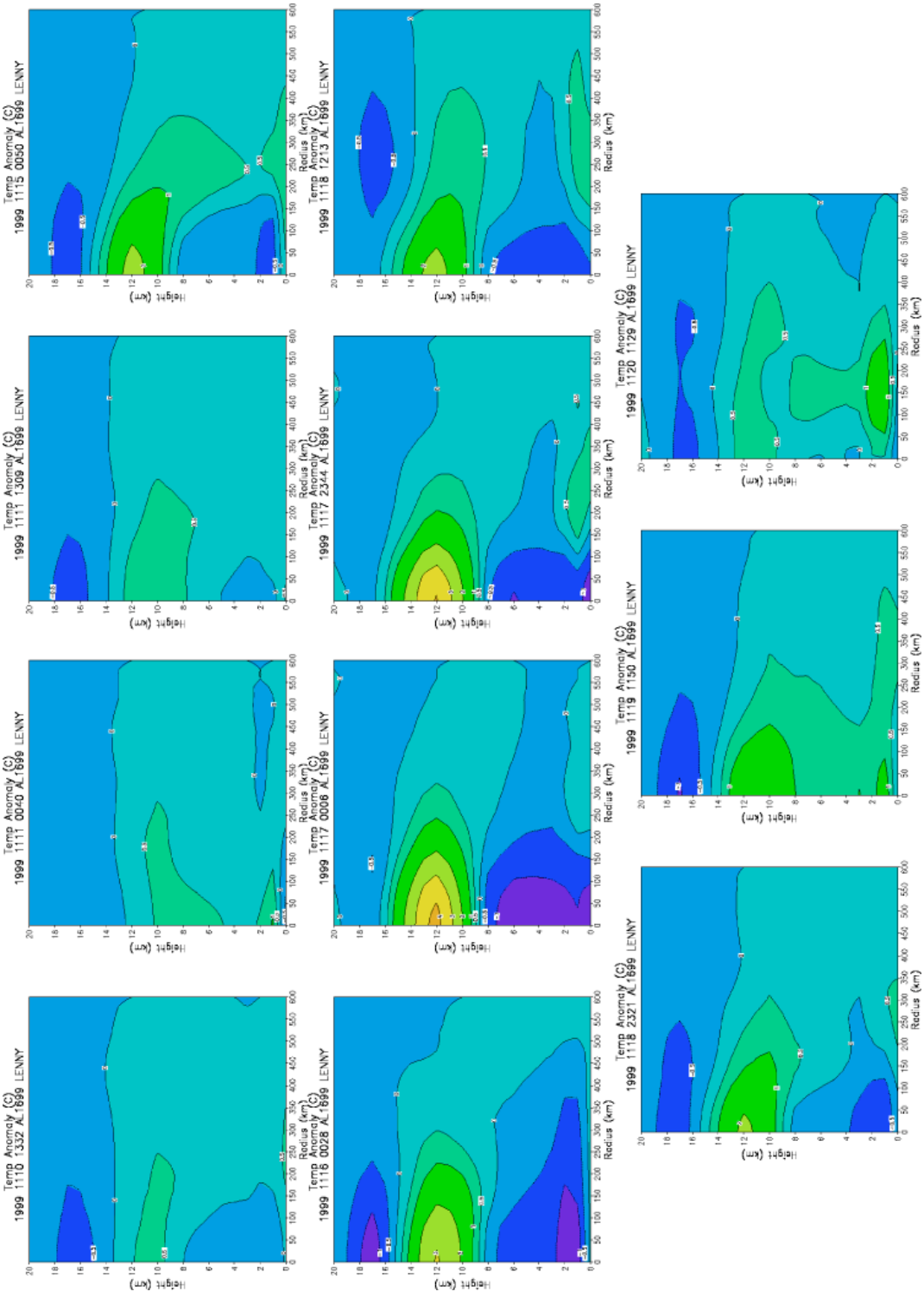

Figure 59: AMSU temperature anomalies for Hurricane Lenny (1999).

7.6 Alberto (ATL, 2000)

Hurricane Alberto was the longest-lived Atlantic tropical cyclone ever to form in August. The hurricane formed as a Cape Verde storm and stayed in the Atlantic, never making land fall. It became a hurricane three times – August 6th, 10th, and 18th. Just before its last intensification phase, Alberto made a five daylong anti-cyclonic loop encircling its own cold wake. Alberto reached Category 3 status on the Saffir-Simpson Scale and never had a convective burst episode.

7.6.1 Alberto: characteristic variables

Hurricane Alberto oscillated between tropical storm and hurricane strength three times during it lifecycle. The first intensification phase, 8/03 through 8/07, was interrupted by an episode of increased vertical shear. Despite this weakening, Alberto regained strength on 8/09 as the storm reached an oceanic area characterized by anomalously high SSTs. A first glance at Figure 60 reveals a strong connection between "Wind Speed" and "SST_{ICW}-SST_A". In fact the Pearson correlation coefficient between these two variables for this storm indicates strong correlation (r=0.6). This positive correlation is evident in Figure 60 especially from 8/08 onward. A very interesting characteristic to note is that the SST_{ICW}-SST_A variable seems to lead the change in wind speed in the storm lifecycle.

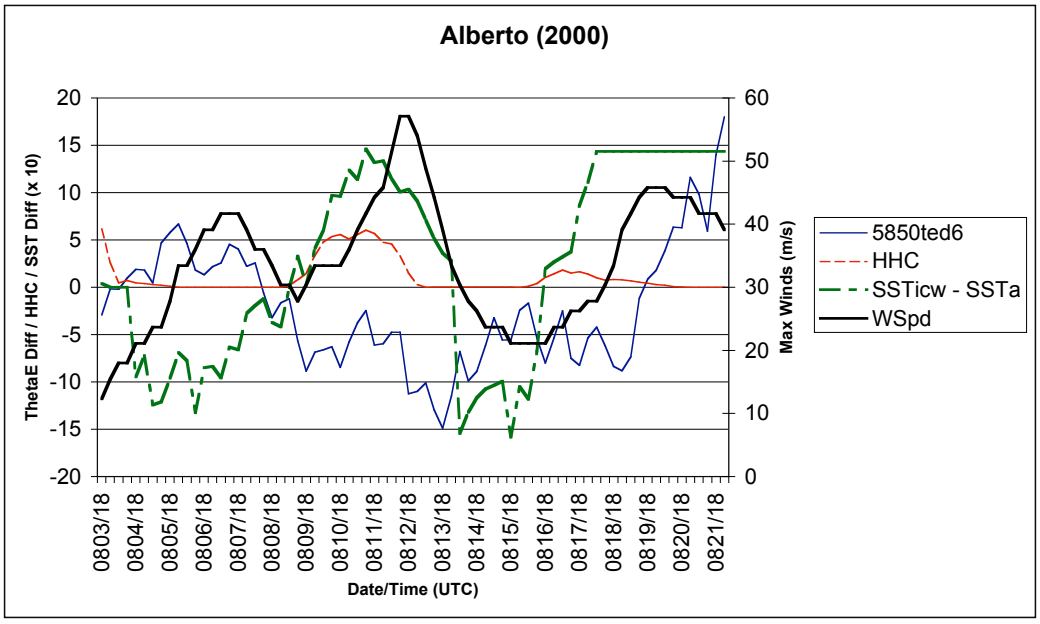

Figure 60: Characteristic variables of Hurricane Alberto (2000).

7.6.2 Alberto SST_{ICW}-SST_A difference analysis

At its inception Hurricane Alberto emerged in an area of relatively warm SSTs. As the storm began to move to the northwest, it entered an area of cooler SSTs and the HHC stayed relatively constant (although near zero). During this time (8/04 – 8/06), the SST_{ICW}-SST_A temperature contrast increased in a negative direction, indicating increased cooling behind the storm. In this case Alberto was moving east-to-west along an SST gradient with warmer water to the south. See Figure 61.

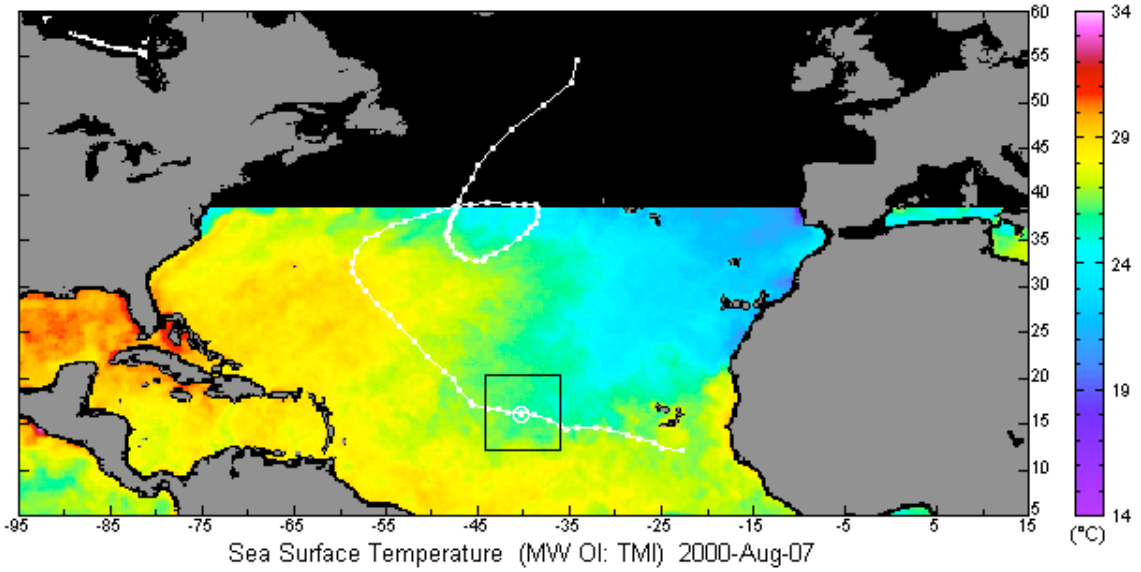

Figure 61: SST plot for Hurricane Alberto. Note the E to W SST gradient to the south.

As Alberto moved through this region of highly variable SST, the storm approached an area of anomalously high SST around 8/09 – 8/11. See Figure 62. At this point HHC increased markedly reaching a peak on 8/11 and the SST_{ICW}-SST_A difference became larger in the positive direction (SST_{ICW}-SST_A > 0) indicating less cooling was occurring in the wake of the storm.

The storm moved back into a region where the wake was cooler than the SST ahead (SST_{ICW}-SST_A < 0) and eventually made an anti-cyclonic loop encircling its own cold wake. A good example can be seen in the SST anomaly plot of 8/16. See Figure 63. At this point Alberto's wind speed had dropped back to the level of a tropical storm. The HHC reached a

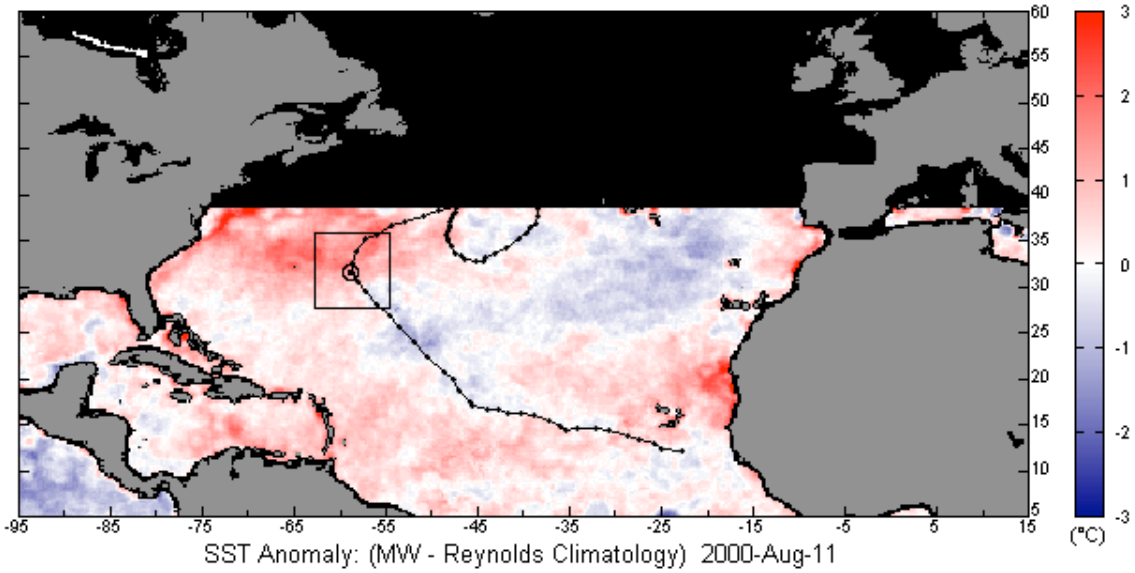

Figure 62: SST Anomaly plot. Hurricane Alberto enters region of high HHC.

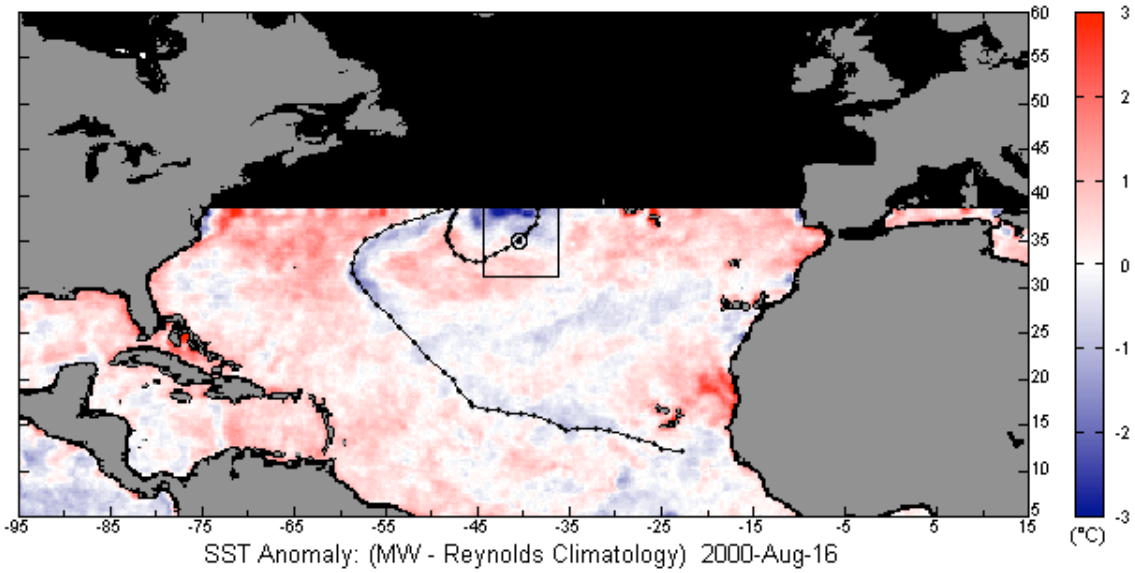

Figure 63: Hurricane Alberto encircles its own cold wake.

secondary maximum at this point and wind speeds increased to hurricane strength once again on 8/18.

7.6.3 Alberto: flux analysis

Since Alberto was never a threat to land, the forecasters never prepared an H*wind analysis for this storm. As a result, fluxes could not be computed. The rain rate proxy is also rather incomplete. See Figure 64. The early wind speed maximum on 8/06 might coincide with a peak in rainfall. A definite decrease in rainfall took place (8/11) just before the storm's maximum intensity. Comparison of the rainfall rate proxy to the "500 mb - 850 mb θ_e difference" plotted in Figure 60 seems to suggest the rainfall rate (and perhaps the fluxes) followed the convective stability tendency in this case. The convective instability plotted on Figure 60 increased from the point the storm reached the elevated HHC (on 8/10) until it reached its peak negative difference on 8/13 just after the peak wind speed on 8/12. Although impossible to tell, this could have been the point of a rainfall minimum as well.

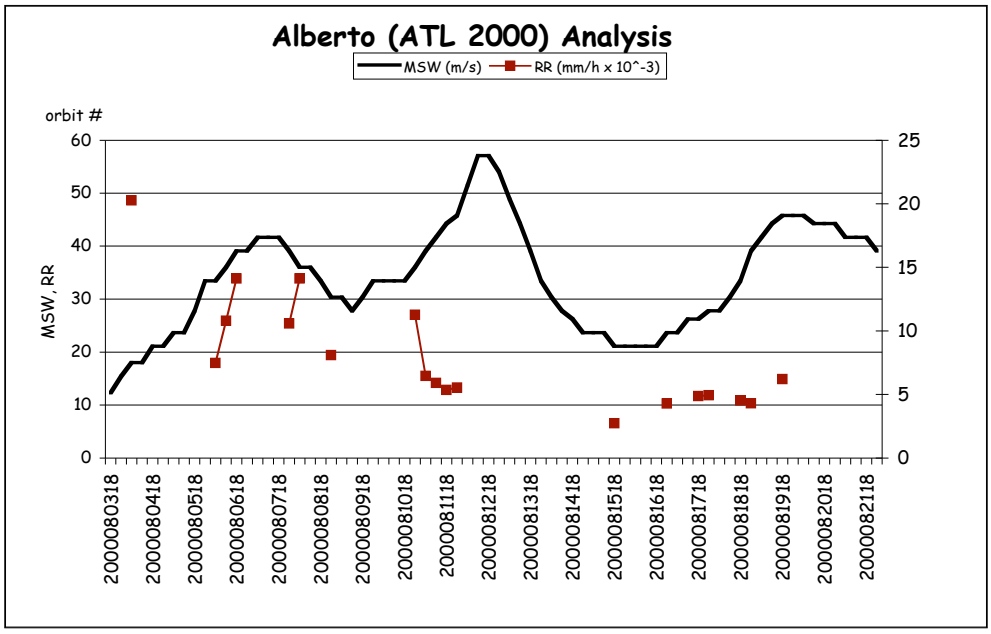

Figure 64: Rainfall rate proxy calculations for Hurricane Floyd. Radius = 0 to 0.5°. (No H*Wind analyses were available.)

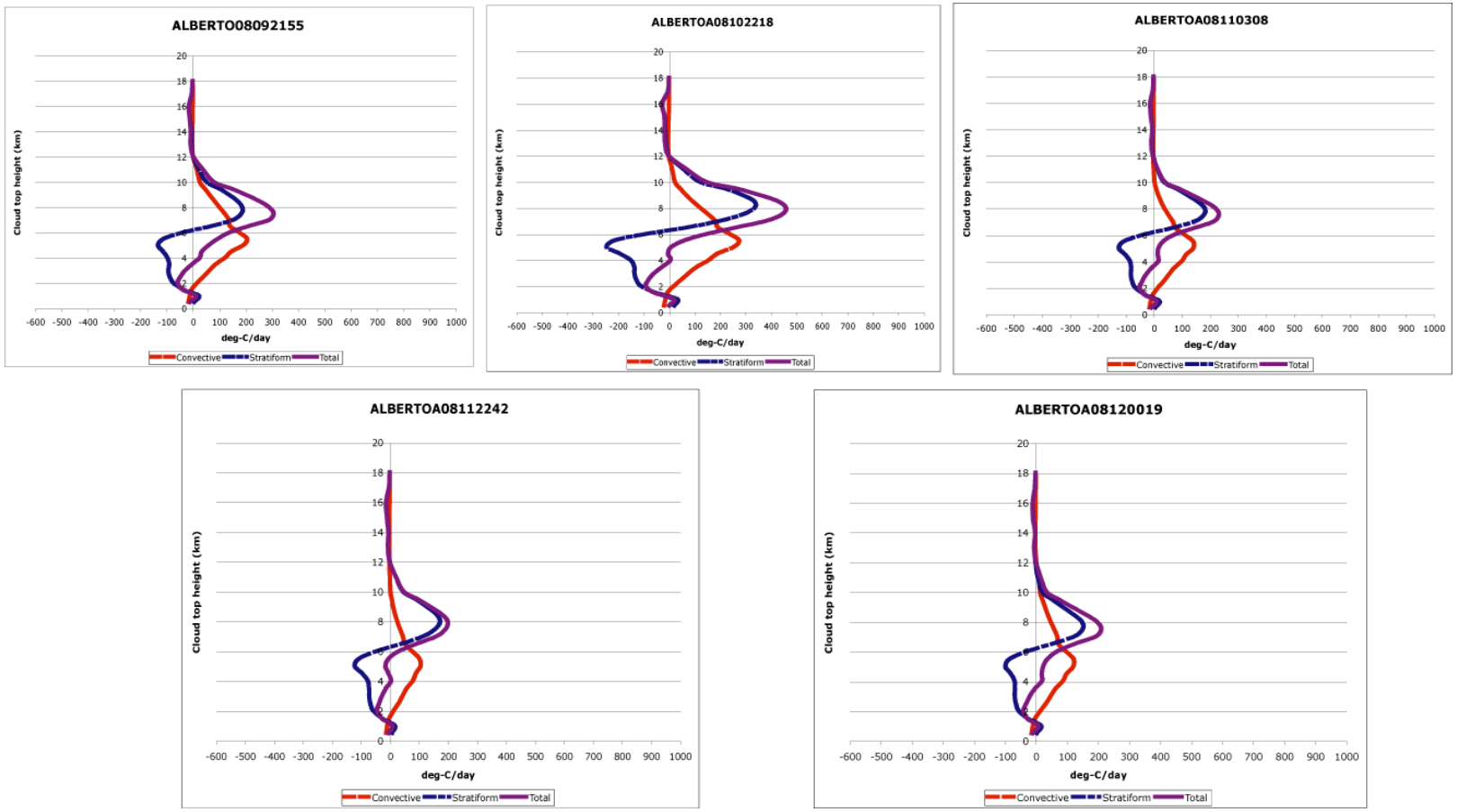

Figure 65: Vertical profiles of latent energy release, Hurricane Alberto (2000).

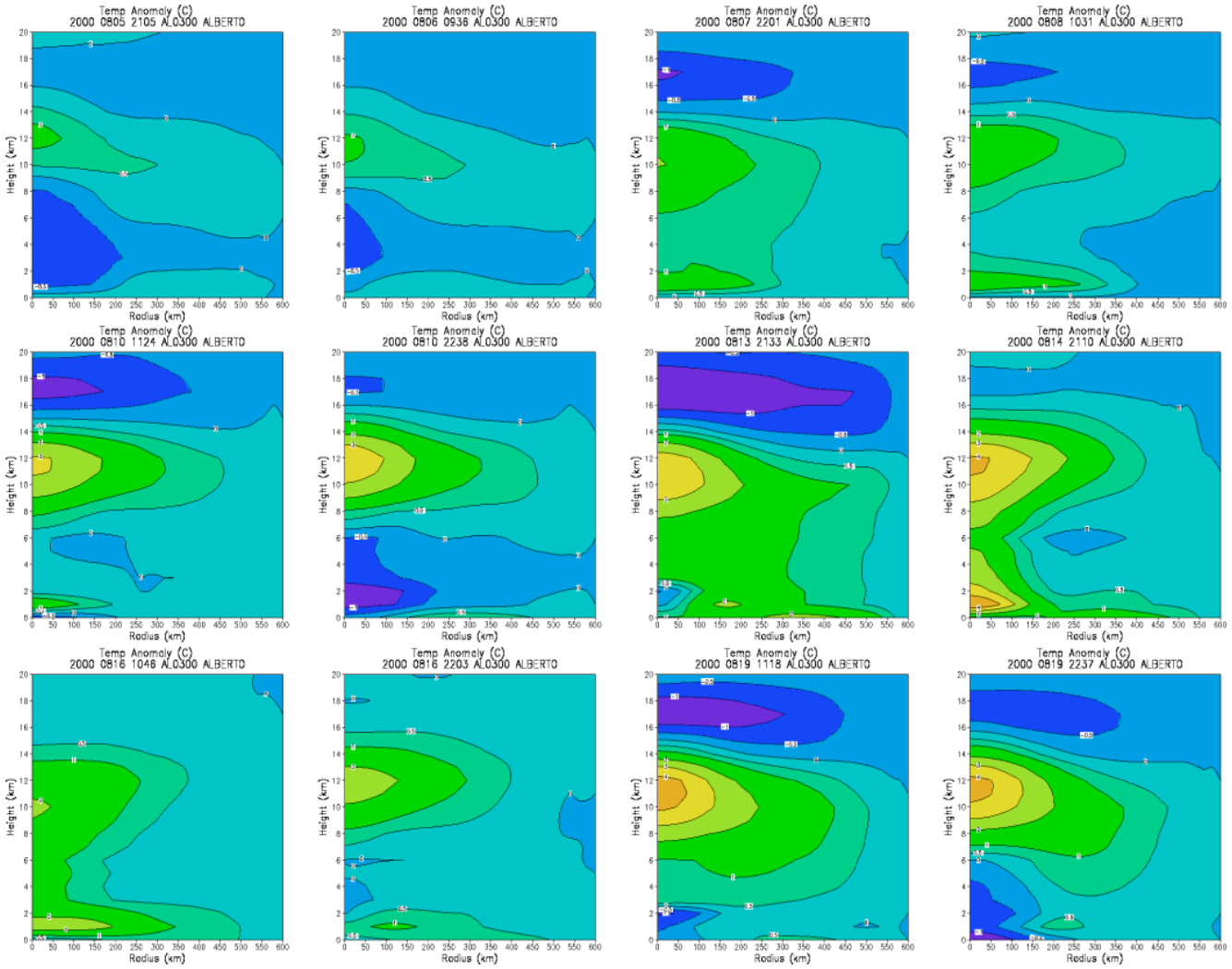

Figure 66: AMSU temperature anomalies for Hurricane Alberto (2000).

7.6.4 Alberto: energetics timeline

The vertical profiles of latent energy release shown in Figure 65 span a short part of Alberto's life cycle, from 8/9 through 8/12. In the second plot (top row, middle) we see increased latent energy release to a moderate 500 °C d^{-1}. This plot corresponds with the peak in the rainfall rate proxy during the first wind speed maxima. The other latent heating profiles are relatively constant with low values. The storm life cycle is not very well represented however so it is hard to draw conclusions from this set of plots.

Figure 66 shows the AMSU temperature anomalies for Hurricane Alberto. A small upper level warm anomaly is indicated in the first two plots (top row, left and middle left). This time period corresponds to the point in the storm lifecycle just before the first peak in wind speed. This anomaly dissipates, then reforms starting on 8/10 (middle row left and middle left) just before the storm's maximum wind speed. The maximum latent energy release shown in the vertical profiles on 8/10 corresponds to this temperature anomaly of +3°C. This warm anomaly is almost completely dissipated by 8/16 (bottom row, left). The third intensification of Alberto is captured in the second from last plot (bottom row, middle right) with a warm anomaly of +4°C.

7.7 Florence (ATL, 2000)

Florence was a Category 1 Hurricane on the Saffir-Simpson Scale that developed as a sub-tropical system, developing a warm core by 9/11. The storm meandered in a tight knot around its place of origin for four days until a short-wave trough in the westerlies accelerated Florence to the north-north east on 9/15.

7.7.1 Florence: characteristic variables

Perhaps the most dominating feature on Figure 67 in the deep negative difference in SST_{ICW}-SST_A apparent on 9/15 at 0000 UTC. Florence had been almost motionless for a few days and the local reduction in SST that resulted was almost -6°C. (Off the scale on Figure 68.) By 9/15 Florence was moving to the north-northeast and approached an area of warmer water (also seen in Figure 68) and HHC has a small maximum about a day before the peak wind speed on 8/16. The cold wake recovered quite rapidly. The 500 mb - 850 mb θ_e difference was smallest during both periods of elevated intensity. The two periods of convective instability (9/13 and 9/17) occur just after the minimum differences in SST_{ICW}-SST_A, and wind speed maxima.

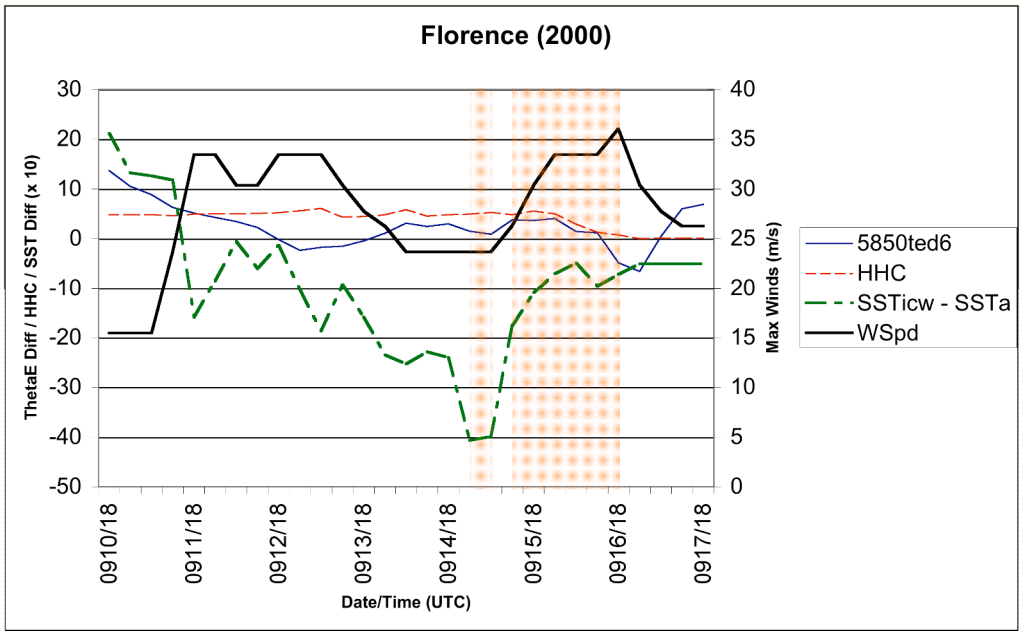

Figure 67: Characteristic variables of Hurricane Florence (2000).

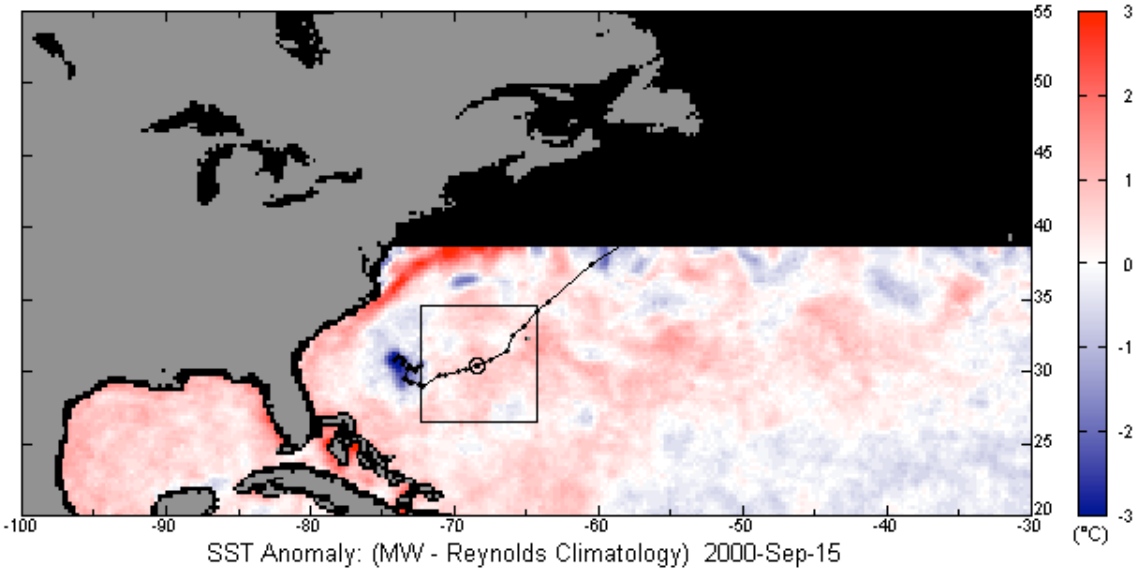

Figure 68: Hurricane Florence's storm-induced SST minimum before moving N-NE into warmer water.

7.7.2 Florence: flux analysis

The fluxes calculated for Hurricane Florence are shown in Figure 69. Not much is apparent due to the temporal resolution of the flux calculations, but the first peak in the rainfall rate proxy, on 9/12 corresponds with the first period of hurricane force winds. SST_{ICW}-SST_A begins to grow larger and more negative after this point, as the storm is trapped circling around its own cold wake. The rainfall rate proxy reaches its maximum value on 9/16 during the major convective burst event (shortly after the storm's SST_{ICW}-SST_A difference was near its minima) as the storm moved into warmer waters.

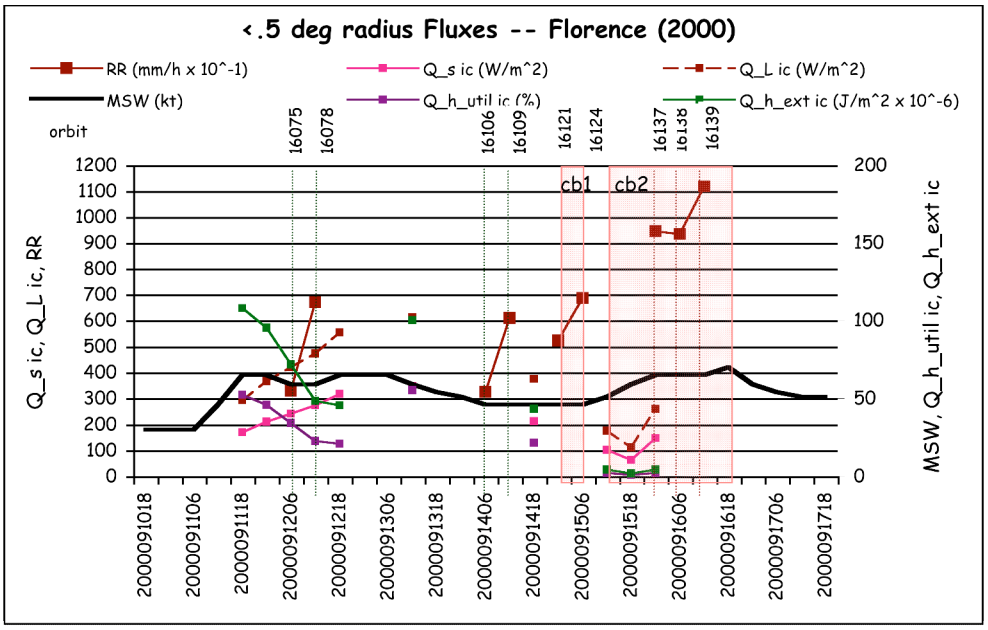

Figure 69: Flux calculations for Hurricane Florence. Radius = 0 to 0.5°.

7.7.3 Florence: energetics timeline

The time period from 9/15 at 0426 UTC through 9/16 0807 UTC is represented by the vertical latent heating profiles in Figure 70. The first figure (top left) corresponds to the period of the maximum negative SST_{ICW}-SST_A difference in Figure 67. As the storm moves into warmer water and is not influenced by its cold wake, latent energy increases as seen in the rest of the plots in Figure 70. The AMSU warm anomalies in Figure 71 show a 1°C temperature anomaly aloft on 9/12 (in plot 4, top row, right) that falls apart by 9/14. Temperature

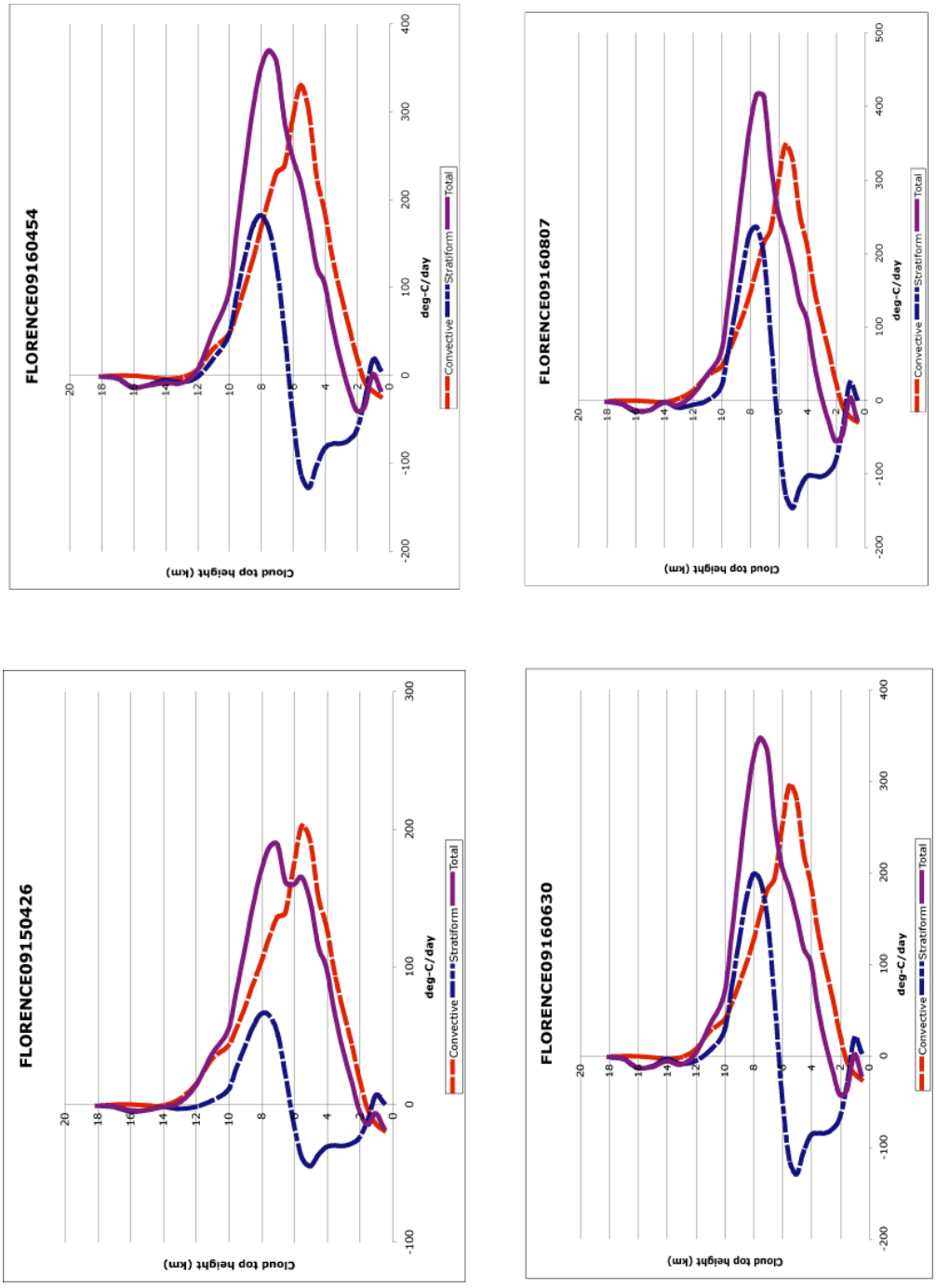

Figure 70: Vertical profiles of latent energy release, Hurricane Florence (2000).

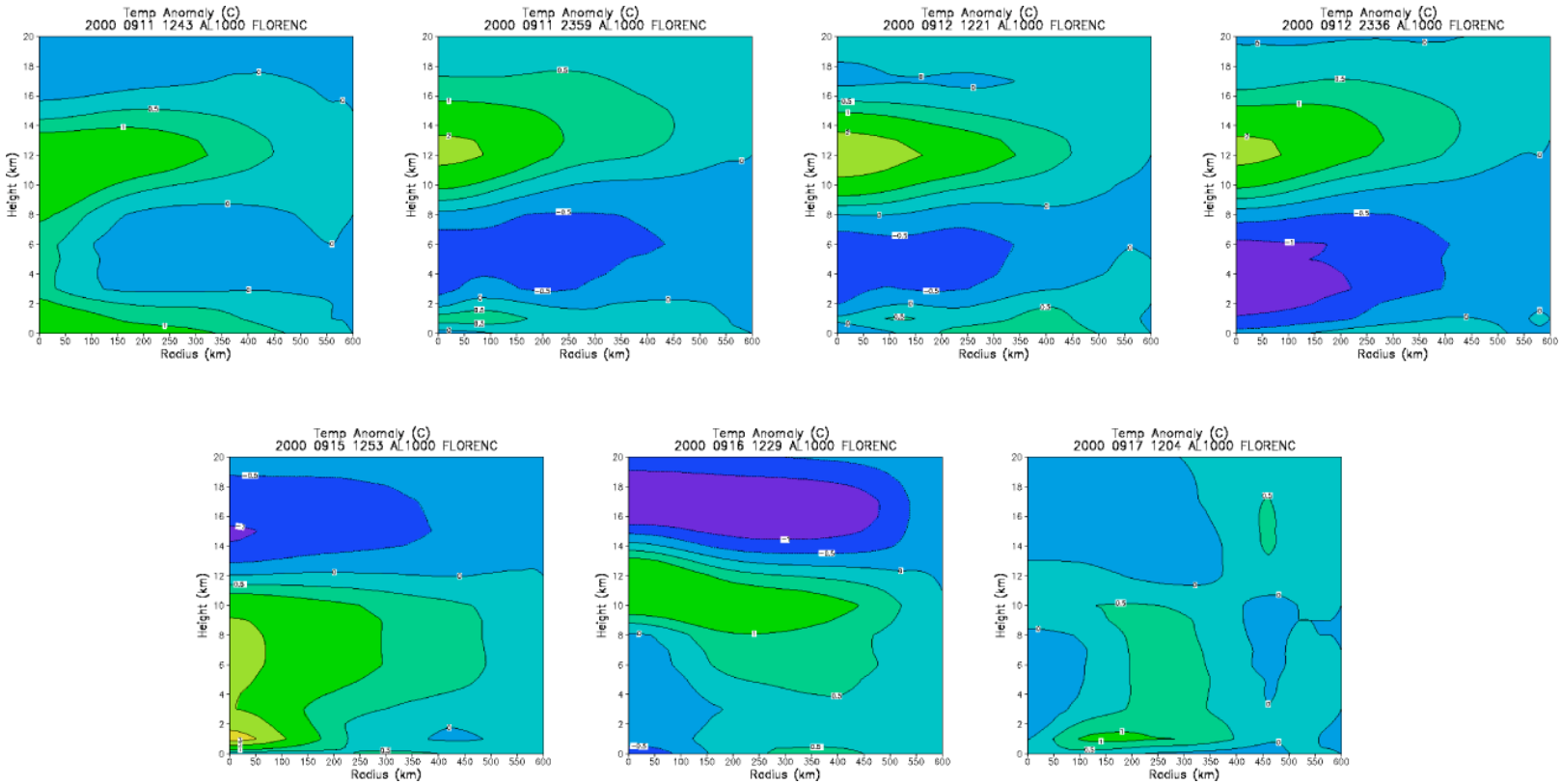

Figure 71: AMSU temperature anomalies for Hurricane Florence (2000).

stratification increases again as seen on 9/16 (bottom row, middle) when Florence's winds return to hurricane strength. Only a weak 1°C temperature anomaly develops however.

7.8 Chantal (ATL, 1999)

Tropical Storm Chantal was never very well organized. The system was dominated by strong low-mid level easterly flow, a rapid translation speed, and vertical wind shear. The storm became better organized just before making landfall at the Mexico/Belize border.

7.8.1 Chantal: characteristic variables

At first, the wind speed increase in Chantal seemed to be encouraged by the increasing HHC. Once the first convective burst occurred on 8/17 however the wind speed led the HHC variable by 6 to 12 hours. A small decrease in the SST_{ICW}-SST_A difference (in a positive direction) occurs just at the beginning of the second convective burst, just after the HHC reached its first maxima, decreased, and started upward again on 8/19.

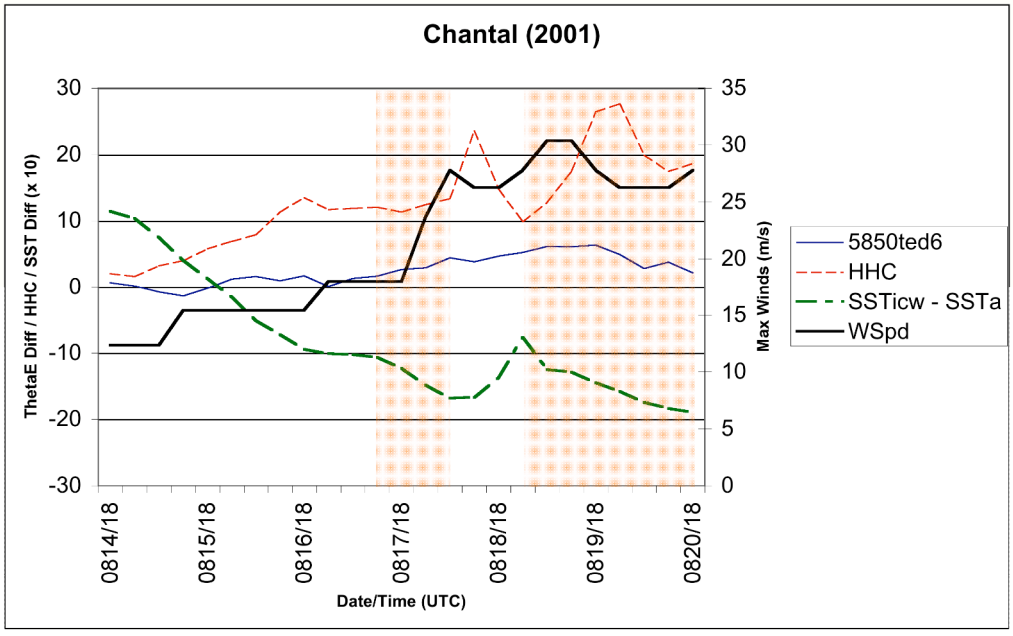

Figure 72: Characteristic variables of Tropical Storm Chantal (2001).

7.8.2 Chantal: flux analysis

No TMI data was available for Chantal. The TRMM satellite's orbit was being adjusted at this time. However H*Wind analysis was available. The flux data is shown in Figure 73. The timing of the maximum fluxes, especially during the first convective burst episode, corresponds nicely to the initial intensification of the wind speeds on 8/18. The fluxes precede the wind speed change by 6 to 12 hours (which fits the convective timescale.) The second peak in the Q_{h_ext} on 8/19 at 0000 UTC seems to be a result of the storm using up the energy available to it from the elevated HHC period 24 hours previously. (First HHC peak on Figure 72.

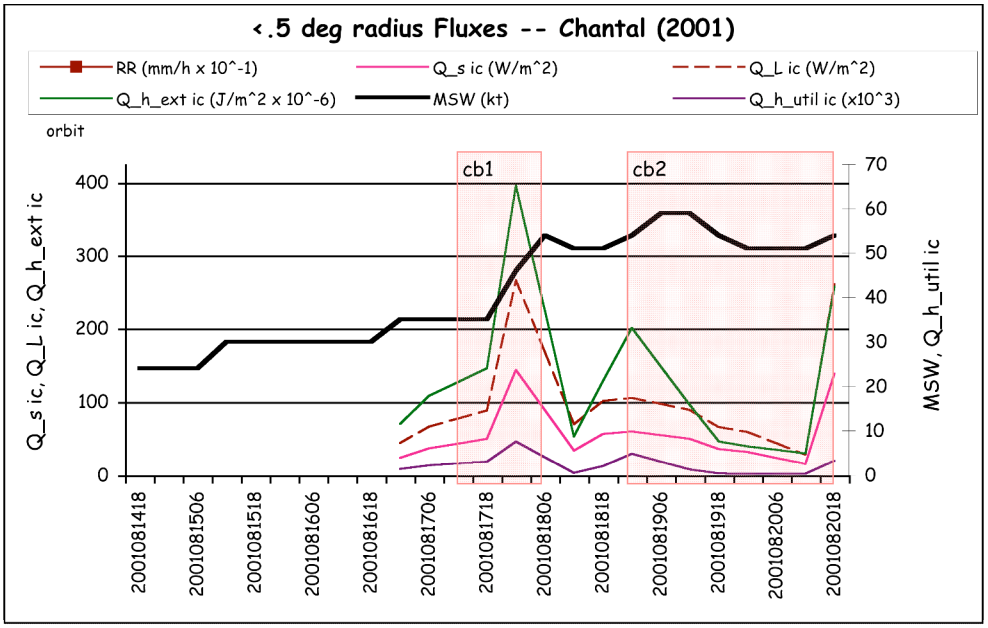

Figure 73: Flux calculations for Hurricane Floyd. Radius = 0 to .5°. (No rainfall rate proxy was available.)

7.8.3 Chantal: energetics timeline

Since no TMI data was available for Chantal, no vertical profiles of latent energy release are available. The AMSU temperature anomaly product was available and is shown in Figure 74. The first plot (top row, left) corresponds to the time when Chantal was

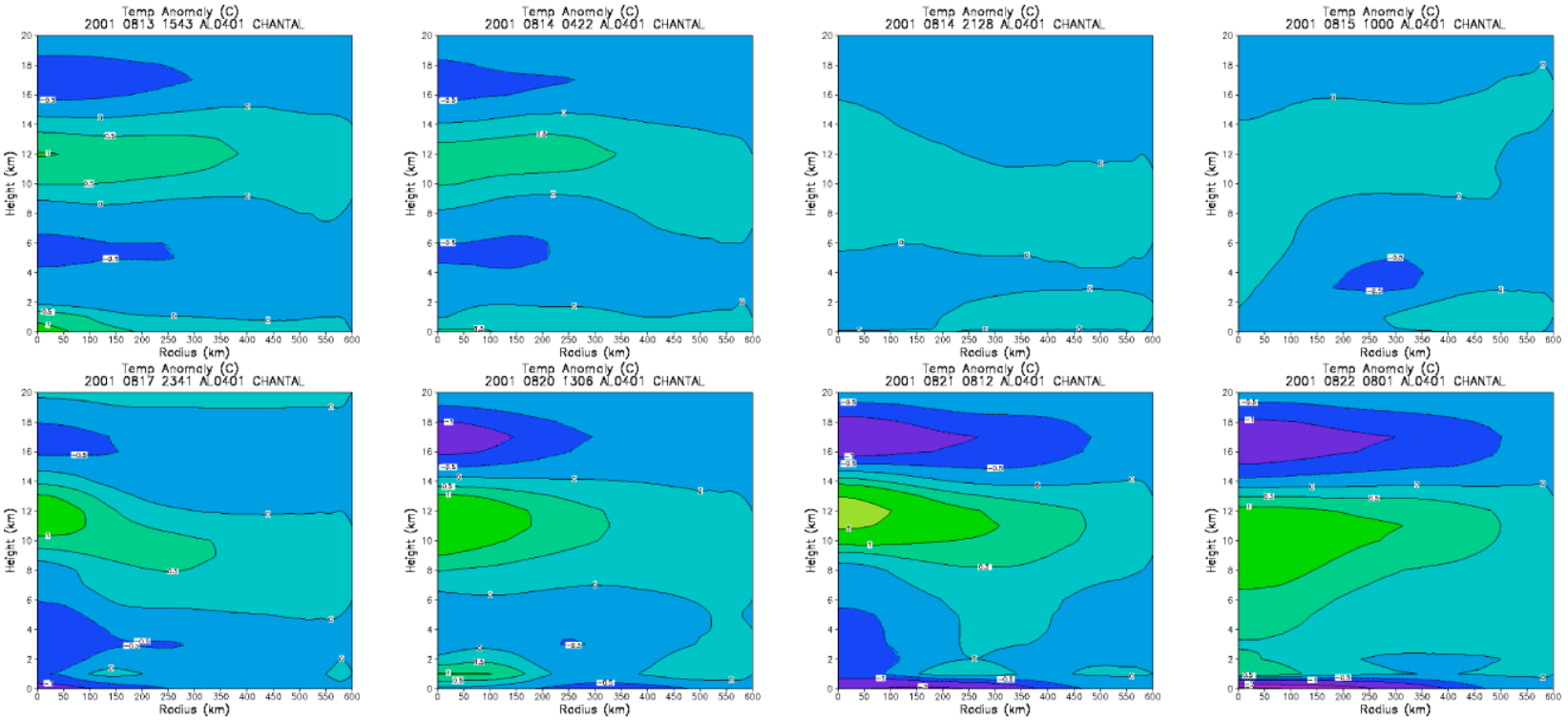

Figure 74: AMSU temperature anomalies for Hurricane Chantal (2001).

first named a tropical storm. A very small +1°C temperature anomaly is apparent aloft. The temperature anomaly of +1°C during the first convective burst episode is shown as well (bottom row, left). The largest temperature anomaly (+2°C) appears in the second-to-last plot (bottom row middle right) and corresponds to the period of rising fluxes just prior to landfall.

7.9 Case study summary

Seven case studies from the convective burst survey were presented in this chapter to try to detect some pattern amongst the variables to support the hypothesis chain central to this study. The analysis of each case began with a set of "characteristic variables" that emerged as "typical" in the convective burst environment. The flux calculations were presented followed by the rain rate proxy, the vertical profiles of latent heating and finally, the AMSU temperature anomalies. A summary of these case studies is presented in Table 23. Some very consistent patterns emerged by the end of the case study analysis:

- the SST_{ICW}-SST_A difference increases in a negative direction (SST_{ICW}-SST_A<0) immediately preceding or at the very beginning of each convective burst event.
- the SST_{ICW}-SST_A difference is coupled to the wind speed change (either precedes or lags)
- fluxes are coupled to the wind speed change
- in most cases, the 500 mb – 850 mb θ_e difference shows increased convective instability during the periods of maximum intensification and wind speeds
- the surface fluxes and the maximum rainfall rate proxy correspond temporally to the maximum AMSU temperature anomaly.

These observed patterns seem to validate the general energetic flow hypothesized in this study, however some of the lags/leads of the variables suggest the energy flow may adjust itself to different situations. In a very strong storm such as Floyd, the wind speed is the driving force behind the fluxes and even the ocean mixed layer structure. A storm without too much interference from other processes like Alberto responded directly to the ocean thermal structure. Anomalous warm or cold features in the ocean as seen in Floyd, Gert, Jose, Alberto, and Florence seem to impact the fluxes directly, perhaps through modification of the θ_e structure of the hurricane boundary layer environment. What is still unknown, and may never be known unless more in-situ data becomes available at small enough spatial and temporal scales, is just how far in advance the storm "feels" the presence of changes in the ocean structure – whether present in the environment, or self-induced.

	Wind speed	HHC	SST_{ICW}-SST_A	Convective instability	Fluxes	RR	LHR	Temp anomaly
Floyd	steady ↑ peak MSW +24h after CB	↑ w/s after HHC max	negatively ↑s at beginning of CB	peak just before CB	max during CB	max during CB	max at end of CB	max (+6°C) +14h after peak LHR
Gert	steady ↑ peak MSW +24h after CB	HHC max +12 h after peak MSW	negatively ↑s at beginning of CB	Small increase just before CB. Maxima just after peak MSW	max at peak MSW +24h after CB	↑ during CB	LHR only for CBs	max (+6°C) +64h after peak LHR
Jose	steady ↑ peak MSW during CB	HHC max + 12h after peak MSW	negatively ↑s during CB at time of peak MSW	Maxima during CB at peak MSW	max during each of 2 CBs	max during CB	max during 2 CBs	max (+1°C) +18h after peak LHR
Lenny	steady ↑ peak MSW +6h after CB	2 small HHC max during each CB	negatively ↑s at beginning of CB. Mirrors w/s.	Maxima at peak MSW +12h after CB. Small increase at beginning of CB.	Secondary max during major CB. Peak Q_L +6h after peak MSW when SST_{ICW}-SST_A>0	max during major CB	max during CB	max (+4°C) +12h after peak LHR
Alberto	no CB	HHC peak leads w/s ↑	highly correlated (r=.6) with w/s	Maxima during peak MSW	no fluxes	max with maximum convective instability	max at 1st peak MSW	max (+4°C) after 3rd peak MSW
Florence	steady ↑ peak MSW at end of CB	small peak during CB	negatively ↑s at beginning of CB. Leads w/s.	Maxima at peak MSW just after peak MSW. Small increase at beginning of CB.	can't tell	Secondary max with peak MSW. Max during CB when SST_{ICW}-SST_A>0	max during 2nd CB	max (+1°C) –72h before peak MSW
Chantal	steady ↑ peak MSW during CB	w/s leads HHC	negatively ↑s during CB	no change evident	max during CBs	no RR	no LHR	max (+1°C) during 1st CB

Table 23: Case study summary by storm by variable of interest

CHAPTER 8
CONVECTIVE BURSTS AND TROPICAL CYCLONE INTENSITY CHANGE

8.1 Statistical test

To get a general sense of how well the variables investigated in this study relate to tropical cyclone intensity change, a regression analysis was run using the independent variables from Chapter 3, Tables 1 and 2. In addition to these variables, the variable "CB/no CB" was added to the analysis to see if convective bursts were linearly related to intensity change.

The dependent variable was tropical cyclone intensity change as measured by wind speed change in knots at some interval of time in the future. The test was run for wind speed change 6 hours, 12 hours, 18 hours, and 24 hours in the future.

8.2 Results of the regression analysis

The results are presented in Table 24:

Hours in future	R	R^2
+6 hrs	.453	.206
+12 hrs	.530	.281
+18n hrs	.577	.332
+24 hrs	.609	.371

Table 24: Results of regression analysis of all atmospheric and oceanic variables and convective burst state on wind speed change in the future.

The Beta coefficients of the regression analysis for predicting wind speed change 24 hours in the future are in Table 25. The variables with at least weak correlation with wind speed 24 hours in the future are highlighted in yellow.

Variable	Coefficient (Standardized)	Correlation
Storm translation speed	.033	-.078
Coriolis parameter	.015	.018
SST_{IC}-SST_A	-.184	-.047
SST_{ICW}-SST_A	.056	-.026
SSHA	.001	-.006
HHC	**.033**	**.384**
SST_{IC}	**.380**	**.416**
Wind speed	**-.323**	**-.301**
200 – 850 mb wind shear (300 km)	**-.157**	**-.188**
150 mb wind divergence	**.104**	**.239**
200 –850 mb wind shear (600 km)	**-.084**	**-.172**
700 – 500 mb moisture divergence (200 km)	.009	.047
500 – 925 mb θ_e difference (300 km)	.033	.022
700 – 500 mb moisture divergence (500 km)	-.004	.057
500 – 850 mb θ_e difference (600 km)	.030	.013
PWAT (200 km)	-.067	.042
PWAT (500 km)	.032	.070
850 mb moisture divergence (200 km)	0.013	-.078
850 mb moisture divergence (600 km)	**-.013**	**-.110**
Convective burst or no convective burst	**.094**	**.322**

Table 25: Beta coefficients for regressions analysis – 24 hours in the future intensity change.

8.3 Discussion

The variables with at least a weak correlation are, as expected, the thermal structure of the ocean, the SST feedback in the inner core, weak shear, good upper level outflow, a moist tropopause, and convective burst occurrence.

The three variables most highly correlated with wind speed 24 hours in the future are the ocean variables, HHC and SST_{IC} and the convective burst occurrence. This relationship is probably non-linear in nature due to multiple interacting feedbacks. The storm changes the ocean environment and the ocean impacts the storm. Only more in-situ data will help resolve many of the remaining questions in this research.

CHAPTER 9
SUMMARY, FUTURE WORK, AND CONCLUSIONS

9.1 Summary

This research is based on a global survey of convective burst episodes observed in tropical storms and cyclones from 1999-2001. Before this research began, no one knew how prevalent convective bursts were in tropical cyclones. "How often do they occur?" "Are they rare episodes of extreme eyewall convection?" "Do they occur in storms in all ocean basins?" The forcing mechanisms of convective burst were only speculation. "Do convective bursts enhance a storm's structure or interfere with it?" "What role does shear play in a convective burst?" "How does a convective burst affect storm symmetry?" and, ultimately, "How does a convective burst affect storm intensity?"

In an attempt to gain some fundamental understanding of convective bursts and their implications for tropical cyclone intensity change, this study employed an ensemble of discriminant analysis procedures based on atmospheric and oceanic variables thought to be important to convective burst existence. These statistical tests were not meant to "predict" convective burst existence necessarily, although they do. They were meant to "tease out" any important underlying structure in the variables that could be important to understand the phenomena. The discriminant analysis was divided into two spheres of influence – first the atmosphere then the ocean. Finally the variables that emerged from these procedures as having discriminatory abilities were combined into a final analysis considering both the atmosphere and the ocean. Both atmospheric and oceanic variables – kinematic and thermodynamic – were important in discerning the existence of convective burst events. The following observations emerged as important "characteristics" typical of the convective burst environment:

- a good supply of moist air in the ambient environment
- lower tropospheric convergence near the storm (200 km)
- warm ocean temperature structure
- low wind shear
- a larger scale (600 km radius) well mixed, fairly stable mid troposphere
- a slow moving storm with a longer dwell rate

- moderate wind speed
- a tendency to modify the near-storm ocean environment.

A hypothesis chain was presented that attempts to link enhanced sea-air fluxes with convective burst development, upper level latent energy release, and finally, subsiding air leading to an upper level warm anomaly – the warm core of the tropical cyclone.

In an attempt to link the thermal structure of the ocean to increased surface fluxes and convective burst development, this study adapted a method of calculating fluxes, upper ocean heat content, and upper ocean energy extracted (used by Cione et al. with in-situ buoy and dropsonde data) based on remotely sensed data from a variety of satellite platforms. There is not much precedent for this methodology at the storm-size scale in the literature. The method proved useful, but is limited by the surface wind analysis available on a case-by-case basis.

To see how the sea-air processes may be influencing the energetics aloft, the TMI data from a set of 26 storms was processed, and composite vertical profiles of latent energy release were constructed for each of three groups: time periods with convective burst events coincident with intensification (> 15 kt.), time periods with convective burst events coincident with no or little intensification (<15 kt.), and time periods with no convective burst present. Time periods with a convective burst (regardless of the concurrent intensity change) had a 2-1/2 to 3 time greater magnitude in mid to upper level latent heating than the null cases. Clearly, the convective burst cases transfer more latent energy.

To investigate the translation of this latent energy release into real effects on the warm anomaly aloft in a tropical cyclone, the AMSU temperature anomalies were constructed for each of the case studies. More work is needed to definitively "prove" that subsidence provides energy to "warm" the tropical cyclone core, but this analysis of the time coincidence between the latent energy release and the AMSU observed warming provides more than the anecdotal evidence than previously existed.

The case studies presented were a few of the total number processed for this study. A variety of storm intensities and types of relationships were captured in the seven selected. The following relationships were observed:

- the SST_{ICW}-SST_A difference increases in a negative direction (SST_{ICW}-SST_A<0) immediately preceding or at the very beginning of each convective burst event.
- the SST_{ICW}-SST_A difference is coupled to the wind speed change (either precedes or lags)
- changes in fluxes are coupled to the wind speed change

- in most cases, the 500 mb – 850 mb θ_e difference shows increased convective instability during the periods of maximum intensification and wind speeds
- the surface fluxes and the maximum rainfall rate proxy correspond temporally to the maximum AMSU temperature anomaly.

In general, the hypothesized flow of energy is viable, but there may be rearrangement of the driving forces depending on the storm's large-scale environment and history. In any case, a warm ocean structure seems to work with wind speed to generate enhanced surface fluxes that affect the convective instability of the tropical cyclone boundary layer. These effects make the environment more likely to be able to sustain the extreme convective burst event. The convective burst events are characterized by more energy aloft, which may contribute to the development of the warm core (as seen from AMSU.)

A regression analysis of the atmospheric and oceanic variables that emerged as statistically descriptive of convective burst events and the condition of burst presence versus no presence was performed to try to predict wind speed change in the next 24 hour period. Results were quite strong ($r = .609$) and instill confidence in the ability of the processes investigated to work together to intensify tropical cyclones.

9.2 Future work

The future work from this dissertation can be split into a few different lines of research. The "big-picture" of tropical cyclone intensity change mechanisms, of which convective bursts are just one, can be split into its inherent sub-categories: ocean forcings, atmospheric forcings, kinematic forcings, thermodynamic forcings, etc. No attempt was made in this study to be "all-inclusive". Only the role of these extreme convective events was considered. As such there is considerable future work to be done in trying to complete the hypothesis chain of tropical cyclone intensification, even with regard to convective burst events.

9.2.1 Atmospheric forcings

The data set employed in this study, the NCEP/NCAR Re-analysis may, have too coarse of a grid resolution to effectively study the role of atmospheric processes. In particular, the structure of moist static energy in the hurricane boundary layer environment may exist at too fine of a scale to detect the θ_e gradients which correspond to the ocean mixed layer structure below. Potential kinematic forcing mechanisms in the atmosphere, vertical shear and moisture divergence in particular, will also benefit from finer scale data

resolution. An alternative data set, NOGAPS 1° x 1° data, may be the next best choice. A more comprehensive look at these variables is an important follow-up to this study.

9.2.2 Oceanic forcings

The oceanic forcing of local convection is just beginning to be researched. This study did not show direct causation between increased sea-air flux and increased convective activity. The relationship is hypothesized and examined and found to be consistent, but the forcing of convection by ocean processes will have to be modeled. Perhaps a relatively simple coupled ocean-atmosphere model on the "cloud" resolving scale is a next step in this process. This study examined the feasibility of computing various variables from remotely sensed data of fine resolution. Perhaps these fields could be modeled, or at the very least incorporated into a "Maximum Potential Intensity" analysis, as is already a common tool in hurricane intensity analysis. A current Joint Test-bed Project at the National Hurricane Center is testing the feasibility of incorporating some storm-scale ocean variables into the Statistical Hurricane Intensity Prediction Scheme (SHIPS model, DeMaria and Kaplan, 1999) in the coming hurricane season.

9.2.3 Flux calculations

The rough-estimate flux calculations employed in this research are highly dependent on the current state of the research of the hurricane boundary layer. The drag coefficients under high wind speeds, the low-level shear present, the downdraft structures, and the influence the storm itself has on its low-level environment are all current (and controversial!) research topics in need of more observational data for testing. Hopefully more boundary layer experiments like Coupled Boundary Layers/Air-Sea Transfer (CBLAST) will provide a better understanding of these processes in the future. A large research effort is currently underway to attempt to calculate fluxes using remotely sensed data on a larger scale. Using H*Wind analyses for many storms is not a feasible means of estimating the surface wind speed in near real-time. A more objective scheme to eliminate bad observational data and rain-flagged scatterometer data is needed. New scatterometer sensors and algorithms are making progress in this regard.

9.3 Importance of this work

This work represents the most complete attempt to date to link the thermodynamics of the ocean to eyewall convection and the energetics of the tropical cyclone using remotely sensed data from many platforms. The global survey of convective burst events has shown

that convective burst are ubiquitous in tropical cyclones, and not just a sporadic feature of interest. The typical characteristics of convective burst environments have been described and statistically tested. These results may lead to the ability to discern critical thresholds for some of the important variables in the future to be able to predict convective burst development. A new method of computing fluxes from remotely sensed data was employed. The ocean has been found to be at least as important as the atmosphere in influencing convective tendencies. And finally, the latent energy released during the intensification stage of a tropical cyclone with a convective burst event is 2-1/2 to 3 times greater than the corresponding stage in a tropical cyclone with no convective burst.

More specifically, this study has shown:

- 80% of tropical cyclones have at least one convective burst event
- Convective burst events usually occur during the intensification phase of the storm life cycle.
- Convective bursts are usually accompanied by a moderate (5-15 kt) wind speed increase, although some have little or no wind speed change during the burst itself.
- Peak convective burst incidence is in the late summer, mirroring the peak in upper ocean heat content and therefore, the peak supply of moist static energy.
- Convective bursts typically form within 1° of the tropical cyclone center within the vortical Rossby radius of deformation. This placement is efficient for channeling energy upward from the ocean to the troposphere to affect tropical cyclone intensity.
- Four main atmospheric variables typify convective burst existence when compared to times with no convective burst:
  - sufficient precipitable water at 200 km and 500 km
  - increased 150 mb divergence at 600 km
  - 2-1/2 times more convective instability in the large-scale environment (500 mb – 850 mb difference in θ_e at 600 km)
  - 1-1/2 to 2 times more 850 mb moisture divergence at 200 km and 600 km.
- Six main oceanic variables show characteristic differences in convective burst events:
  - the mean climatological SST is 1.25°C greater during convective burst events

  - the hurricane heat content is double for convective burst times
  - SST_{ICW}-SST_A indicates less inner-core cooling for the convective burst time periods. A deeper mixed layer or less upwelling of cold water slows mixing.
  - SST_{ICW} and SST_{IC} are approximately 1.4°C warmer for convective burst times also reflecting the strong warm thermal structure of the ocean.
- The moist static energy provided by the warm ocean is more influential on convective burst occurrence than simply having "enough" available atmospheric moisture.
- Storms with convective bursts actively modify their own environments to a greater extent than storms with no convective burst.
- Tropical cyclones generally utilize only about 8% of the total enthalpy flux available from the ocean/atmosphere boundary layer.
- Storms with convective bursts utilize more energy from the ocean (11%) than storms with no convective burst (2%).
- Sea-air fluxes are greatly enhanced (doubled) during convective burst time periods.
- Convective burst time periods exhibit twice as much latent energy release in the mid-upper troposphere than non-burst time periods regardless of the concurrent wind speed change.

The upscale energy cascade of the tropical cyclone with a convective burst event has been shown to be consistent with the hypothesized energy chain as illustrated in Figure 75.

A very warm ocean with a deep mixed layer is the base of the energy supply for the intensifying tropical cyclone. The undilute convection of the convective burst mines the enhanced boundary layer gaining almost twice the total enthalpy flux of a storm with no convective burst. This twofold energy utilization is apparent in the mid-upper troposphere as TRMM vertical profiles of latent energy release show 2 to 2-1/2 times the magnitude of profiles of non-convective burst time periods. Finally, in most cases and after a 12 to 24 hour lag, an enhanced warm core anomaly appears in AMSU analyses. This lag time is consistent with the convective timescale necessary for adiabatic warming through subsidence along the inner edge of the tropical cyclone eyewall.

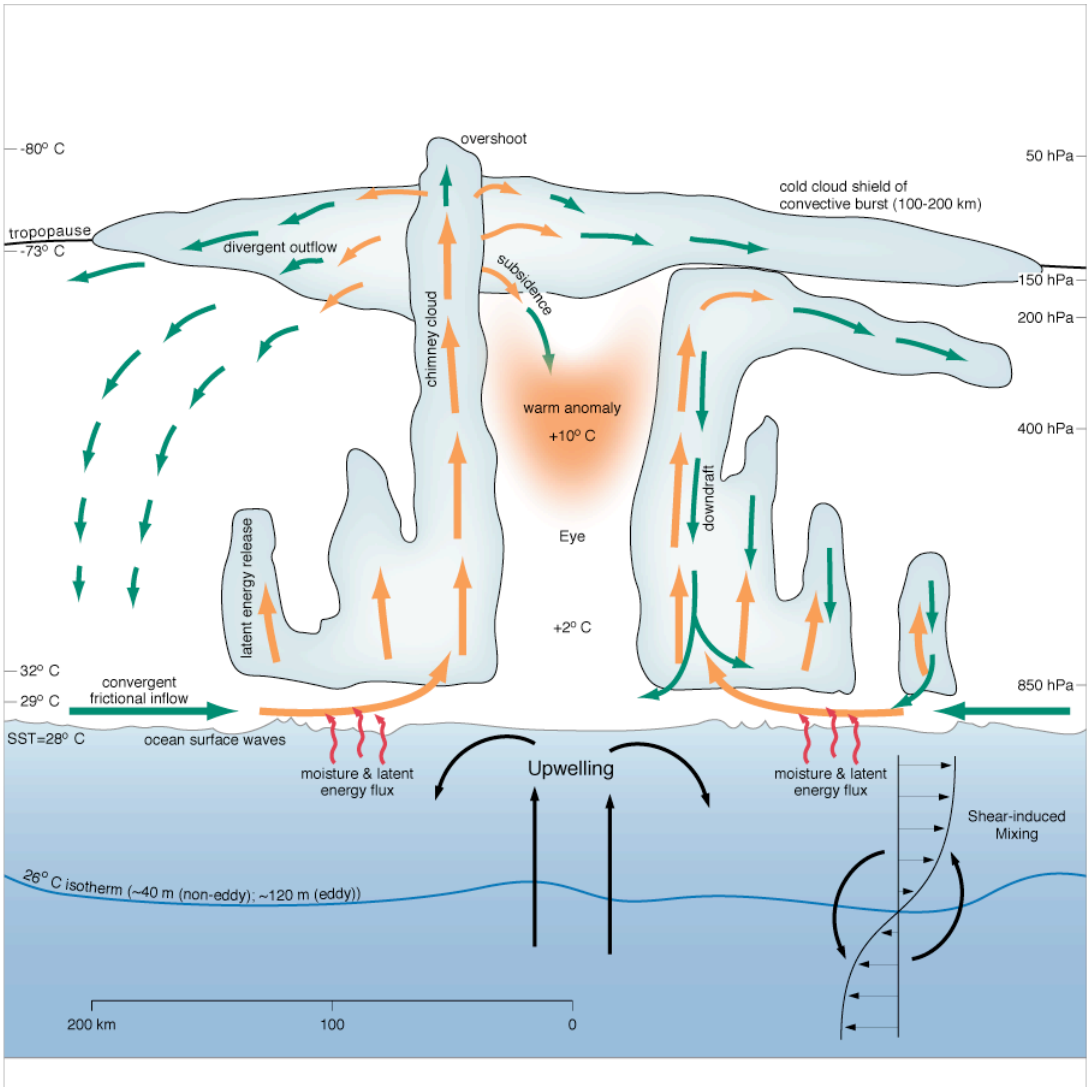

Figure 75: Recap of the energetics of the tropical cyclone augmented with a convective burst event. A warm ocean provides energy to the TC through the boundary layer sea-air fluxes. The convective burst is efficient at mining the enhanced boundary layer fluxes and channeling this increased energy into the mid-upper tropospheric levels. The enhanced upper tropospheric latent energy is transformed into adiabatic warming as the air slowly subsides in the eye of the tropical cyclone, increasing and maintaining the warm core of the tropical cyclone. This warming, drier air subsiding along the inside edge of the hurricane eyewall leads to surface pressure decrease and eventually an increase in tangential wind velocities.

APPENDIX

TRMM OVERPASS DATES AND TIMES FOR COMPOSITE VERTICAL LATENT HEATING PROFILES

Basin	Year	Storm Name	Orbit Date	Orbit Time (UTC)
SHEM	1999	Alda	01/17	1734
SHEM	1999	Alda	01/18	1131
SHEM	1999	Alda	01/18	1622
EPAC	1999	Beatriz	07/09	2258
EPAC	1999	Beatriz	07/10	1338
EPAC	1999	Beatriz	07/12	2230
EPAC	1999	Beatriz	07/13	1311
EPAC	1999	Beatriz	07/14	2140
ATL	2000	Alberto	08/09	2155
ATL	2000	Alberto	08/10	2218
ATL	2000	Alberto	08/11	0308
ATL	2000	Alberto	08/11	2242
ATL	2000	Alberto	08/12	0019
ATL	2000	Nadine	10/20	1401
ATL	2000	Nadine	10/21	1113
EPAC	2001	Flossie	08/27	1843
EPAC	2001	Flossie	08/29	0158
ATL	2001	Karen	10/12	1857
ATL	2001	Karen	10/12	2035
ATL	2001	Olga	11/24	2327
ATL	2001	Olga	11/25	1915
ATL	2002	Cristobal	08/06	1143
ATL	2002	Cristobal	08/06	1636
ATL	2003	Ana	04/21	0031
ATL	2003	Ana	04/21	2337

Table 26: TRMM overpass storm names, dates and times included in the “no convective burst” composite vertical latent heating profile.

Basin	Year	Storm Name	Orbit Date	Orbit Time (UTC)
ATL	1999	Cindy	08/19	2037
ATL	1999	Cindy	08/21	1947
ATL	1999	Cindy	08/22	1028
ATL	1999	Cindy	08/26	1024
ATL	1999	Cindy	08/26	1651
ATL	1999	Cindy	08/27	1048
ATL	1999	Cindy	08/30	1201
ATL	1999	Cindy	08/30	1337
ATL	1999	Floyd	09/09	1109
ATL	1999	Floyd	09/10	0954
ATL	1999	Floyd	09/11	0215
ATL	1999	Floyd	09/11	1019
ATL	1999	Floyd	09/12	0238
ATL	1999	Floyd	09/12	0905
ATL	1999	Lenny	11/14	0222
ATL	1999	Lenny	11/15	0246
ATL	1999	Lenny	11/15	1730
ATL	1999	Lenny	11/16	0136
ATL	1999	Lenny	11/16	1615
ATL	1999	Lenny	11/17	0024
ATL	1999	Lenny	11/17	1506
ATL	1999	Lenny	11/19	2224
ATL	1999	Lenny	11/20	1306
WPAC	2000	Damrey	05/07	00832
WPAC	2000	Damrey	05/07	1817
WPAC	2000	Damrey	05/08	0857
WPAC	2000	Damrey	05/08	1705
EPAC	2000	Carlotta	06/19	0224
EPAC	2000	Carlotta	06/20	1053
WPAC	2000	Bilis	08/19	1210
WPAC	2000	Bilis	08/20	0252
WPAC	2000	Bilis	08/20	1058
WPAC	2000	Saomai	09/02	1804
WPAC	2000	Saomai	09/03	1829
WPAC	2000	Saomai	09/04	0233
WPAC	2000	Saomai	09/04	1713
WPAC	2000	Saomai	09/05	1739
WPAC	2000	Saomai	09/06	0145
WPAC	2000	Saomai	09/06	1623
WPAC	2000	Saomai	09/07	0207
WPAC	2000	Saomai	09/08	0052
ATL	2000	Isaac	09/26	0411
ATL	2000	Isaac	09/26	1852
ATL	2000	Isaac	09/26	0257
ATL	2000	Keith	09/30	2017
ATL	2000	Keith	10/02	1932
ATL	2000	Keith	10/03	0337
ATL	2000	Keith	10/05	0247

ATL	2001	Erin	09/05	0247
ATL	2002	Isidore	09/17	1207
ATL	2002	Isidore	09/19	1155
ATL	2002	Isidore	09/19	2006
ATL	2002	Lili	09/24	0719
ATL	2002	Lili	09/24	1710
ATL	2002	Lili	09/25	0802
ATL	2002	Lili	09/28	0651
ATL	1999	Gert	09/14	0823
ATL	1999	Gert	09/14	2303

Table 27: TRMM overpass storm names, dates and times included in the "convective burst with intensification" composite vertical latent heating profile.

Basin	Year	Storm Name	Orbit Date	Orbit Time (UTC)
WPAC	1999	Kate	04/22	1444
WPAC	1999	Kate	04/23	2316
WPAC	1999	Kate	04/24	1358
WPAC	1999	Kate	04/26	1311
WPAC	1999	Kate	04/26	1939
EPAC	1999	Hilary	09/18	0138
EPAC	1999	Hilary	09/19	1008
ATL	1999	Jose	10/19	1434
ATL	1999	Jose	10/20	0513
ATL	1999	Jose	10/21	0539
ATL	1999	Jose	10/21	1345
ATL	1999	Jose	10/23	0451
ATL	1999	Jose	10/24	0514
ATL	1999	Jose	10/24	0651
ATL	1999	Jose	10/25	0717
EPAC	2000	Aletta	05/24	0127
EPAC	2000	Aletta	05/24	1608
EPAC	2000	Aletta	05/26	0037
EPAC	2000	Aletta	05/26	1518
WPAC	2000	Wukong	09/05	0426
WPAC	2000	Wukong	09/06	1932
ATL	2000	Florence	09/15	0426
ATL	2000	Florence	09/16	0454
ATL	2000	Florence	09/16	0630
ATL	2000	Florence	09/16	0807
EPAC	2001	Dalila	07/21	1230
EPAC	2001	Dalila	07/22	1116

EPAC	2001	Dalila	07/22	2059
EPAC	2001	Dalila	07/23	1140
EPAC	2001	Dalila	07/24	1204
EPAC	2001	Dalila	07/24	2009
EPAC	2001	Dalila	07/26	1112
EPAC	2001	Gil	09/04	1430
EPAC	2001	Gil	09/05	2325
EPAC	2001	Gil	09/07	1320
EPAC	2001	Gil	09/07	2132

Table 28: TRMM overpass storm names, dates and times included in the "convective burst with little or no intensification" composite vertical latent heating profile.

LIST OF REFERENCES

Adler, R. F. and E. B. Rodgers (1977). "Satellite-Observed Latent Heat Release in a Tropical Cyclone." Monthly Weather Review **105**(8): 956-963.

Andreas, E. L. and K. A. Emanuel (2001). "Effects of Sea Spray on Tropical Cyclone Intensity." Journal of the Atmospheric Sciences **58**(24): 3741-3751.

Anis, A. and J. N. Moum (1994). "Prescriptions for Heat Flux and Entrainment Rates in the Upper Ocean during Convection." Journal of Physical Oceanography **24**(10): 2142-2155.

Barnes, G. M. and P. B. Bogner (2001). "Comments on "Surface Observations in the Hurricane Environment"." Monthly Weather Review **129**(5): 1267-1269.

Barnes, G. M., J. F. Gamache, et al. (1991). "A Convective Cell in a Hurricane Rainband." Monthly Weather Review **119**(3): 776-794.

Barnes, G. M. and M. D. Powell (1995). "Evolution of the Inflow Boundary Layer of Hurricane Gilbert (1988)." Monthly Weather Review **123**(8): 2348-2368.

Barnes, G. M., E. J. Zipser, et al. (1983). "Mesoscale and Convective Structure of a Hurricane Rainband." Journal of the Atmospheric Sciences **40**(9): 2125-2137.

Bender, M. A. and I. Ginis (2000). "Real-Case Simulations of Hurricane-Ocean Interaction Using A High-Resolution Coupled Model: Effects on Hurricane Intensity." Monthly Weather Review **128**(4): 917-946.

Bentamy, A., K. B. Katsaros, et al. (2003). "Satellite Estimates of Wind Speed and Latent Heat Flux over the Global Oceans." Journal of Climate **16**(4): 637-656.

Betts, A. K. and J. Simpson (1987). "Thermodynamic Budget Diagrams for the Hurricane Subcloud Layer." Journal of the Atmospheric Sciences **44**(5): 842-849.

Bister, M. (2001). "Effect of Peripheral Convection on Tropical Cyclone Formation." Journal of the Atmospheric Sciences **58**: 3463-3476.

Black, M. L., R. W. Burpee, et al. (1996). "Vertical Motion Characteristics of Tropical Cyclones Determined with Airborne Doppler Radial Velocities." Journal of the Atmospheric Sciences **53**(13): 1887-1909.

Black, P. G. (1978). "Mesoscale Cloud Patterns Revealed by Apollo-Soyuz Photographs." Bulletin of the American Meteorological Society **59**(11): 1409-1419.

Black, P. G. (1983). Ocean temperature changes induced by tropical cyclones. University Park, PA, The Penn State University**:** 278.

Black, P. G., R. W. Burpee, et al. (1986). "Appearance of the Sea Surface in Tropical Cyclones." Weather and Forecasting **1**(1): 102-107.

Black, P. G., R. L. Elsberry, et al. (1988). "Atmospheric Boundary Layer and Oceanic Mixed Layer Observations in Hurricane Josephaine Obtained from Air-Deployed Drifting Buoys and Research Aircraft." Journal of Atmospheric and Oceanic Technology **5**(6): 683-698.

Black, P. G. and G. J. Holland (1995). "The Boundary Layer of Tropical Cyclone Kerry (1979)." Monthly Weather Review **123**(7): 2007-2028.

Bogner, P. B., G. M. Barnes, et al. (2000). "Conditional Instability and Shear for Six Hurricanes over the Atlantic Ocean." Weather and Forecasting **15**(2): 192-207.

Bosart, L. F., C. S. Velden, et al. (2000). "Environmental Influences on the Rapid Insensification of Hurricane Opal (1995) over the Gulf of Mexico." Monthly Weather Review **128**: 322-352.

CDC (2005). The NCEP/NCAR Reanalysis project. C. D. Center, Internet. **2005**.

Cecil, D. J. and E. J. Zipser (1999). "Relationships between Tropical Cyclone Intensity and Satellite-Based Indicators of Inner Core Convection: 85-GHz Ice-Scattering Signature and Lightning." Monthly Weather Review **127**(1): 103-123.

Chan, J. C. L., Y. Duan, et al. (2001). "Tropical Cyclone Intensity Change from a Simple Ocean-Atmosphere Coupled Model." Journal of the Atmospheric Sciences **58**(2): 154-172.

Chang, C.-P. and C. R. I. Miller (1977). "Comparison of Easterly Waves in the Tropical Pacific during Two Contrasting Periods of Sea Surface Temperature Anomalies." Journal of the Atmospheric Sciences **34**(4): 615-628.

Chang, S. W. and R. A. Anthes (1979). "The Mutual Response of the Tropical Cyclone and the Ocean." Journal of Physical Oceanography **9**(1): 128-135.

Chen, S. S. and W. M. Frank (1993). "A Numerical Study of the Genesis of Extratropical Convective Mesovortices. Part I: Evolution and Dynamics." Journal of the Atmospheric Sciences **50**(15): 2401-2426.

Cione, J., P. G. Black, et al. (2000). "Surface Observations in the Hurricane Environment." Monthly Weather Review **128**: 1550-1561.

Cione, J. and E. W. Uhlhorn (2003). "Sea Surface Temperature Variability in Hurricanes: Implications with Respect to Intensity Change." Monthly Weather Review **131**: 1783-1796.

Clark, W. A. V. and P. L. Hosking (1986). Statistical Methods for Geographers. New York, John Wiley & Sons.

Davis, C. A. and L. F. Bosart (2001). "Numerical Simulations of the Genesis of Hurricane Diana (1984). Part I: Control Simulation." Monthly Weather Review **129**(8): 1859-1881.

DeMaria, M. and J. Kaplan (1994). "Sea surface temperature and the maximum intensity of Atlantic tropical cyclones." Journal of Climate **7**: 1324-1334.

DeMaria, M., M. Mainelli, et al. (2005). "Further Improvements to the Statistical Hurricane Intensity Prediction Scheme (SHIPS)." Weather and Forecasting **20**(4): 531-543.

Donelan, M. A., W. M. Drennan, et al. (1997). "The Air-Sea Momentum Flux in Conditions of Wind Sea and Swell." Journal of Physical Oceanography **27**(10): 2087-2099.

Doswell, C. A. I. (1987). "The Distinction between Large-Scale and Mesoscale Contribution to Severe Convection: A Case Study Example." Weather and Forecasting **2**(1): 3-16.

Dvorak, V. F. (1975). "Tropical Cyclone Intensity Analysis and Forecasting from Satellite Imagery." Monthly Weather Review **103**(5): 420-430.

Eastin, M. D., W. M. Gray, et al. (2005). "Buoyancy of Convective Vertical Motions in the Inner Core of Intense Hurricanes. Part I: General Statistics." Monthly Weather Review **133**(1): 188-208.

Eastin, M. D., W. M. Gray, et al. (2005). "Buoyancy of Convective Vertical Motions in the Inner Core of Intense Hurricanes. Part II: Case Studies." Monthly Weather Review **133**(1): 209-227.

Ebert, E. E. and G. J. Holland (1992). "Observations of Record Cold Cloud-Top Temperatures in Tropical Cyclone Hilda (1990)." Monthly Weather Review **120**(10): 2240-2251.

Emanuel, K. A. (1986). "An Air-Sea Interaction Theory for Tropical Cyclones. Part I: Steady-state Maintenance." Journal of the Atmospheric Sciences **43**(6): 585-605.

Emanuel, K. A. (1988). "The maximum intensity of hurricanes." Journal of the Atmospheric Sciences **45**: 1143-1156.

Emanuel, K. A. (1995). "Sensitivity of Tropical Cyclones to Surface Exchange Coefficients and a Revised Steady-State Model incorporating Eye Dynamics." Journal of the Atmospheric Sciences **52**(22): 3969-3976.

Emanuel, K. A. (1999). "Thermodynamic control of hurricane intensity." Nature **401**: 665-669.

Emanuel, K. A., C. DesAutels, et al. (2004). "Environmental Controls of Tropical Cyclone Intensity." Journal of the Atmospheric Sciences **61**: 843-858.

Evans, J. L. (1993). "Sensitivity of tropical cyclone intensity to sea surface temperature." Journal of Climate **6**: 1133-1140.

Frank, W. M. (1977). "Convective Fluxes in Tropical Cyclones." Journal of the Atmospheric Sciences **34**(10): 1554-1568.

Frank, W. M. and E. A. Ritchie (1999). "Effects of Environmental Flow upon Tropical Cyclone Structure." Monthly Weather Review **127**(9): 2044-2061.

Frank, W. M. and E. A. Ritchie (2001). "Effects of Vertical Wind Shear on the Intensity and Structure of Numerically Simulated Hurricanes." Monthly Weather Review **129**(9): 2249-2269.

Franklin, C. N., G. J. Holland, et al. (2005). "Sensitivity of Tropical Cyclone Rainbands to Ice-Phase Microphysics." Monthly Weather Review **133**(8): 2473-2493.

Fritsch, J. M. and G. S. Forbes (2001). Mesoscale convective systems. Severe Convective Storms. C. A. I. Doswell. Boston, MA, American Meteorological Society. **1:** 323-357.

Garratt, J. R. (1977). "Review of Drag Coefficients over Oceans and Continents." Monthly Weather Review **105**(7): 915-929.

Gentry, R. C., T. T. Fujita, et al. (1970). "Aircraft, spacecraft, satellite and radar observations of Hurricane Gladys." Journal of Applied Meteorology **9**: 837-850.

Gentry, R. C., E. Rodgers, et al. (1980). "Predicting tropical storm intensity using satellite measured equivalent blackbody temperature of cloud tops." Monthly Weather Review **108**: 445-455.

Ginis, I., A. P. Khain, et al. (2004). "Effects of Large Eddies on the Structure of the Marine Boundary Layer under Strong Wind Conditions." Journal of the Atmospheric Sciences **61**: 3049-3063.

Giordani, H. and G. Caniaux (2001). "Sensitivity of Cyclogenesis to Sea Surface Temperature in the Northwestern Atlantic." Monthly Weather Review **129**(6): 1273-1295.

Goni, G., L. K. Shay, et al. (2000). Role of the upper ocean structure on the intensification of Hurricane Bret from satellite altimetry. 24th Conference on Hurricanes and Tropical Meteorology, Ft. Lauderdale, FL, American Meteorological Society.

Gray, W. M. (1965). "Calculations of Cumulus Vertical Draft Velocities in Hurricanes from Aircraft Observations." Journal of Applied Meteorology **4**(4): 463-474.

Gray, W. M. (1998). "The Formation of Tropical Cyclones." Meteor. Atmos. Phys **67**: 37-69.

Gray, W. M. and R. W. J. Jacobson (1977). "Diurnal Variation of Deep Cumulus Convection." Monthly Weather Review **105**(9): 1171-1188.

Hawkins, H. F. and S. M. Imbembo (1976). "The Structure of a Small, Intense Hurricane -- Inez 1966." Monthly Weather Review **104**(4): 418-442.

Hendricks, E. A. and M. T. Montgomery (2004). "The Role of "Vortical" Hot Towers in the Formation of Tropical Cyclone Diana (1984)." Journal of the Atmospheric Sciences **61**(11): 1209-1231.

Henning, R. G. (2000). Observations of low level wind maxima using GPS Dropsondes and their link to 200 millibar clues identifying the onset of rapid intensification.

Heymsfield, A. J., L. M. Miloshevich, et al. (2005). "Homogeneous Ice Nucleation in Subtropical and Tropical Convection and Its Influenceon Cirrus Anvil Microphysics." Journal of the Atmospheric Sciences **62**(1): 41-64.

Heymsfield, G. M., S. W. Bidwell, et al. (1996). "The EDOP Radar System on the High-Altitude NASA ER-2 Aircraft." Journal of Atmospheric and Oceanic Technology **13**(4): 795-809.

Heymsfield, G. M., J. B. Halverson, et al. (2001). "ER-2 Doppler Radar Investigations of the Eyewall of Hurricane Bonnie during the Convection and Moisture Experiment-3." Journal of Applied Meteorology **40**(8): 1310-1330.

Hobgood, J. S. (2003). "Maximum Potential Intensities of Tropical Cyclones near Isla Socorro, Mexico." Weather and Forecasting **18**(6): 1129-1139.

Holland, G. J. (1997). "The Maximum Potential Intensity of Tropical Cyclones." Journal of the Atmospheric Sciences **54**: 2519-2540.

Holliday, C. R. and A. H. Thompson (1979). "Climatological characteristics of rapidly intensifying typhoons." Monthly Weather Review **107**: 1022-1034.

Hong, X., S. W. Chang, et al. (2000). "The Interaction between Hurricane Opal (1995) and a Warm Core Ring in the Gulf of Mexico." Monthly Weather Review **128**: 1347-1365.

Huber, M. M., L. K. Shay, et al. (1998). Atlantic ocean's role on intensity change. 23rd Conference on Hurricanes and Tropical Meteorology, American Meteorological Society.

Huber, M. M., L. K. Shay, et al. (2000). Operational heat content charts at the Tropical Prediction Center. 24th Conference on Hurricanes and Tropical Meteorology, Ft. Lauderdale, Florida, American Meteorological Society.

Jacob, S. D., F. D. Marks, et al. (2000). "The 3D oceanic mixed layer response to Hurricane Gilbert." Journal of Physical Oceanography **30**: 1407-1429.

Jarvinen, B. R., C. J. Neumann, et al. (1984). A tropical cyclone data tape for the North Atlantic Basin, 1886-1983: Contents, limitations, and uses. NWS NHC-22. N. T. Memo. Miami, FL, National Hurricane Center**:** 21.

Jensen, M. P. and A. D. Del Genio (2003). "Radiative and Microphysical Characteristics of Deep Convective Systems in the Tropical Western Pacific." Journal of Applied Meteorology **42**(9): 1234-1254.

Kalnay, E. a. c.-a. (1996). "The NCEP/NCAR 40-year reanalysis project." Bulletin of the American Meteorological Society **77**: 437-471.

Kaplan, J. and M. DeMaria (2003). "Large-Scale Characteristics of Rapidly Intensifying Tropical Cyclones in the North Atlantic Basin." Weather and Forecasting **18**(6): 1093-1108.

Kelley, O. A., J. Stout, et al. (2005). "Hurricane intensification detected by continuously monitoring tallprecipitation in the eyewall." Geophysical Research Letters **32**(L20819).

Kelley, O. A., J. Stout, et al. (2004). "Tall precipitation cells in tropical cyclone eyewalls are associated with tropical cyclone intensification." Geophysical Research Letters **31**(L24112).

Kelly, K. A. and B. Qiu (1995). "Heat Flux Estimates for the Western North Atlantic. Part I: Assimilation of Satellite Data into a Mixed Layer Model." Journal of Physical Oceanography **25**(10): 2344-2360.

Khain, A. P., I. Ginis, et al. (1997). The influence of sea surface temperature inhomogeneity on motion of binary tropical cyclones. 22nd Conference on Hurricanes and Tropical Meteorology, American Meteorological Association.

Klecka, W. (1980). Discriminant Analysis. Beverly Hills, CA, Sage Publications.

Knaff, J. A., C. R. Sampson, et al. (2005). "An Operational Statistical Typhoon Intensity Prediction Scheme for the Western North Pacific." Weather and Forecasting **20**(4): 688-699.

Knaff, J. A., S. A. Seseske, et al. (2004). "On the Influences of Vertical Wind Shear on Symmetric Tropical Cyclone Structure Derived from AMSU." Monthly Weather Review **132**(10): 2503-2510.

Kossin, J. P. and M. D. Eastin (2001). "Two Distinct Regimes in the Kinematic and Thermodynamic Structure of the Hurricane Eye and Eyewall." Journal of the Atmospheric Sciences **58**(9): 1079-1090.

Kummerow, C., W. S. Olson, et al., Eds. (1996). A simplified scheme for obtaining precipitation and vertical hydrometeor profiles from passive microwave sensors. IEEE Transactions in Geoscience and Remote Sensing, IEEE.

Lackmann, G. M. and R. M. Yablonsky (2004). "The Importance of the Precipitation Mass Sink in Tropical Cyclones and Other Heavily Precipitating Systems." Journal of the Atmospheric Sciences **61**(14): 1674-1692.

Laing, A. G. and J. M. Fritsch (2000). "The Large-Scale Environments of the Global Populations of Mesoscale Convective Complexes." Monthly Weather Review **128**(8): 2756-2776.

Lander, M. A. (1999). "A Tropical Cyclone with an Enormous Central Cold Cover." Monthly Weather Review **127**(1): 132-136.

Larson, K. and D. L. Hartmann (2003). "Interactions among Cloud, Water Vapor, Radiation, and Large-Scale Circulation in the Tropical Climate. Part II: Sensitivity to Spatial Gradients of Sea Surface Temperature." Journal of Climate **16**(10): 1441-1455.

Leipper, D. F. (1967). "Observed ocean conditions and hurricane Hilda." Journal of the Atmospheric Sciences **24**: 182-196.

Leipper, D. F. and D. Volgenau (1972). "Hurricane Heat Potential of the Gulf of Mexico." Journal of Physical Oceanography **2**: 218-224.

LeMone, M. A., E. J. Zipser, et al. (1998). "The Role of Environmental Shear and Thermodynamic Conditions in Determining the Structure and Evolution of Mesoscale Convective Systems during TOGA COARE." Journal of the Atmospheric Sciences **55**(23): 3493-3518.

Liu, C. and M. W. Moncrieff (2001). "Cumulus Ensembles in Shear: Implications for Parameterization." Journal of the Atmospheric Sciences **58**(18): 2832-2842.

Lonfat, M., F. D. J. Marks, et al. (2004). "Precipitation Distribution in Tropical Cyclones Using the Tropical Rainfall Measuring Mission (TRMM) Microwave Imager: A Global Perspective." Monthly Weather Review **132**(7): 1645-1660.

Lyons, W. A. and C. S. Keen (1994). "Observations of Lightning in Convective Supercells within Tropical Storms and Hurricanes." Monthly Weather Review **122**(8): 1897-1916.

Mack, R. A. and D. P. Wylie (1982). "An Estimation of the Condensation Rates in Three Severe Storm Systems from Satellite Observations of the Convective Mass Flux." Monthly Weather Review **110**(7): 725-744.

Malkus, J. S. (1962). Large-scale interactions. The Sea: Ideas and Observations on Progress in the Study of teh Seas, John Wiley and Sons**:** 88-294.

Malkus, J. S. and H. Riehl (1960). "On the dynamics and energy transformations in steady-state hurricanes." Tellus **12**: 1-20.

Mao, Q., S. W. Chang, et al. (2000). "Influence of Large-Scale Initial Oceanic Mixed Layer Depth on Tropical Cyclones." Monthly Weather Review **128**: 4058-4070.

Marks, F. D. and L. K. Shay (1998). "Landfalling tropical cyclones: Forecast problems and associated research opportunities: Report of the 5th prospectus development team to the U.S. Weather Research Program." Bulletin of the American Meteorological Sociey **79**: 1-19.

McBride, J. L. (1981). "Observational Analysis of Tropical Cyclone Formation. Part I: Basic Description of Data Sets." Journal of the Atmospheric Sciences **38**(6): 1117-1131.

McBride, J. L. (1981). "Observational Analysis of Tropical Cyclone Formation. Part III: Budget Analysis." Journal of the Atmospheric Sciences **38**(6): 1152-1166.

McBride, J. L. and R. Zehr (1981). "Observational Analysis of Tropical Cyclone Formation. Part II: Comparison of Non-Developing versus Developing Systems." Journal of the Atmospheric Sciences **38**(6): 1132-1151.

Miller, B. I. (1958). "On the maximum intensity of hurricanes." Journal Meteorlogika **15**: 184-195.

Miller, D. and J. M. Fritsch (1991). "Mesoscale Convective Complexes in the Western Pacific Region." Monthly Weather Review **119**(12): 2978-2992.

Miller, D. K. and K. B. Katsaros (1992). "Satellite-derived Surface Latent Heat Fluxes in a Rapidly Intensifying Marine Cyclone." Monthly Weather Review **120**(7): 1093-1107.

Miller, R. A. and W. M. Frank (1993). "Radiative Forcing of Simulated Tropical Cloud Clusters." Monthly Weather Review **121**(2): 482-498.

Molinari, J., D. Vollaro, et al. (2005). "Tropical Cyclone Formation in a Sheared Environment: A Case Study." Journal of the Atmospheric Sciences **61**(21): 2493-2509.

Nesbitt, S. W. and E. J. Zipser (2003). "The Diurnal Cycle of Rainfall and Convective Intensity according to Three Years of TRMM Measurements." Journal of Climate **16**(10): 1456-1475.

Olson, W., C. Kummerow, et al. (1996). "A method for combined passive-active microwave retreivals of cloud and precipitation profiles." Journal of Applied Meteorology **35**: 1763-1789.

Ooyama, K. (1969). "Numerical Simulation of the Life Cycle of Tropical Cyclones." Journal of the Atmospheric Sciences **26**(1): 3-40.

Palmen, E. (1948). "On the formation and structure of tropical cyclones." Geophysica **3**: 26-38.

Pan, J., X.-H. Yan, et al. (2004). "A New Method for Estimation of the Sensible Heat Flux under Unstable Conditions Using Satellite Vector Winds." Journal of Physical Oceanography **34**(4): 968-977.

Powell, M. D. (1990). "Boundary Layer Structure and Dynamics in Outer Hurricane Rainbands. Part I: Mesoscale Rainfall and Kinematic Structure." Monthly Weather Review **118**(4): 891-917.

Powell, M. D. (1990). "Boundary Layer Structure and Dynamics in Outer Hurricane Rainbands. Part II: Downdraft Modification and Mixed Layer Recovery." Monthly Weather Review **118**(4): 918-938.

Price, J. F. (1981). "Upper ocean response to a hurricane." Journal of Physical Oceanography **11**: 153-175.

Reasor, P. D. and M. T. Montgomery (2005). "Mesoscale Observations of the Genesis of Hurricane Dolly (1996)." Journal of the Atmospheric Sciences **62**(9): 3151-3171.

Riehl, H. (1950). "A model for hurricane formation." Journal of Applied Physics **21**: 917-925.

Riehl, H. (1954). Tropical Meteorology, McGraw-Hill.

Riehl, H. and J. S. Malkus (1958). "On the heat balance in the equatorial trough zone." Geophysica **6**: 503-538.

Ritchie, E., J. Simpson, et al. (2003). Present Day Satellite Technology for Hurricane Research: A Closer Look at Formation and Intensification. Hurricane!: coping with disaster: progress and challenges since Galveston, 1900. R. Simpson.

Rodgers, E., W. Olson, et al. (2000). "Environmental Forcing of Supertyphoon Paka's (1997) Latent Heat Structure." Journal of Applied Meteorology **39**(12): 1983-2006.

Rodgers, E. B., J.-J. Baik, et al. (1994). "The Environmental Influence on Tropical Cyclone Precipitation." Journal of Applied Meteorology **33**(5): 573-593.

Rodgers, E. B., S. W. Chang, et al. (1994). "A Satellite Observational and Numerical Study of Precipitation Characteristics in Western North Atlantic Tropical Cyclones." Journal of Applied Meteorology **33**(2): 129-139.

Rodgers, E. B., S. W. Chang, et al. (1991). "Satellite Observations of Variations in Tropical Cyclone Convection Caused by Upper-Tropospheric Troughs." Journal of Applied Meteorology **30**(8): 1163-1184.

Rodgers, E. B., W. S. Olson, et al. (1998). "Satellite-Derived Latent Heating Distribution and Environmental Influences in Hurricane Opal (1995)." Monthly Weather Review **126**(5): 1229-1247.

Rodgers, E. B. and H. F. Pierce (1995). "Environmental Influence on Typhoon Bobbie's Precipitation Distribution." Journal of Applied Meteorology **34**(11): 2513-2532.

Rodgers, E. B. and H. F. Pierce (1995). "A Satellite Observational Study of Precipitation Characteristics in Western North Pacific Tropical Cyclones." Journal of Applied Meteorology **34**(12): 2587-2599.

Roebber, P. J. (1989). "The Role of Surface Heat and Moisture Fluxes Associated with Large-Scale Ocean Current Meanders in Maritime Cyclogenesis." Monthly Weather Review **117**(8): 1676-1694.

Rogers, R. F. and J. M. Fritsch (2001). "Surface Cyclogenesis from Convectively Driven Amplification of Midlevel Mesoscale Convective Vortices." Monthly Weather Review **129**(4): 605-637.

Sanford, T. B., P. G. Black, et al. (1987). "Ocean Response to a Hurricane. Part I: Observations." Journal of Physical Oceanography **17**(11): 2065-2083.

Schade, L. R. (1994). The ocean's effect on hurricane intensity. Earth, Oceans, and Planetary Science. Cambridge, Mass., Massechusetts Institute of Technology**:** 127.

Schade, L. R. (2000). "Tropical Cyclone Intensity and Sea Surface Temperature." Journal of the Atmospheric Sciences **57**(18): 3122-3130.

Schade, L. R. and K. A. Emanuel (1999). "The ocean's effect on the intensity of tropical cyclones: Results from a simple coupled atmosphere-ocean model." Journal of the Atmospheric Sciences **56**: 642-651.

Schubert, W. H., J. J. Hack, et al. (1980). "Geostrophic Adjustment in an Axisymmetric Vortex." Journal of the Atmospheric Sciences **37**(7): 1464-1484.

Schumacher, C., R. A. J. Houze, et al. (2004). "The Tropical Dynamical Response to Latent Heating Estimates Derived from the TRMM Precipitation Radar." Journal of the Atmospheric Sciences **61**(12): 1341-1358.

Schwartz, B. E., D. M. Rodgers, et al. (1987). "The Use and Interpretation of Numerical Weather Prediction Model Output in Identifying Synoptic-Scale Environments Associated with Development of Mesoscale Convective Systems." Weather and Forecasting **2**(1): 50-69.

Shay, L. K., G. J. Goni, et al. (2000). "Effects of a warm oceanic feature on Hurricane Opal." Monthly Weather Review **128**: 1366-1383.

Shay, L. K., G. J. Goni, et al. (1998). Role of warm ocean features on intesity change: Hurricane Opal. Symposium on Tropical Cyclone Intensity Change, Boston, MA, American Meteorological Society.

Simpson, J., J. B. Halverson, et al. (1998). "Eyeing the eye: Exciting early stage science results from TRMM." Bulletin of the American Meteorological Sociey **79**: 1711.

Simpson, J., E. Ritchie, et al. (1997). "Mesoscale Interactions in Tropical Cyclone Genesis." Monthly Weather Review **125**(10): 2643-2661.

Steranka, J., E. B. Rodgers, et al. (1984). "The Diurnal Variation of Atlantic Ocean Tropical Cyclone aoud Distribution Inferred from Geostationary Satellite Infrared Measurements." Monthly Weather Review **112**(11): 2338-2344.

Steranka, J., E. B. Rodgers, et al. (1986). "The relationship between satellite measured convective bursts and tropical cyclone intensification." Monthly Weather Review **114**: 1539-1546.

Stewart, S. and S. W. Lyons (1996). "A WSR-88D Radar View of Tropical Cyclone Ed." Weather and Forecasting **11**(1): 115-135.

Stossmeister, G. J. and G. M. Barnes (1992). "The Development of a Second CIrculation Center within Tropical Storm Isable (1985)." Monthly Weather Review **120**(5): 685-697.

Su, H., J. D. Neelin, et al. (2003). "Sensitivity of Tropical Tropospheric Temperature to Sea Surface Temperature Forcing{ast}." Journal of Climate **16**(9): 1283-1301.

Titley, D. W. and R. L. Elsberry (2000). "Large Intensity Changes in Tropical Cyclones: A Case Study of Supertyphoon Flo during TCM-90." Monthly Weather Review **128**(10): 3556-3573.

Uhlhorn, E. W., P. G. Black, et al. (2000). Warm core ocean features in the central and eastern Gulf of Mexico. 24th Conference on Hurricanes and Tropical Meteorology, Fort Lauderdale, Florida, American Meteorological Society.

Velasco, I. and J. M. Fritsch (1987). "Mesoscale convective complexes in the Americas." J. Geophys. Res. **92**: 9591-9613.

Velden, C. S. (1992). "Satellite-based Microwave Observations of Tropopause-Level Thermal Anomalies: Qualitative Applications in Extratropical Cyclone Events." Weather and Forecasting **7**(4): 669-682.

Wang, Y., J. D. Kepert, et al. (2001). "The Effect of Sea Spray Evaporation on Tropical Cyclone Boundary Layer Structure and Intensity." Monthly Weather Review **129**: 2481-2500.

Weatherford, C. L. and W. M. Gray (1988). "Typhoon Structure as Revealed by Aircraft Reconnaissance. Part I: Data Analysis and Climatology." Monthly Weather Review **116**(5): 1032-1043.

Webster, P. J. and R. Lukas (1992). "TOGA COARE: The Coupled Ocean-Atmosphere Response Experiment." Bulletin of the American Meteorological Society **73**(9): 1377-1416.

Wentz, F. J., C. Gentemann, et al. (2000). "Satellite Measurements of Sea Surface Temperature Through Clouds." Science **288**(5467): 847-850.

Wilcox, E. M. and V. Ramanathan (2001). "Scale Dependence of the Thermodynamic Forcing of Tropical Monsoon Clouds: Results from TRMM Observations." Journal of Climate **14**(7): 1511-1524.

Yu, H. and H. J. Kwon (2005). "Effect of TC-Trough Interaction on the Intensity Change of Two Typhoons." Weather and Forecasting **20**(2): 199-211.

Yu, J.-Y. and J. D. Neelin (1997). "Analytic Approximations for Moist Convectively Adjusted Regions." Journal of the Atmospheric Sciences **54**(8): 1054-1063.

Zehr, R. (1988). "Use of VAS Data to Diagnose the Mesoscale Environment of Convective Storms." Weather and Forecasting **3**(1): 33-49.

Zehr, R. M., J. F. W. Purdom, et al. (1988). "Use of VAS Data to Diagnose the Mesoscale Environment of Convective Storms." Weather and Forecasting **3**(1): 33-49.

Zhang, D.-L. and N. Bao (1996). "Oceanic Cyclogenesis as Induced by a Mesoscale Convective System Moving Offshore. Part I: A 90-h Real-Data Simulation." Monthly Weather Review **124**(7): 1449-1469.

Zhu, T., D.-L. Zhang, et al. (2002). "Impact of the Advanced Microwave Sounding Unit Measurements on Hurricane Prediction." Monthly Weather Review **130**(10): 2416-2432.